

THERMOPHYSICS 2000

Meeting of the Thermophysical Society
Working Group of the Slovak Physical Society

Nitra, October 20, 2000

Editor Libor Vozár



Constantine the Philosopher University in Nitra
Faculty of Natural Sciences
2000

© CPU Nitra, 2000

THERMOPHYSICS 2000
Proceedings of the Meeting of the Thermophysical Society - Working
Group of the Slovak Physical Society
Nitra, October 20, 2000

Editor Libor Vozár

Issued by Constantine the Philosopher University in Nitra
First Edition
Released in 2000
Printed by Oto Kanás, Nitra

Published with the support by the Slovak Science Grant Agency under the contract
1/6115/99.

ISBN 80-8050-361-3

CONTENTS

PERFACE	5
EFFECTIVE THERMAL DIFFUSIVITY IN POROUS MATERIALS <i>Štefan Barta</i>	7
EFFECTIVE THERMAL CONDUCTIVITY OF FIBROUS COMPOSITE MATERIALS <i>Štefan Barta</i>	13
HYGRIC AND THERMAL PROPERTIES OF CEMENTITIOUS COMPOSITES AFTER THERMAL AND MECHANICAL LOAD <i>J. Toman, R. Černý</i>	19
FRIGICHIPS TESTING FOR THE HEAT FLOW MEASUREMENTS <i>V. Bahyl, Š. Dubnička</i>	25
MEASUREMENT OF THE THERMAL CONDUCTIVITY OF THE AIR PERMEABLE INSULATION MATERIAL IN A HORIZONTAL GUARDED HOT PLATE APPARATUS <i>P. Matiašovský, O. Koronthályová</i>	33
TRANSIENT METHODS FOR THE MEASUREMENT OF THERMOPHYSICAL PROPERTIES <i>L. Kubičár, V. Boháč</i>	39
THICKNESS DEPENDENCY OF THERMOPHYSICAL PROPERTIES OF PERSPEX <i>V. Boháč, L. Kubičár, M.K. Gustafsson</i>	49
DETERMINATION OF THE RESPONSE DELAY PARAMETERS FOR A MEASUREMENT SYSTEM USING THE FLASH METHOD <i>J. Spišiak, T. Šrámková</i>	55
DETERMINATION OF TEMPERATURE-DEPENDENT THERMAL CONDUCTIVITY WITHOUT INTERNAL MEASUREMENTS <i>J. Lukovičová, J. Zámečník</i>	59
UNCERTAINTY OF THE THERMAL CONDUCTIVITY MEASUREMENT BY THE TRANSIENT HOT WIRE METHOD <i>G. Labudová, V. Vozárová</i>	65

MODELLING OF THE THERMAL CONDUCTIVITY PROPERTIES OF ULTRA-THIN LAYERS 1-DIMENSIONAL CASE	71
<i>A. Teleki</i>	
HIGH-TEMPERATURE ALUMINA ROD DILATOMETER	77
<i>I. Štubňa, L. Vozár</i>	
AN APPARATUS FOR THE THERMAL DIFFUSIVITY MEASUREMENT USING THE FLASH METHOD	83
<i>L. Vozár, W. Hohenauer</i>	

PREFACE

It is a pleasure for our research group at the Department of Physics, Faculty of Natural Sciences at the Constantine the Philosopher University in Nitra to host the fifth meeting of the Thermophysical Society - Working Group of the Slovak Physical Society.

The tradition of series of meetings has been initiated by prof. Štefan Barta who organized the first meeting on January 22, 1996 at the Department of Physics, Faculty of Electrical Engineering and Information Technology at the Slovak University of Technology in Bratislava. Then Dr. Ľudovít Kubičár acted as the coordinator of the group and organized meetings at the Institute of Physics of the Slovak Academy of Sciences in Bratislava in the following three years – 1997, 1998 and 1999.

The Thermophysics workshop has now been established as a periodical meeting of scientists working in the field of investigation of heat transfer and measurement of thermophysical and other transport properties of materials.

Organizers of the last meeting were delighted to have heard an increased number of contributions – participants delivered 13 original lectures in which their authors presented current research progress and original results achieved at their home institutions.

A special thank goes to MSc. student Ľubomír Veselý for his contribution in the preparation of the proceedings.

The proceedings are also available in a digital form at the homepage of the Thermophysics – <http://www.tpl.ukf.sk/thermophysics>, or upon a request at the e-mail address vozar@uniag.sk.

Libor Vozár

EFFECTIVE THERMAL DIFFUSIVITY IN POROUS MATERIALS

Štefan Barta

Department of Physics, Faculty of Electrical Engineering and Information Technology,
Slovak University of Technology, Ilkovičova 3, SK-812 19 Bratislava, Slovakia
Email: bartas@elf.stuba.sk

Abstract

The effective heat equation and the formula for the effective thermal diffusivity in a particulate and fibrous composite and porous materials are derived.

Key words: effective thermal diffusivity, effective thermal conductivity, effective heat capacity

1 Introduction

The aim of this paper is to derive the effective heat equation and the relation for the effective thermal diffusivity of composite and porous materials. The composite materials on the submacroscopic level are heterogeneous ones, and therefore the heat equation can be written as

$$\gamma(\vec{r}) \frac{\partial T}{\partial t} = \nabla \cdot \lambda(\vec{r}) \nabla T, \quad (1)$$

where $\gamma(\vec{r}) = \rho(\vec{r})c(\vec{r})$, is the heat capacity of the unit volume, $\rho(\vec{r})$ is the density, $c_p(\vec{r})$ is the specific heat capacity at the constant pressure, $\lambda(\vec{r})$ is the thermal conductivity, T is the thermodynamic temperature.

In (1) we assume that the individual components are isotropic. On the macroscopic level usually the composite is isotropic and homogeneous therefore, the effective heat equation reads

$$\gamma_p \frac{\partial T_p}{\partial t} = \lambda_p \Delta T_p, \quad (2)$$

where thermophysical parameters γ_p (effective heat capacity of the unit volume) and λ_p (effective thermal conductivity) do not depend on the space coordinates. The physical meaning of the parameters λ_p and γ_p will be given later. In this situation there arises the problem how the thermophysical parameters λ_p and γ_p depend on the volume fractions of the individual components. This problem will be solved in the next part of this paper.

2 Formal solution of the stochastic heat equation

We arrange equation (1) in the form

$$\frac{\partial T}{\partial t} = \nabla \cdot a(\vec{r}) \nabla T + \frac{\nabla \gamma(\vec{r})}{\gamma(\vec{r})} a(\vec{r}) \cdot \nabla T, \quad (3)$$

where $a(\vec{r}) = \frac{\lambda(\vec{r})}{\gamma(\vec{r})}$ is the thermal diffusivity. Applying Laplace's transformation on equations (2) and (3) one obtains

$$p\tilde{T} - T(0, \vec{r}) = \nabla a(\vec{r}) \cdot \nabla \tilde{T} + \frac{\nabla \gamma(\vec{r})}{\gamma(\vec{r})} a(\vec{r}) \cdot \nabla \tilde{T} \quad \text{and} \quad p\tilde{T}_p - T(0, \vec{r}) = a_p \Delta \tilde{T}_p \quad (4)$$

where $a_p = \frac{\lambda_p}{\gamma_p}$ is the effective thermal diffusivity. In equations (4) we consider the same boundary conditions. Introducing the notation $a^* = a - a_p$ into equation (4) we obtain the equation

$$\left[\Delta - \frac{p}{a_p} + \nabla \frac{a^*(\vec{r})}{a_p} \cdot \nabla + \frac{\nabla \gamma(\vec{r})}{\gamma(\vec{r})} \frac{a(\vec{r})}{a_p} \cdot \nabla \right] \tilde{T} = \left[\Delta - \frac{p}{a_p} \right] \tilde{T}_p \quad (5)$$

The formal solution of (5) is the following one

$$\tilde{T} = \left[\Delta - \frac{p}{a_p} + \nabla \frac{a^*(\vec{r})}{a_p} \cdot \nabla + \frac{\nabla \gamma(\vec{r})}{\gamma(\vec{r})} \frac{a(\vec{r})}{a_p} \cdot \nabla \right]^{-1} \left[\Delta - \frac{p}{a_p} \right] \tilde{T}_p \quad (6)$$

We arrange the inverse operator in (6) with the help of the following operator identity:

$$\left[\hat{L}_0 + \hat{L}_1 \right]^{-1} = \sum_{n=0}^{\infty} (-1)^n \left\{ \hat{L}_0 \hat{L}_1 \right\}^n \hat{L}_0^{-1} \quad (7)$$

Using (7) we can write

$$\left[\Delta - \frac{p}{a_p} + \nabla \frac{a^*(\vec{r})}{a_p} \cdot \nabla + \frac{\nabla \gamma(\vec{r})}{\gamma(\vec{r})} \frac{a(\vec{r})}{a_p} \cdot \nabla \right]^{-1} = \sum_{n=0}^{\infty} (-1)^n \left\{ \left[\Delta - \frac{p}{a_p} + \nabla \frac{a^*(\vec{r})}{a_p} \cdot \nabla \right]^{-1} \frac{\nabla \gamma(\vec{r})}{\gamma(\vec{r})} \frac{a(\vec{r})}{a_p} \cdot \nabla \right\}^n \left[\Delta - \frac{p}{a_p} + \nabla \frac{a^*(\vec{r})}{a_p} \cdot \nabla \right]^{-1} \quad (8)$$

Again using (7) one can write

$$\nabla \left[\Delta - \frac{p}{a_p} + \nabla \frac{a^*(\vec{r})}{a_p} \cdot \nabla \right]^{-1} = \sum_{m=0}^{\infty} (-1)^m \left\{ \hat{H} \frac{a^*}{a_p} \right\}^m \cdot \hat{G}, \quad (9)$$

$$\text{where } \hat{H} = \nabla \nabla \left[\Delta - \frac{p}{a_p} \right]^{-1} \dots \hat{G} = \nabla \left[\Delta - \frac{p}{a_p} \right]^{-1} \quad (10)$$

With the help of (6), (8) and (9) it may be shown that

$$\nabla \hat{T} = \sum_{n=0}^{\infty} (-1)^n \left\{ \sum_{m=0}^{\infty} (-1)^m \left[\hat{H} \frac{a^*}{a_p} \right]^m \cdot \hat{G} \frac{\nabla \gamma}{\gamma} \frac{a}{a_p} \right\}^n \cdot \sum_{m=0}^{\infty} (-1)^m \left\{ \hat{H} \frac{a^*}{a_p} \right\}^m \cdot \nabla \tilde{T}_p \quad (11)$$

2 Properties of the operators \hat{H} and \hat{G}

The operator $\hat{L}_0 = \left[\Delta - \frac{p}{a_p} \right]^{-1}$ is defined by the relation

$$\hat{L}_0 f(\vec{r}) = \int G(\vec{r} - \vec{r}') f(\vec{r}') d\vec{r}' \quad (12)$$

Applying operator $\left[\Delta - \frac{p}{a_p} \right]$ on relation (12) one obtains

$$f(\vec{r}) = \int \left[\Delta - \frac{p}{a_p} \right] G(\vec{r} - \vec{r}') d\vec{r}' \quad (13)$$

If equation (13) has to be fulfilled it has to hold

$$\left[\Delta - \frac{p}{a_p} \right] G(\vec{r} - \vec{r}') = \delta(\vec{r} - \vec{r}') \quad (14)$$

For the infinite large surroundings the solution of equation (14) is expressed by the relation

$$G(\vec{r} - \vec{r}') = -\frac{1}{4\pi} \frac{1}{r} e^{-r \sqrt{\frac{p}{a_p}}} \quad (15)$$

in the three dimensional case and

$$G(\vec{r} - \vec{r}') = -\frac{1}{2\pi} K_0 \left(|\vec{r} - \vec{r}'| \sqrt{\frac{p}{a_0}} \right) \quad (16)$$

in the two dimensional case. $K_0(x)$ is the Bessel function of second order [2].

The composite material on the submacroscopic level represents the random medium and therefore the macroscopic quantities can be obtained by averaging. For averaging it is

necessary to pass from the operator form to the integral form. That can be done by the following way: According to (10), and (12) one can write

$$\hat{\hat{H}}f(\vec{r}) = \int \nabla \nabla G(\vec{r} - \vec{r}') f(\vec{r}') d\vec{r}' = \int \vec{\vec{H}}(\vec{r} - \vec{r}') f(\vec{r}') d\vec{r}' \quad (17)$$

and

$$\hat{\hat{G}}f(\vec{r}) = \int \nabla G(\vec{r} - \vec{r}') f(\vec{r}') d\vec{r}' = \int \vec{\vec{G}}(\vec{r} - \vec{r}') f(\vec{r}') d\vec{r}' \quad (18)$$

For example the operator form $\left[\frac{\hat{\hat{H}} a^*}{a_p} \right]^m \cdot \hat{\hat{G}}$ can be rewritten in the integral form with

the help of (17) and (18) as

$$\begin{aligned} \left[\frac{\hat{\hat{H}} a^*}{a_p} \right]^m \cdot \hat{\hat{G}} &= \int \vec{\vec{H}}(\vec{r} - \vec{r}_1) \frac{a^*(\vec{r}_1)}{a_p} d\vec{r}_1 \cdot \int \vec{\vec{H}}(\vec{r}_1 - \vec{r}_2) \frac{a^*(\vec{r}_2)}{a_p} \dots \int \vec{\vec{H}}(\vec{r}_{m-1} - \vec{r}_m) \frac{a^*(\vec{r}_m)}{a_p} \cdot \int \vec{\vec{G}}(\vec{r}_m - \vec{r}') = \\ &= \vec{\vec{B}}(\vec{r}, \vec{r}') \end{aligned} \quad (19)$$

Using relation (19) one can write

$$\sum_{m=0}^{\infty} (-1)^m \left[\frac{\hat{\hat{H}} a^*}{a_p} \right]^m \cdot \hat{\hat{G}} = \sum_{m=0}^{\infty} \vec{\vec{B}}_m(\vec{r}, \vec{r}') = \vec{\vec{B}}(\vec{r}, \vec{r}') \quad (20)$$

Introducing (20) into (11) one can write

$$\begin{aligned} \nabla \tilde{T} &= \sum_{n=0}^{\infty} (-1)^n \int B(\vec{r}, \vec{r}'_1) \frac{\nabla \gamma(\vec{r}'_1) a(\vec{r}'_1)}{\gamma(\vec{r}'_1) a_p} d\vec{r}'_1 \cdot \int B(\vec{r}'_1, \vec{r}'_2) \frac{\nabla \gamma(\vec{r}'_2) a(\vec{r}'_2)}{\gamma(\vec{r}'_2) a_p} \dots \int B(\vec{r}'_{n-1}, \vec{r}'_n) \frac{\nabla \gamma(\vec{r}'_n) a(\vec{r}'_n)}{\gamma(\vec{r}'_n) a_p} d\vec{r}'_n \cdot \\ &\left[\Delta_{\vec{r}'_{n+1}} - \frac{p}{a_p} \right] \hat{T}_p(\vec{r}'_{n+1}) d\vec{r}'_{n+1} \end{aligned} \quad (21)$$

Due to the macroscopic character of measuring instrument an experimentalist measures the temperature averaged over large number of grains or fibres and, therefore $\tilde{T}_{exp} = \langle \tilde{T} \rangle$,

where $\langle \rangle$ means the average value over the representative volume element. For averaging one needs to know all n -points correlation functions, what usually is unknown. Further it is evident that the heat equation becomes nonlocal. But all experimental methods for measuring thermophysical parameters are based on the solution of the local heat equation. In the further text we will assume that the heat transport in composite materials can be described by the local effective heat equation of the type (2). In this case it is sufficient to consider only the singular parts of the operators $\hat{\hat{H}}$ and $\hat{\hat{G}}$. The singular parts of the operators $\hat{\hat{H}}$ and $\hat{\hat{G}}$ are defined by the following way:

$$\hat{\hat{H}}^{sing} = \lim_{R \rightarrow 0} \int_{\Omega_R} \nabla \nabla G(\vec{r}) d\vec{r} \quad \text{and} \quad \vec{\vec{G}}^{sing} = \lim_{R \rightarrow 0} \int_{\Omega_R} \nabla G(\vec{r}) d\vec{r}, \quad (22)$$

where Ω_R is the region of the globular form in the three dimensional case.

$$\hat{\vec{H}}^{sing} = \lim_{R \rightarrow 0} \int_{S_R} \nabla \nabla G(\vec{r}) d\vec{r} \quad \text{and} \quad \hat{G}^{sing} = \int_{S_R} \nabla G(\vec{r}) d\vec{r}, \quad (23)$$

where S_R is the region of circular form in the two dimensional case. Using (15),(16) and the Gauss's theorem one can write

$$\vec{\vec{H}}^{sing} = \lim_{R \rightarrow 0} \oint_{\Sigma_R} d\vec{S} \frac{\vec{R}}{R} \frac{dG(R)}{dR} = \frac{1}{3} \vec{\vec{I}} \dots \text{and} \quad \vec{G}^{sing} = \lim_{R \rightarrow 0} \oint_{\Sigma_R} d\vec{S} G(R) = 0, \quad (24)$$

in the three dimensional case. $\vec{\vec{I}}$ is the unit tensor. In the two dimensional case:

$$\begin{aligned} \hat{\vec{H}}^{sing} &= \lim_{R \rightarrow 0} \oint d\vec{S} \frac{\vec{R}}{R} \frac{dG(R)}{dR} = \lim_{R \rightarrow 0} \int_0^{2\pi} R d\alpha (\cos^2 \alpha \vec{i}\vec{i} + \sin^2 \alpha \vec{j}\vec{j}) \sqrt{\frac{p}{a_p}} \dots K_1 \left(R \sqrt{\frac{p}{a_p}} \right) = \\ &= \frac{1}{2} (\vec{i}\vec{i} + \vec{j}\vec{j}) \quad \text{and} \quad \hat{G}^{sing} = \lim_{R \rightarrow 0} \int_{S_R} \nabla G(\vec{r}) d\vec{r} = \lim_{R \rightarrow 0} \oint d\vec{S} G(R) = 0, \end{aligned} \quad (25)$$

where we used the asymptotical form of $K_1(x) \approx \frac{1}{x}$ [2].

3 Effective thermal diffusivity

Considering only the singular parts of the operators $\hat{\vec{H}}$ and \hat{G} relation (11) can be written in the close form

$$\nabla \tilde{T} \approx \sum_{n=0}^{\infty} (-1)^n \left\{ \frac{\hat{\vec{H}}^{sing}}{a_p^*} \right\}^n \cdot \nabla \tilde{T}_p = \sum_{n=0}^{\infty} (-1)^n \left\{ g \frac{\vec{\vec{I}}}{a_p} \right\}^n \cdot \nabla \tilde{T}_p = \frac{1}{1 + g \frac{a^*}{a_p}} \nabla \tilde{T}_p \quad (26)$$

where $g = \frac{1}{3}$ in the three dimensional case and $g = \frac{1}{2}$ in the two dimensional case.

We would obtain this result if we neglected the second term on the right side of equation (4). Averaging (26) one obtains

$$\nabla \langle \tilde{T} \rangle = \nabla \tilde{T}_{exp} = \left\langle \frac{1}{1 + g \frac{a^*}{a_p}} \right\rangle \nabla \tilde{T}_p \quad (27)$$

If we put $\tilde{T}_p = \tilde{T}_{exp}$ then it follows immediatelly from (26)

$$\left\langle \frac{1}{1 + g \frac{a^*}{a_p}} \right\rangle = 1 \quad (28)$$

It is easy to show that from (28) it follows also

$$\left\langle \frac{a^*}{1 + g \frac{a^*}{a_p}} \right\rangle = 0 \quad (29)$$

Averaging (4) and neglecting the second term on the right side of equation (4) we obtain

$$p\langle\tilde{T}\rangle - T(0, \vec{r}) = \nabla \cdot \langle a(\vec{r}) \nabla \tilde{T} \rangle = a_p \Delta \langle T \rangle + \nabla \cdot \langle a^* \nabla \tilde{T} \rangle \quad (30)$$

Considering (26) and (27) equation (28) transforms to the effective heat equation

$$p\langle\tilde{T}\rangle - T(0, \vec{r}) = a_p \Delta \langle \tilde{T} \rangle \quad \text{or} \quad \frac{\partial \langle T \rangle}{\partial t} = a_p \Delta \langle T \rangle \quad (31)$$

For the n -components composite equation (29) has the form

$$\sum_{i=1}^n c_i \frac{a_i - a_{eff}}{1 + g \frac{a_i - a_{eff}}{a_{eff}}} = 0 \quad (32)$$

where c_i is the volume fraction of i^{th} component. In (32) instead of a_p we used the a_{eff} which we call the effective thermal diffusivity.

In the stationary heat transport the heat equation is the following one

$$\nabla \cdot \lambda(\vec{r}) \nabla T = 0 \quad (33)$$

Proceeding similarly as in the preceding case we obtain the following equation for the calculation of the effective thermal conductivity

$$\sum_{i=1}^n c_i \frac{\lambda_i - \lambda_{eff}}{1 + g \frac{\lambda_i - \lambda_{eff}}{\lambda_{eff}}} = 0 \quad (34)$$

Now we define the effective heat capacity of the unit volume as

$$\gamma_{eff} = \frac{\lambda_{eff}}{a_{eff}} \quad (36)$$

Introducing (35) into (30) one obtains

$$\gamma_{eff} \frac{\partial \langle T \rangle}{\partial t} = \lambda_{eff} \Delta \langle T \rangle. \quad (37)$$

This is the effective heat equation for composite materials.

References

- [1] Beran M.J, 1974 Application of Statistical Theories for the Determination of Thermal, Electrical and Magnetic Properties of Heterogeneous Materials. In *Composite Materials, Vol.2* (New York, Academic Press) p.209
- [2] Gradshteyn J.S, Ryzhik J.M, 1965 Table of Integrals, Series, and Products (Academic Press, New York) p.558 Eq.4.293.3

EFFECTIVE THERMAL CONDUCTIVITY OF FIBROUS COMPOSITE MATERIALS

Štefan Barta

Department of Physics, Faculty of Electrical Engineering and Information Technology, Slovak University of Technology, Ilkovičova 3, 812 19 Bratislava, Slovak Republic

Abstract

The formula for the effective thermal conductivity tensor in fibrous composite materials is derived.

Keywords: fibrous composite, effective thermal conductivity, average field approximation

1 Introduction

The aim of this paper is to derive the relation for the effective thermal conductivity tensor for fibrous composite material. Fibrous material is regarded as that one consisting of fibres, possibly in a matrix. Generally the composite material on the submacroscopic level is heterogeneous because it is composed of some components which on the one hand are spacially separated from each other and on the other hand are randomly distributed over all sample. Due to this randomness the physical quantities of composite on the submacroscopic level are not only dependent on space coordinates but they are also the random quantities. However, on the macroscopic level composite usually is homogeneous and may be characterized by the effective parameters which are independent on space coordinates. For an experimentalist it is very important to know in which cases the composite material on the macroscopic level may be characterized by effective parameters because only in these cases it is justifiable to use the standard method for their measurement. The necessary and sufficient conditions for using effective parameters are discussed in Beran's work [1]. In the further text we will assume that all conditions for using the effective parameters are fulfilled. In this situation, we meet with a problem of the determination how the effective parameters depend on the structure of composite on the submacroscopic level and also on the quantities, which characterize individual components of composite material. This information is very important especially for technologist. Knowing the relation for the effective parameters it is possible to manufacture composite material with the prescribed values of the parameters ("tailoring" of materials). The statistics of the structure of composite on the submacroscopic level is very often unknown and only the volume fractions are known from the manufacturing process. If the composite on the macroscopic level is a homogeneous one then we will use the *Assumption: The probability of the occupation of certain place with the i^{th} component is equal to its volume fraction.* The derivation of the relation for effective parameter is a very difficult problem. When solving this problem we have to face two difficulties. The first one is connected with the necessity of becoming familiar with the statistics of the structure of the composite on the submacroscopic level, which as a rule is unknown. The second one

is connected with the mathematical difficulties of exact calculation of effective parameters and, therefore one is obliged to use approximate methods. One of those approximate method is an average field approximation method, which will be used in this article.

2 Average field approximation

The average field approximation method is based on the idea that a randomly chosen isotropic fibre of circular form characterized by the thermal conductivity λ is submerged into an unlimited effective medium, which is characterized by the effective thermal conductivity λ_{eff} . We will consider that all fibres are parallel and go through the whole sample. The fibres are covered with the surface layer characterized by the thermal conductivity λ_m . The average field approximation method does not require knowlege of the n -point correlation function, but only the local distribution function. This fact is advantageous, but it represents only an approximate method because it uses incomplete information about the statistics of the structure of the composite on the submacroscopic level.

The fibrous composite on the macroscopic level is anisotropic. The effective thermal conductivity along the fibres is other than that one perpendicular to the fibres. The effective thermal conductivity along the fibres can be derived easily because it represents the parallel connected thermal conductivities. If we consider the binary fibrous composite where the fibres are submerged into a matrix, which is characterized by the thermal conductivity λ_2 then

$$\lambda_{effalong} = \frac{S_1\lambda_1 + S_m\lambda_m + S_2\lambda_2}{S} \quad (1)$$

where $S_1 = \pi R_1^2$ is the area of the cross-section of fibre,

R_1 is the radius of the cross-section of fibre,

$S_m = \pi(R_2^2 - R_1^2)$ is the area of the cross-section of the surface layer of fibre,

R_2 is the radius of the cross-section of fibre and his surface layer,

$S_2 = S - S_1 - S_m$,

S is the area of the cross-section of the sample.

The calculation of the effective thermal conductivity perpendicular to the fibres differs from the standard method because the fibres are covered by the surface layer. The calculation will be done by two steps. At first step we will consider the fibre of the radius R_2 which consists of the matrix material and is put in the effective medium of the thermal conductivity λ_{eff} . In the stationary case the heat equation has the following form

$$\Delta T = 0, \quad (2)$$

where T is the temperature. The solution of equation (2) reads

$$T^{(I)} = -B\vec{E}_0 \cdot \vec{r} \quad \text{in the region I (fibre)} \quad (3)$$

$$T^{(II)} = -\vec{E}_0 \cdot \vec{r} + A\vec{E}_0 \cdot \frac{\vec{r}}{r^2} \quad \text{in the region II (effective medium)} \quad (4)$$

The constants A and B are determined from the boundary conditions:

At $r=R_2$

$$T^{(I)}(R_2) = T^{(II)}(R_2) \quad (5)$$

$$-\lambda_2 \nabla T^{(I)} \cdot \vec{r}_0 = -\lambda_{eff} \nabla T^{(II)} \cdot \vec{r}_0 \quad (6)$$

where \vec{r}_0 is the unit vector parallel to \vec{r} . The condition (6) expresses the equality of the heat current densities in the radial direction. From the boundary conditions (5) and (6) it follows

$$B = \frac{I}{I + \frac{1}{2} \frac{\lambda_2 - \lambda_{eff}}{\lambda_{eff}}} \quad (7)$$

and

$$\nabla T^{(I)} = -\frac{I}{I + \frac{1}{2} \frac{\lambda_2 - \lambda_{eff}}{\lambda_{eff}}} \vec{E}_0 \quad (8)$$

In the second step we will consider the fibre with the surface layer, which is put in the effective medium. In this case we have three regions. In the first region there is the fibre with the thermal conductivity λ_l and the radius R_l . In the second region there is the surface layer with the thermal conductivity λ_m and the third region is the effective medium. The solution of heat equation (2) is the following

In region I

$$T^{(I)} = -B\vec{E}_0 \cdot \vec{r} \quad (9)$$

In region II

$$T^{(II)} = -C\vec{E}_0 \cdot \vec{r} + D\vec{E}_0 \cdot \frac{\vec{r}}{r^2} \quad (10)$$

In region III

$$T^{(III)} = -\vec{E}_0 \cdot \vec{r} + A\vec{E}_0 \cdot \frac{\vec{r}}{r^2} \quad (11)$$

The constants B, C, D and A are determined from the boundary conditions:

At $r = R_l$

$$T^{(I)}(R_l) = T^{(II)}(R_l) \quad (12)$$

$$-\lambda_l \nabla T^{(I)}(R_1) \cdot \vec{r}_0 = -\lambda_m \nabla T^{(II)}(R_1) \cdot \vec{r}_0 \quad (13)$$

At $r = R_2$

$$T^{(II)}(R_2) = T^{(III)}(R_2) \quad (14)$$

$$-\lambda_m \nabla T^{(II)}(R_2) \cdot \vec{r}_0 = -\lambda_{eff} \nabla T^{(III)}(R_2) \cdot \vec{r}_0 \quad (15)$$

Introducing (9),(10) and (11) into (12),(13),(14) and (15) one obtains

$$B = C - \frac{D}{R_1^2}, \quad C - \frac{D}{R_2^2} = I - \frac{A}{R_2^2} \quad (16)$$

$$\lambda_l B = \lambda_m \left(C + \frac{D}{R_1^2} \right) \quad \lambda_m \left(C + \frac{D}{R_2^2} \right) = \lambda_{eff} \left(I + \frac{A}{R_2^2} \right) \quad (17)$$

The heat current density on the semicircle with the radius R_2 is expressed by the relation

$$\vec{q}(R_2) = -\lambda_m \nabla T^{(II)}(R_2) = C \vec{E}_0 - \frac{D}{R_2^2} \vec{E}_0 + \frac{D}{R_2^2} \vec{E}_0 \cdot \vec{r}_0 \vec{r}_0 \quad (18)$$

We choose the x -axis in the direction of \vec{E}_0 . The average heat current density in the direction of \vec{E}_0 on the semicircle with the radius R_2 has the following form:

$$\begin{aligned} \langle \vec{q}_x(R_2) \rangle &= \frac{\lambda_m}{\pi R_2} \int_{-\frac{\pi}{2}}^{+\frac{\pi}{2}} \vec{q}(R_2) \cdot \vec{i} \vec{i} R_2 d\alpha = \lambda_m C \vec{E}_0 - \lambda_m \frac{D}{R_2^2} \vec{E}_0 + \frac{\lambda_m}{\pi R_2} \int_{-\frac{\pi}{2}}^{+\frac{\pi}{2}} \frac{D}{R_2^2} E_0 \cos^2 \alpha R_2 d\alpha = \\ &= \lambda_m \left(C + \frac{D}{R_2^2} \right) \vec{E}_0 \end{aligned} \quad (19)$$

The heat current density at $r = R_1$ in the region I is expressed by the relation

$$\vec{q}^{(I)} = -\lambda_l \nabla T^{(I)}(R_1) = \lambda_l B \vec{E}_0 = \lambda_m \left(C + \frac{D}{R_1^2} \right) \vec{E}_0,$$

where we used the first relation in (17). We see that at the boundary $r = R_1$ the heat current densities in both sides are equal. From (16) and (17) it follows

$$C + \frac{D}{R_2^2} = \frac{2\lambda_{eff} \lambda_l^*}{\lambda_{eff}} \frac{I}{\lambda_m} \quad (20)$$

where

$$\lambda_l^* = \lambda_m \frac{I + \gamma + \alpha(I - \gamma)}{I + \gamma - (\alpha - \gamma)}, \quad \gamma = \frac{\lambda_m}{\lambda_l}, \quad \alpha = \left(\frac{R_1}{R_2} \right)^2$$

Introducing (20) into (19) one obtains

$$\langle q_x(R_2) \rangle = \frac{2\lambda_{eff}\lambda_l^*}{\lambda_{eff} + \lambda_l^*} \bar{E}_0 = \frac{\lambda_l^*}{I + \frac{I}{2} \frac{\lambda_l^* - \lambda_{eff}}{\lambda_{eff}}} \bar{E}_0 \quad (21)$$

From (21) it follows

$$\langle \nabla T^{(II)}(R_2) \rangle = - \frac{I}{I + \frac{I}{2} \frac{\lambda_l^* - \lambda_{eff}}{\lambda_{eff}}} \bar{E}_0 \quad (22)$$

It is obvious that λ_l^* is the thermal conductivity of fibre with the surface layer. According to (8) and (22) and the *Assumption* the configurational average value of $\langle \nabla T^{(II)}(R_2) \rangle$ is defined by the relation

$$\nabla \langle T \rangle_c = \langle \langle \nabla T^{(II)}(R_2) \rangle \rangle_c = - \left[c_1 \frac{I}{I + \frac{I}{2} \frac{\lambda_l^* - \lambda_{eff}}{\lambda_{eff}}} + c_2 \frac{I}{I + \frac{I}{2} \frac{\lambda_2 - \lambda_{eff}}{\lambda_{eff}}} \right] \bar{E}_0 \quad (23)$$

where c_1 is the area fraction of fibres with surface layers,
 c_2 is the area fraction of matrix.

Now we choose $\nabla \langle T \rangle_c = \bar{E}_0$ and from that assumption it follows

$$c_1 \frac{I}{I + \frac{I}{2} \frac{\lambda_l^* - \lambda_{eff}}{\lambda_{eff}}} + c_2 \frac{I}{I + \frac{I}{2} \frac{\lambda_2 - \lambda_{eff}}{\lambda_{eff}}} = I \quad (24)$$

The configurational average of $\langle \bar{q}(R_2) \rangle$ can be calculated from the relation

$$\langle \langle \bar{q}(R_2) \rangle \rangle_c = \left[c_1 \frac{\lambda_l^*}{I + \frac{I}{2} \frac{\lambda_l^* - \lambda_{eff}}{\lambda_{eff}}} + c_2 \frac{\lambda_2}{I + \frac{I}{2} \frac{\lambda_2 - \lambda_{eff}}{\lambda_{eff}}} \right] \bar{E}_0 = -\lambda_{eff} \nabla \langle T \rangle_c +$$

$$+ \left[c_1 \frac{\lambda_1^* - \lambda_{eff}}{1 + \frac{1}{2} \frac{\lambda_1^* - \lambda_{eff}}{\lambda_{eff}}} + c_2 \frac{\lambda_2 - \lambda_{eff}}{1 + \frac{1}{2} \frac{\lambda_2 - \lambda_{eff}}{\lambda_{eff}}} \right] \nabla \langle T \rangle_c \quad (25)$$

Due to the macroscopic character of measuring the experimentalist measures the temperature averaged over large number of fibres and, therefore $\langle T \rangle_c = T_{exp}$, where $\langle \rangle$ means the average value over the representative volume element. From (24) it follows immediately

$$c_1 \frac{\lambda_1^* - \lambda_{eff}}{1 + \frac{1}{2} \frac{\lambda_1^* - \lambda_{eff}}{\lambda_{eff}}} + c_2 \frac{\lambda_2 - \lambda_{eff}}{1 + \frac{1}{2} \frac{\lambda_2 - \lambda_{eff}}{\lambda_{eff}}} = 0 \quad (26)$$

and therefore

$$\langle \langle \vec{q}(R_2) \rangle \rangle_c = -\lambda_{eff} \nabla \langle T \rangle_c \quad (27)$$

Relation (27) expresses the Fourier's law for the fibrous composite perpendicular to fibres. The effective thermal conductivity can be calculated from (24) or from (27) according to the relation

$$\lambda_{eff} = -\frac{c_1(\lambda_1^* - \lambda_2) + c_2(\lambda_2 - \lambda_1^*)}{2} + \sqrt{\frac{1}{4} [c_1(\lambda_1^* - \lambda_2) + c_2(\lambda_2 - \lambda_1^*)]^2 + \lambda_2 \lambda_1^*} \quad (28)$$

The effective thermal conductivity tensor according to relations (1) and (28) is expressed by the relation

$$\lambda_{eff} = \lambda_{eff} (\vec{i}\vec{i} + \vec{j}\vec{j}) + \lambda_{eff\,along} \vec{k}\vec{k} \quad (29)$$

The above introduced method can be used also for fibres with more layers than one. The application of fibres in composite is the cause of the mechanical reinforcement of composite. But on the other hand due to the difference of the thermal expansibility of fibre and matrix there arises on the boundary between the fibre and matrix a thermal stress which causes the failure in a material. The problem is how aptly to choose the surface layer to prevent the failure in composite material.

References

- [1] Beran M.J, 1974 Application of Statistical Theories for the Determination of Thermal, Electrical and Magnetic Properties of Heterogeneous Materials. *In Composite Materials. Vol. 2.* (New York, Academic Press) p.209

HYGRIC AND THERMAL PROPERTIES OF CEMENTITIOUS COMPOSITES AFTER THERMAL AND MECHANICAL LOAD

Jan Toman¹ and Robert Černý²

¹Department of Physics, Faculty of Civil Engineering, Czech Technical University, Thákurova 7, 166 29 Prague 6, Czech Republic

²Department of Structural Mechanics, Faculty of Civil Engineering, Czech Technical University, Thákurova 7, 166 29 Prague 6, Czech Republic
Email toman@fsv.cvut.cz, cernyr@fsv.cvut.cz

Abstract

Thermal conductivity λ , water vapor permeability δ and liquid moisture diffusivity κ of cement mortar are measured on four types of samples, unloaded, mechanically loaded to 90% of compressive strength, thermally loaded by the 800°C exposure for two hours, and loaded both mechanically and thermally. The values of κ are found to depend on the way of loading in a very significant way, the maximum differences compared to the unloaded samples being as high as 3 orders of magnitude. On the other hand, the values of δ increase by only about 40% compared to the basic unloaded material. The thermal conductivity in the high temperature region is found to be affected by both mechanical and thermal load in a significant way. Two competing mechanisms, namely the increase of the total pore volume and the intensification of convective heat transfer, can result in both positive and negative changes of thermal conductivity compared to the basic samples not exposed to any load.

Key words: thermal conductivity, moisture diffusivity, water vapor permeability, high temperature exposure, mechanical load

1 Introduction

For a long time, hygric and thermal properties of building materials were considered in the form of single room-temperature values. Later, also their dependence on temperature and moisture content was taken into account. However, some weakly studied areas remained until now. One of them is the influence of mechanical load on the hygric and thermal properties of materials used for load bearing structures which are often a part of building envelope. Another one is the influence of high temperatures both at the moment of their application and after thermal load removal which is an interesting topic for instance in fire engineering. In this paper, the effect of mechanical and thermal load on the thermal conductivity, moisture diffusivity and water vapor permeability of cement mortar is studied.

2 Methods for measuring the hygric and thermal properties

For the determination of moisture diffusivity κ we employed a simple method based on the assumption that κ can be considered as piecewise constant with respect to the moisture density [1]. The measuring method for determination of the water vapor permeability δ is described in [2], in more details. The measuring apparatus consists of two airtight glass chambers separated by a plate-type specimen of the measured material. In the first chamber, a state near to 100% relative humidity is kept (achieved with the help of a cup of water), while in the second one there is a state close to 0% relative humidity (set up using some absorption material, such as silica gel). The changes in the mass of water in the cup, Δm_w , and of the silica gel, Δm_a , are measured in dependence on time. For high temperature measurements of thermal conductivity, we used a double integration method based on the analysis of the temperature field [3].

3 Material samples

In the experimental measurements, we studied the samples of cement mortar as a typical representant of cement composites. The composition for one charge was the following: Portland cement ENV 197 - 1 CEM I 42.5 R (Kraluv Dvur, CZ) - 450 g, natural quartz sand with continuous granulometry I, II, III (the total screen residue on 1.6 mm 2%, on 1.0 mm 35%, on 0.50 mm 66%, on 0.16 mm 85%, on 0.08 mm 99.3%) - 1350 g, water - 225 g.

The mortar was prepared by mixing and compacting using mixing machine and vibrator. The samples for measurements of hygric parameters had a cylindrical shape, with the diameter of 105 mm and the height of 20 mm.

The samples were left in moulds for the first 24 hours in a high relative humidity environment under wetted cloth. After mould removal, the time remaining to 28 days spent the samples in 20°C water and then they were put in protected external environment (a metal-sheet shed) with the relative humidity approximately 65%. After 28 days, the compressive strength was determined on selected samples (57.4 MPa). The density of dry material was found to be 2130 kg/m³, the moisture content at saturation 8%kg/kg.

4 Experimental results

In the experimental measurements of hygric parameters, four deferent types of specimens of cement mortar were analyzed:

- 1) specimen not exposed to any load (we will denote it NL in what follows),
- 2) specimen exposed to a gradual temperature increase up to 800°C during two hours and then left for another 2 hours at 800°C but without previous mechanical load (TL),
- 3) specimen exposed to mechanical load of 90% of compressive strength but without thermal load (ML),
- 4) specimen exposed first to mechanical load of 90% of compressive strength, then to a gradual temperature increase up to 800 °C during two hours and finally left for another 2 hours at 800°C (MTL). Always three samples of each type were tested.

Table 1 Hygric parameters of cement mortar

Sample	$\kappa(\text{m}^2\text{s}^{-1})$	$\delta(\text{s})$
NL	$9,7 \cdot 10^{-9}$	$3,34 \cdot 10^{-12}$
ML	$9,0 \cdot 10^{-8}$	$3,18 \cdot 10^{-12}$
TL	$1,0 \cdot 10^{-5}$	$4,03 \cdot 10^{-12}$
MTL	$1,3 \cdot 10^{-6}$	$4,56 \cdot 10^{-12}$

The experimental results of measurements of hygric parameters are summarized in Table 1. Apparently, the influences of thermal and mechanical load were more pronounced for moisture diffusivity κ than for water vapor permeability δ . While the values of δ increased only by 40% in maximum, the values of κ increased up to 3 orders of magnitude.

The effect of mechanical load was significant for κ only where it has led to about one order of magnitude increase, the differences between NL and ML in δ were within the errorbar of experimental measurements. The thermal load appeared as the most important factor affecting the values of κ , and resulted in about 3 orders of magnitude difference compared to NL. On the other hand, the influence of thermal load on δ was relatively small, only about 20% increase was observed in comparison to NL samples. The effect of the combination of mechanical and thermal load was for κ less significant than that of thermal load but more important than mechanical load itself, the observed increase in κ was about 2 orders of magnitude. The 10% increase of δ for MTL compared to TL is somewhere on the edge of the errorbar of the experimental method for δ determination, therefore we cannot be sure whether this difference is really significant.

In the high temperature measurements of thermal conductivity, six different types of specimens of cement mortar (five specimens in each group) were analyzed: 1) specimen not exposed to any load (we will denote it NL in what follows), 2) specimen exposed to a gradual temperature increase up to 800°C during two hours and then left for another 2 hours at 800°C but without previous mechanical load (TL), 3) specimen exposed suddenly to the temperature of 800°C (i.e. to a thermal shock) and then left for 2 hours at that temperature, again without previous mechanical loading (TSL), 4) specimen exposed to mechanical load of 90% of compressive strength but without thermal load (ML), 5) specimen exposed first to mechanical load of 90% of compressive strength, then to a gradual temperature increase up to 800°C during two hours and finally left for another 2 hours at 800°C (MTL), 6) specimen exposed first to mechanical load of 90% of compressive strength, then suddenly to the temperature of 800°C (i.e. to a thermal shock) and finally left for 2 hours at that temperature (MTSL).

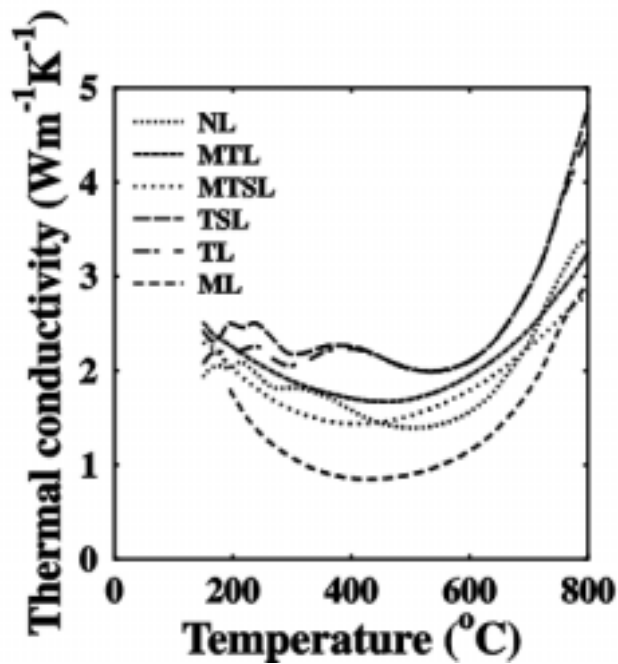


Fig. 1 Thermal conductivity vs. temperature relation of cement mortar, depending on the thermal and mechanical load

In Fig. 1, three groups of $\lambda(T)$ curves can be distinguished. Highest λ values achieved the TL and TSL samples, the lowest values exhibited ML samples, and the remaining MTL, MTSL and NL samples formed a third group in between. As the measured results have shown a reproducibility better than 10% which can be considered as very good, only characteristic results were chosen for the presentation in Fig. 1. According to the analysis which was done before [3], the overall accuracy of the determination of the thermal conductivity using the double integration method is $\pm 15\%$. The differences between the particular specimens within each group were smaller than those between the groups, therefore it can be concluded that the differences between the groups are outside the errorbar of our measurements.

5 Discussion

In order to analyze the reasons for the remarkable changes in the hygric and thermal parameters induced by the mechanical and thermal load we used scanning electron microscopy (SEM) and mercury porosimetry (MP).

Scanning electron microscope Jeol JXA-733 was employed to study the structural changes in the surface region of the samples induced by the thermal and mechanical load. A typical sample mechanically loaded to 90% of compressive strength exhibited cracks approximately 1-2 μm wide. A similar view we could see for images of thermally loaded samples, only the cracks were wider, up to 5 μm .

Porosimetric measurements were performed using the mercury porosimeter AutoPore 200 - Micromeritics on four types of specimens, NL, ML, MTL, TL, using the notation introduced before. Only minor changes in global parameters appeared,

when mechanical load was applied, for instance the total intrusion volume V_p increased only by 10% and the median pore radius by volume r_v by 30% compared to the reference specimen NL. On the other hand, thermal load exhibited much more pronounced effects. The median pore radius increased 17 times compared to the reference specimen NL, V_p increased by almost 100% and even ρ decreased by 10%. The combination of mechanical and thermal load (MTL) has led to very similar results as in the case when only thermal load (TL) was applied, V_p was almost the same (i.e., within the errorbar of experimental measurements). However, the median pore radius for MTL decreased two and a half times compared to TL and the total pore area increased almost two times. A comparison of differential distribution functions of the pore volume by pore radius for the studied specimens has shown that mechanical load (ML) has led to certain increase of pore volume in the region $0.3 \mu\text{m} - 2 \mu\text{m}$ compared to the reference specimen NL. This is in a qualitative agreement with the results of scanning electron microscopy measurements which revealed for ML specimens an appearance of not very numerous cracks $1-2 \mu\text{m}$ in width. The thermally loaded specimen TL exhibited a very significant increase of pore volume in the region $0.1 \mu\text{m} - 5 \mu\text{m}$ compared to NL but a similarly high decrease was observed in the region of smaller pores, $r < 0,1\mu\text{m}$. The combination of thermal and mechanical load (MTL) resulted in significantly higher volume of smaller pores with $r < 0,1\mu\text{m}$ compared to TL but still lower than for NL, the amount of bigger pores was for MTL very similar to TL. The increase of amount of bigger pores in the μm region for thermally loaded specimens was in a qualitative agreement with our observations and SEM measurements, we could see numerous visible cracks in the material after being heated to 800°C and cooled again.

6 Conclusions

Both mechanical load of 90% of the compressive strength, and the thermal load of 800°C exposure for 2 hours, and their combination as well, were found to be very significant factors affecting the moisture diffusivity κ and thermal conductivity λ . The main reason for the observed differences in the values of κ and λ for the samples loaded in deferent ways was probably the appearance of cracks up to $5\mu\text{m}$ wide which were mostly well visible. In the case of thermal conductivity, the most probable reason for both positive and negative changes compared to the basic samples not exposed to any load were two competing mechanisms, namely the increase of the total pore volume and the intensification of convective heat transfer. On the other and, the values of water vapor permeability δ were affected in much smaller extent than the changes of κ what is related to the fact that water vapor transfer in concrete is much easier than water transfer in normal conditions.

Acknowledgement

This paper is based upon work supported by the Grant Agency of the Czech Republic, under grant # 103/00/0021.

References

- [1] Černý, R., Drchalová, J., 1995. Measuring the Moisture Diffusivity of Board Materials. *Proc. of International Symposium on Moisture Problems in Building Walls*, V.P. de Freitas, V. Abrantes (eds.), pp. 147-156, Univ. of Porto.
- [2] Černý, R., Hošková, Š., Toman, J., 1995. A Transient Method for Measuring the Water Vapor Diffusion in Porous Building Materials. *Proc. of International Symposium on Moisture Problems in Building Walls*, V.P. de Freitas, V. Abrantes (eds.), pp. 137-146, Univ. of Porto.
- [3] Černý, R., Toman, J., 1995. Determination of Temperature- and Moisture-Dependent Thermal Conductivity by Solving the Inverse Problem of Heat Conduction. *Proc. of international Symposium on Moisture Problems in Building Walls*, V.P. de Freitas, V. Abrantes (eds.), Univ. of Porto, pp. 299-308.

FRIGICHIPS TESTING FOR THE HEAT FLOW MEASUREMENTS

Vladimír Bahýl, Štefan Dubnička

Department of Physics and Applied Mechanics, Technical University in Zvolen, T.G.
Masaryka 24, SK-960 53 Zvolen, Slovakia
Email: bahyl@vsld.tuzvo.sk, pistad@pobox.sk

Abstract

There are presented our results with the frigichip Melcor Cp 1-127-05L as the heat flow measuring sensor. The results are very promising for the possible future industrial applications.

The value of the thermal conductivity coefficient is crucial in these measurements. So great amount of work is devoted to its determination. The obtained results are discussed and compared. We have studied the problem of the frigichip efficiency as a heat power machine too. These results are compared with the theoretical ones.

Key words: heat flow measurement, frigichips, thermal conductivity

1 Introduction

The saved up energy is the cheapest energy. To be able to save up the energy, we should be able to measure its used amount. In some special cases it is not very difficult. But in the case of the thermal energy there are many problems associated especially with the heat losses in the parts of the measuring instrument. The heat is everywhere around us. Further as we see the problem of the saving up the thermal energy as the problem for the next century, we decided to realise the measuring device which will be able to give us not only the precise values but the real time values too. And not in the steady state only.

Of course, today, there is possible to buy a huge variety of devices which are able to measure the heat flow. At least they are putting on the appearance of such kind of measurements. With respect to the physical principles of the measurements they are usually a cat in a sac for the end user. We not only strongly disagree with this, but also we wish to go further. We wish to see inside the physical principles of such a device and we wish to be able to use these principles in our scientific goals and to be able technically to improve such kind of a device. Therefore we decided to realise our own research and our own development. We have chosen the frigichips as the base of our effort.

In our research we have obtained some very considerable results. See for example Bahýl and Marčok 1995, Kotrik 1997 and Dubnička 1999. Of course we are not the first who intend to use the frigichip as the heat flow measuring device. See for example the paper of Dittmann and Schneider 1992. Even iff this paper is not physically quite clear it has encouraged us in our research to develop high quality, easy operate and cheap device for the heat flow measurements.

We think that our present paper is also one small step toward this goal too. Mainly if we can see the prevalent interest to use the Peltier and Seebeck phenomenon predominantly in the temperature control systems. As the problems of the so called thermoelectrical converters is well described in the paper Heřman et al. 1984 we give here the basic design of the thermocouple, the ground element of the thermoelectrical converter device.

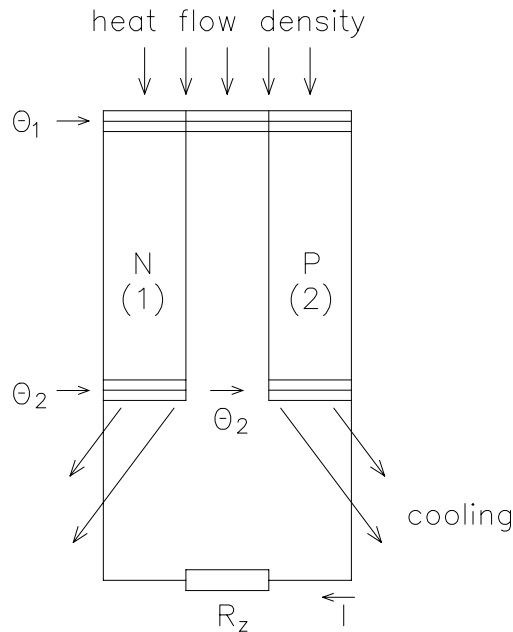


Figure 1. The basic design of the thermocouple

The Peltier and Seebeck phenomena we will not describe here as they are well described in any better physical textbook.

2 Experiments

We have realised the set of experiments in our laboratories in which we have been concentrated on the problem of calibration of our converters i.e. we should determine the function $\bar{q} = f(P)$, where P is the power of the generated electric current. We have devoted great amount of interest to determination of the efficiency of the frighichip as a hot engine. I.e. we paid our attention to the quite opposite event of the frighichip as it is in common use we decided experimentally determine the value of the efficiency

$$\eta = \frac{R \cdot I^2}{Q}$$

generated with the heat Q .

All our experiments we have realised in the steady state conditions and we have used quite classical experimental arrangement. The basic sketch of our experimental device arrangement is given on the figure 2. The heat flow lone have been represented with the set of aluminium joists between which there have been placed the frighichips and the control thermocouples. The calorimeter loaded with melting ice has been used as a heat sink.

The temperatures have been measured in 8 different places. This enables us to determine the heat flow losses in the different Al joists on the way of heat from the room conditions to the heat sink in the calorimeter. For the reference temperature point we have used the calorimeter with zero Celsius degree.

Our measuring device is connected with the personal computer and it is full automated. The measured values have been gathered in every 30 seconds. The scheme of our computer aided working place is in the figure 3. The scheme of the Peltier element circuit is in the figure 4.

The determination of the value of the loading resistor has been very important task of our work. The results of our measurements are given in the figure 5. It is easy to see that we get the maximal performance of our “converters” we got for the loading resistor $R_{LR} = 3.9\Omega$. The resistance of ampermeter is $R_A = 10.5\Omega$. In common we get $R = 14.4\Omega$. As we can see from the figure 5, the dependence of the Peltier element performance on the loading resistor has well defined maximum.

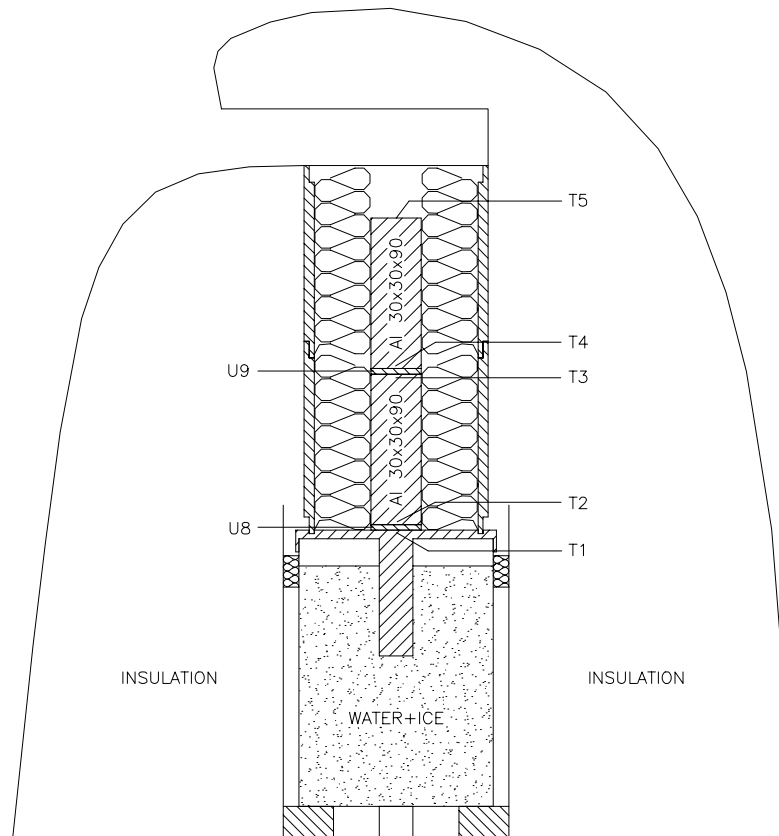


Figure 2. The measuring device scheme with the heat flow line.

Figure 3. The scheme of the data gathering computer aided system.

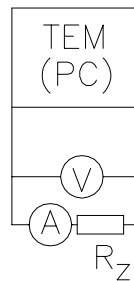
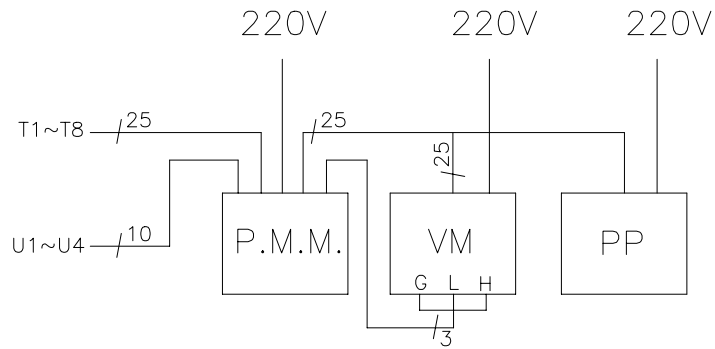


Figure 4. The Peltier element circuit connection.

Toward fig. 3:

T1~T2 – thermoelements

U1~U4 – terminal on measurement of the voltage

P.M.M – switch of the measuring spoil

VM – voltmeter

PP – personal computer

Toward fig. 4:

TEM(PC) – thermoelectric changer
- Peltier element

V – voltmeter

A – ampere-meter

Rz – loading resistance

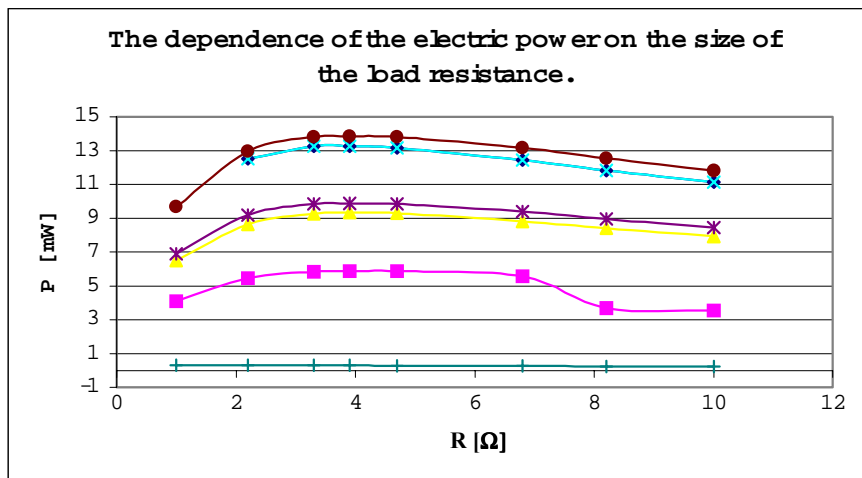


Figure 5. The diagram of the electric power dependence upon the loading resistance.

3 Results

We have realised 12 independent experiments in which we have been looking for the dependence of the performance of the studied Peltier element (PE) upon the heat flowing through it.

As it is in the common use first we have determined the function $U = f(\Delta t)$ in which U is the PE voltage and Δt is the temperature difference between the PE plates. We have obtained the equation

$$U = (0.022 \pm 0.006) \cdot \Delta t + (0.0036 \pm 0.0137) [V] \quad (1)$$

The results from the experiment No. 6 are given in the figure 6.

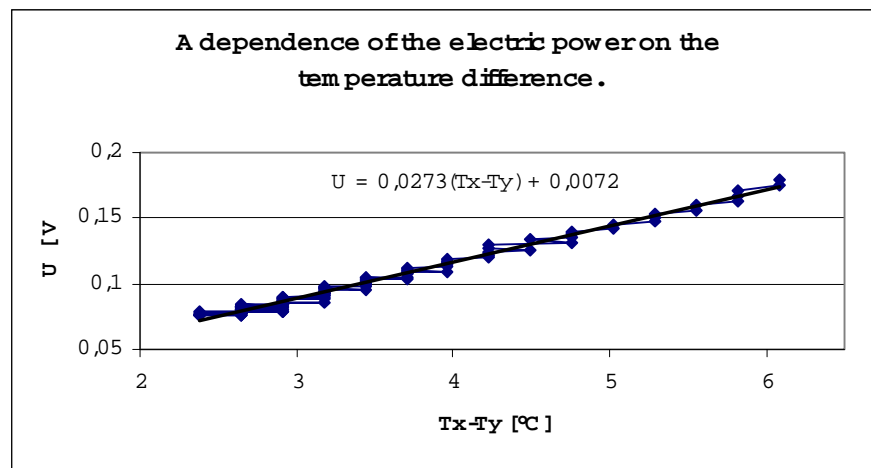


Figure 6. The voltage – temperature difference dependence for the studied PE.

As the q value in the regression equation (1) equals 0.0036 ± 0.0137 and from this we can conclude that this value is statistically equal to zero we can take our results as the precise one. (The value of q should be zero from the theoretical point of view.)

The next proof of our preciseness we can get from the thermal conductivity coefficient λ . According to our computations and measurements we have obtained the value

$$\lambda_{PE} = 1.99 \pm 0.65 [Wm^{-1} \cdot K^{-1}] \quad (2)$$

As it is impossible to find this value in the scientific papers, we ask for it the Melcor Peltier Corporation directly. Via E-mail we have obtained the next form

$$k = (k_0 + k_1 * T_{AVE} + k_2 * T_{AVE}^2) \cdot 10^{-6} [Wcm^{-1} \cdot K^{-1}], \quad (3)$$

where : $k_0 = 62605.0; k_1 = -277.7; k_2 = 0.4131; T_{AVE} = 0.5 * (T_{HOT} - T_{COLD})$

After substitution of our measured values into the form (3) we obtained

$$\lambda_{PE}^{MPC} = 1.712 \pm 0.003 [Wm^{-1} \cdot K^{-1}] \quad (4)$$

We take this as very well agreement with our measurements and as the direct proof of our correctness.

The efficiency of the PE is in comparison with their efficiency in the cooling systems very low. In the conditions of the loading resistance 14.4Ω we have obtained the next value

$$\eta_{PE} = 93.5 \cdot 10^{-5} \pm 43.1 \cdot 10^{-5} . \quad (5)$$

This value we do not think as a definite one, because of the fact that from our theoretical computations in accordance with Heřmann at all. 1984 we obtained the value

$$\eta_{OPT} = 613 \cdot 10^{-5} \pm 249 \cdot 10^{-5} . \quad (6)$$

Our experimental device did not allowed us to measure under the conditions of rather great amount of the heat flow. So we decided to install our measuring device into the wood drying kiln. Our results are depicted in the figure 7. We can conclude that the electric power performance of the PE is the linear function of the heat flow through the Peltier element.

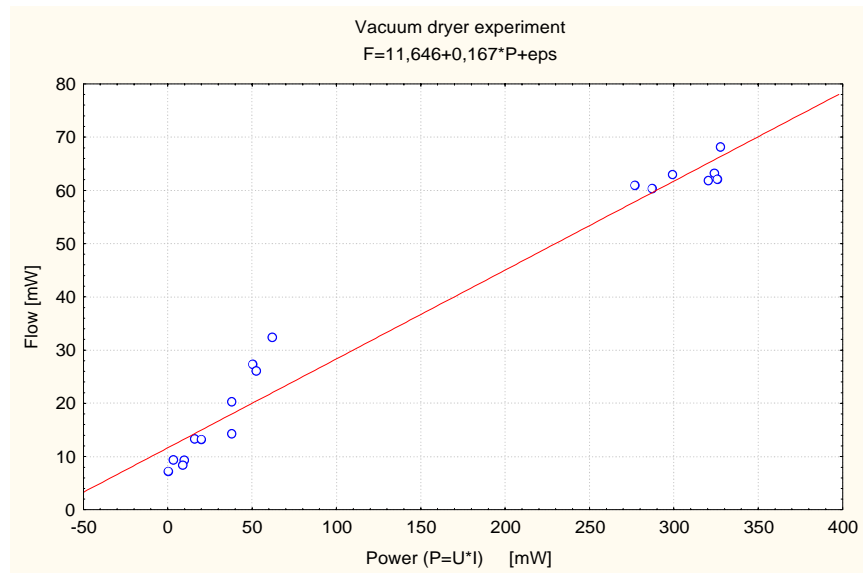


Figure 7. The peltier element performance for the large size of the heat flow values.

Of course we should to take these our results as a preliminary one because of rather great dispersion of the measurements.

4 Discussion

As it has been mentioned in the beginning of the present paper we are dealing with the possibility to use the PE as the direct heat flow measuring device rather long time. It is quite sure that PE is possible to use as the basic element in the heat flow measuring device. We think that it will not take a long time till we will be able to meet it in the technical practice. More we regard them much more precise as the classical ones, fore example the Schmidt carpets. So if we wish fully utilise their sensitivity, we need more

precise experimental device and we should to realise more experiments. But the till now done serve as the clear proof that we are on the true way.

From the point of view of the practice it is important to solve the question of the so called self calibrating system for the PE connected as the heat flow measuring device i. e. in the sense of the Seebeck phenomenon. Normally the PE is used as the heat source or sink part of many modern systems i. e. in the sense of the Peltier phenomenon. The calibrating of the heat flow measuring PE is possible in the obvious way, by usage of the well heat conducting externally heated thin plates. We suppose that such an arrangement will allow us to determine the straight line from the figure 7 in much more uniformly distributed data.

The thermal contact of the PE with the measured object plays very important role in the heat flow measurements. Other way we can introduce rather large systematic errors in the results. So it is inevitable to use the thin layer of the thermopast to be sure that the thermal contact are well. Of course such kind of past have been used in our experiments too.

Acknowledgement

This paper has been done under the support of the Scientific and technical project No. VTP 2903 which is highly appreciated by the authors.

References

- [1] Bahýl V, Marčok M, 1995 The thermal conductivity of the frigichips for using in the heat flow measurements in the vacuum drier. In: Vacuum Drying of Wood '95, Slovak Republik, High Tatras, October 8. - 12. 1995, TU Zvolen, 1995, s. 84 - 93
- [2] Kotrík E, 1997 The Utilization of Frigichips for Measurement of Heat Flows and Thermophysical Characteristics of Materials and Constructions. In Zborník 7. International conference, 5. Section, Budova a energia 2., Košice 6. - 8.5.1997, SF TU Košice, 1997, 175 - 181.
- [3] Dubnička Š, 1999 The Heat Flow Measurement by the Usage of the Peltier Elements, in Proc. "Nové smery vo výrobných technológiách 2000", 15. – 16. jún 2000, Prešov
- [4] Dittmann H, Schneider V. B, 1992 Ein Meßgerät für den Wärmestrom. Physik und Didaktik, 3, 319 – 324.
- [5] Heřman J at all., 1984 Příručka silnoprúdej elektroniky, Praha SNTL 780 p.

MEASUREMENT OF THE THERMAL CONDUCTIVITY OF THE AIR PERMEABLE INSULATION MATERIAL IN A HORIZONTAL GUARDED HOT PLATE APPARATUS

Peter Matiašovský, Oľga Koronthályová

Department of Building Physics, Institute of Construction and Architecture, Slovak Academy of Sciences, Dúbravská cesta 9, 842 20 Bratislava, Slovakia
E-mail: usarmat@savba.sk, usarkoro@savba.sk

Abstract

The apparent thermal conductivity of the lightweight fibrous insulation materials comprehends intensive radiative heat transfer. Under certain boundary conditions also natural convection can play the role. The results of apparent thermal conductivity measurement of the low density mineral wool confirmed the presence of convection at the Rayleigh values significantly lower than 40. This fact was caused by the permeable boundary conditions during the experiment.

Key words: thermal conductivity, natural convection, long-wave radiation, fibrous insulation material, heat and air transfer

1 Introduction

In fibrous insulation materials three modes of heat transfer can be distinguished: conduction, longwave radiation and convection. In the low density fibrous insulating materials the heat transfer by longwave radiation and natural convection can play significant role at certain boundary conditions. For such a cases the apparent thermal conductivity of the material (comprehending longwave radiation, conduction and natural convection) varies with the temperature of the material as well as with the boundary conditions. With the aim to analyse mutual interaction between particular heat transfer modes the measurements of the heat flows and temperatures in horizontal lightweight mineral wool insulation layer were made.

2 Experimental results

The mineral wool used in the experiment had the density $\rho = 9,8 \text{ kg/m}^3$, the porosity $\psi = 0,996$ and the mean fibre diameter $D = 5 \cdot 10^{-6} \text{ m}$. The measurements were done in the guarded hot plate apparatus with horizontal plates and upwardly oriented heat flow (Fig. 1). The sample consisted of mineral wool flocks layer filled in the test frame with internal dimensions of $0,5 \times 0,5 \text{ m}$. The height of the frame 0.1 m has determined thickness of the sample. Two sets of the measurements were done. With the aim to evaluate the temperature dependence of the thermal conductivity due to longwave

radiation in the actual experimental conditions, the effective thermal conductivity of mineral wool was determined for variable mean temperatures at small surface temperature differences (from 3,74 to 4,34° C) in the first set of the measurements. The results are shown in Fig. 2.

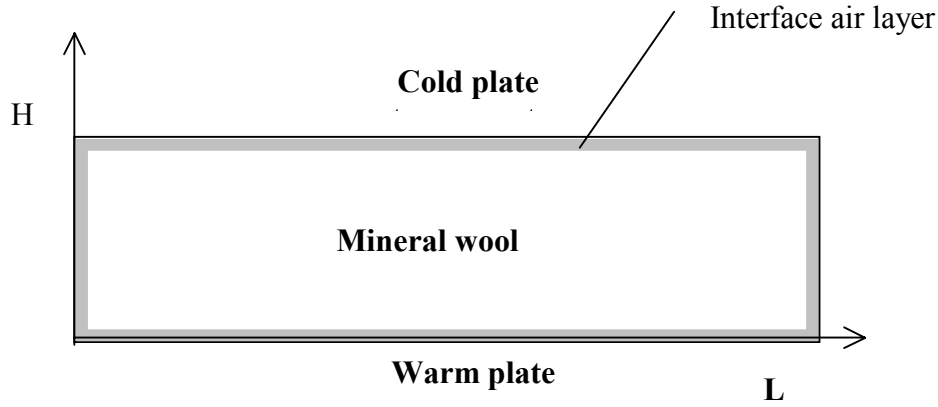


Fig 1 The schematic description of the measurement

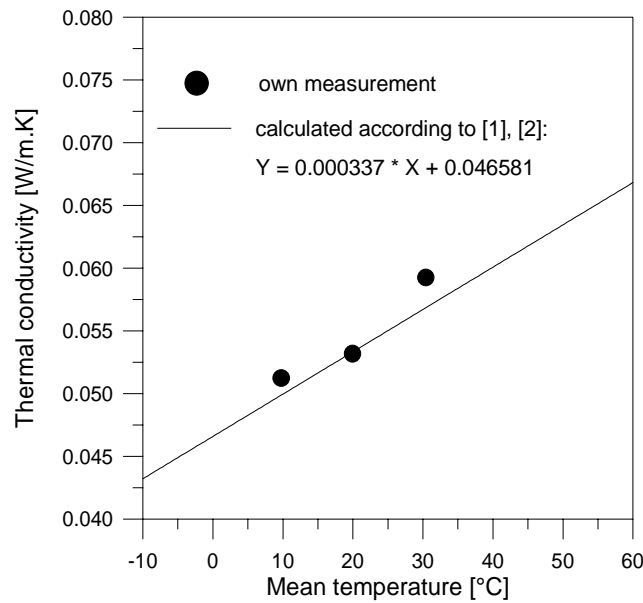


Fig 2 The dependence of the measured thermal conductivity of the mineral wool on its average temperature compared with the theoretical relation according to [1], [2].

The second set of the measurements has been done at variable surface temperature differences (from 5 to 60 °C) and the same mean temperature of the sample (20°C) simultaneously. The results of these measurements are shown in Fig. 3. The measurements confirmed significant dependence of the measured thermal conductivity on the mean temperature of the sample as well as the dependence of the thermal conductivity on the surface temperature difference.

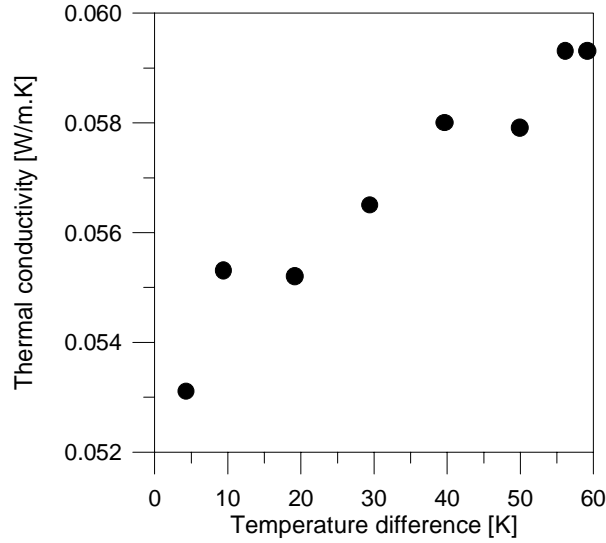


Fig 3 The thermal conductivity of the mineral wool measured for various surface temperature differences

3 Total heat transfer in fibrous materials

3.1 Effective thermal conductivity

In the fibrous materials different types of heat transfer are present: conduction in solid phase constituting the insulation, radiation in the material and heat transfer in gas confined the insulation. The total effective thermal conductivity of a fibrous material may be expressed as:

$$\lambda_{\text{eff}} = \lambda_G + \lambda_F + \lambda_R \quad (1)$$

where λ_G is the effective thermal conductivity due to conduction in gas which results from direct thermal conduction in the gas and conduction in gas and fibres alternatingly. The effective thermal conductivity due to conduction in solids λ_F results from direct conduction in fibers and fiber contacts. The influence of radiation on the effective thermal conductivity of the fibrous material is denoted by λ_R [1].

The effective thermal conductivity (conductive and radiative heat transfer) dependence on temperature “t” can be expressed by the linear relation:

$$\lambda_{\text{eff}} = a + b \cdot t \quad (2)$$

where a and b are the regression coefficients obtained from the measurements (Fig. 2).

3.2 Apparent thermal conductivity

Natural convection in horizontal porous materials occurs if the lower boundary temperature is higher than the upper boundary temperature. The air is stable when the upper surface has a higher temperature than the lower surface. The heat transfer in a fibrous material is described by the following non-dimensional parameters: Modified Rayleigh number:

$$Ra = \rho \cdot c \cdot g \cdot \beta \cdot B_o \cdot H \cdot (t_w - t_c) / (\eta \cdot \lambda_{\text{eff}}) \quad (3)$$

where $\rho(t)$ is density of air [kg/m^3], c is specific heat of air [J/kg.K], g is gravitational acceleration [m/s^2], β is coefficient of thermal expansion [$1/\text{K}$], B_0 is permeability [m^2], H is thickness [m], $\eta(t)$ is dynamic viscosity of air [Pa.s], t_w , t_c are temperatures of the warm and cold surface respectively [$^\circ\text{C}$], $\lambda_{\text{eff}}(t)$ is effective thermal conductivity [W/m.K] and Nusselt Number:

$$Nu = \lambda_{\text{ap}}/\lambda_{\text{eff}} \quad (4)$$

where $\lambda_{\text{ap}}(t)$ is apparent thermal conductivity at the presence of natural convection [W/m.K].

The relation between Nusselt and Rayleigh numbers can be expressed as follows:

$$Nu=f(Ra, \text{ geometry, boundary conditions}) \quad (5)$$

A critical porous Rayleigh number is found when significant natural convection occurs ($Nu > 1$). This number was found to be 40 for a impermeable upper boundary while it decreases to approximately 20 for a porous layer with a permeable upper surface. In the case of upper and lower permeable boundaries or non-isothermal boundaries Ra can reach the values higher than zero (Tab.1) [3] .

Table 1. Values of the critical Rayleigh number for various boundary conditions [3]

lower boundary	upper boundary	lower boundary	upper boundary	Ra_{critical}
impermeable	impermeable	conducting	conducting	39.48
impermeable	impermeable	conducting	insulating	27.10
impermeable	impermeable	insulating	insulating	12
impermeable	free	conducting	conducting	27.10
impermeable	free	insulating	conducting	17.65
impermeable	free	conducting	insulating	9.87
impermeable	free	insulating	insulating	3
free	free	conducting	conducting	12
free	free	conducting	insulating	3
free	free	insulating	insulating	0

4 Discussion

The estimated increase of the effective thermal conductivity with the average temperature (Fig. 2) caused by longwave radiation is in the agreement with calculation according to the model of the heat transfer in fibrous material [1], [2].

The increase of the apparent thermal conductivity caused by the increase of the surface temperature difference begins already at low temperature differences. The effect of the natural convection expressed by the relation between Nusselt number and modified Rayleigh number occurs already at $Ra = 3$ which is the value significantly lower than the critical value 40 for impermeable upper boundary or 20 for permeable upper boundary. The obtained value of critical Rayleigh number corresponds to the boundary conditions defined by both upper and lower permeable boundaries (Tab. 1). The results of the measurements were compared with the results of the measurements by

[4] for fibrous insulation material with comparable properties and under the same boundary conditions and are presented in Fig. 4.

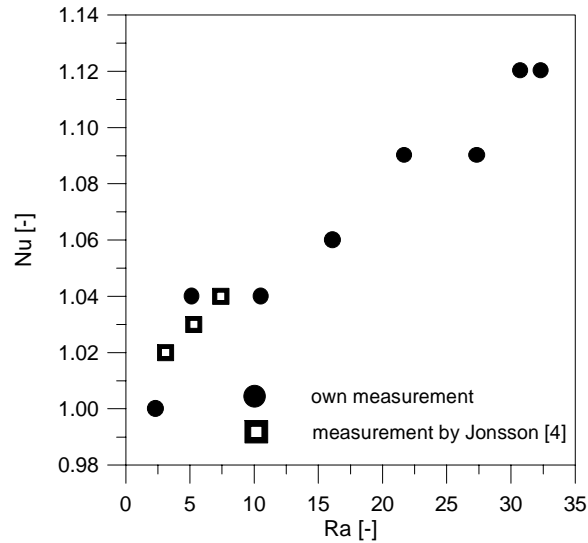


Fig 4 Measured values of Nusselt number versus modified Rayleigh number

The explanation of the existence of the permeable boundaries in the case of the lightweight loose-fill mineral wool follows from the character of its structure. The maximum known permeability of the mineral wools of the density lower than 10 kg/m^3 - adequate to the density of the analysed sample is $1.0 - 1.5 \cdot 10^{-8} \text{ m}^2$ (Fig. 5). The material of the analysed sample consisted of the mineral wool flocks filled in the frame and the permeability of the material varied spatially from the lower permeabilities of the particular flocks to higher permeabilities of the contacts between them. Similarly also the contact between the material and the surrounding plates was not perfect. Continual interface layer with higher permeability was between the sample and the plates of the measuring apparatus (Fig. 1). Further due to its compressibility the material has tendency of settling with subsequent increase of thin continuous air layer between the measuring plate and the upper sample boundary. In this context the increase of the apparent thermal conductivity with temperature difference caused by natural convection in the low density fibrous material is explainable by imperfect contact between the insulation and the impermeable boundaries (Fig. 1). The actual Nu versus Ra values depend on the actual permeable material properties, its geometry and the boundary conditions in an experimental device. The results of the measurements in horizontally oriented mineral wool layer with density below 10 kg/m^3 agree with the measurements of the other authors and confirm that natural convection can occur already at $Ra = 3$.

5 Conclusion

The measurements of the heat transfer in horizontally oriented low density mineral wool plate have been done. The measurements were carried out in order to assess two different relations: the temperature dependence of effective thermal conductivity (heat transfer without natural convection) and the temperature difference dependence of apparent thermal conductivity (heat transfer with natural convection). Due to specific character of their structure only permeable boundaries are characteristic for lightweight mineral wool

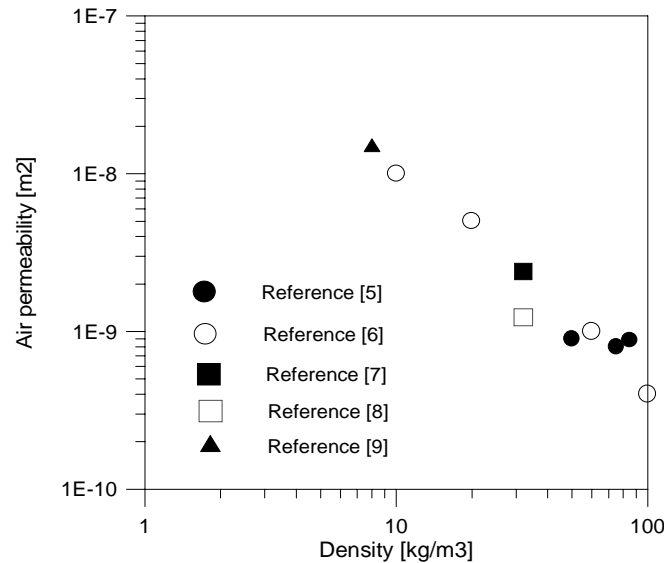


Fig 5 Experimental permeability coefficients of inorganic fibrous insulation materials insulation layers. The assessment of heat transfer by the values of Nusselt number has confirmed the occurrence of natural convection already at the Rayleigh values higher than zero.

Acknowledgement

Authors are grateful to VEGA (Grant No 2/5105/20) for the supporting of this work.

References

- [1] Bankvall, C.G. 1972. *Heat transfer in fibrous materials*. National Swedish Building Research , rapport D4:1972.
- [2] Klarsfeld, S. 1980. La conductivité des isolants fibreux en fonction de leur structure. *Cahiers du CSTB* . N° 213. pp 38-50.
- [3] Serkitjjs, M. 1995. *Natural convection heat transfer in a horizontal thermal insulation layer underlying an air layer*. PhD. Thesis. Chalmers University of Technology, Goteborg.
- [4] Jonsson, B. 1993. *Measurement of the thermal resistance of loose-fill insulation*. In: *Proceedings of the 3rd symposium Building physics in the Nordic countries* (Bjarne Saxhof, editor) . Copenhagen. pp 171- 180.
- [5] Mrlík, F. 1990. *Improvement of building performance by building physics methods*. Scientific report II-8-4/06. VÚPS Praha, Zlín. (In Czech).
- [6] Kronvall, J. 1980. *Air flows in building components*. Report TUBH-1002. Lund Institute of Technology.
- [7] Bankvall, C.G. 1972. *Natural convective heat transfer in insulated structures*. Report 38. Division of Building and Technology, Lund Institute of Technology.
- [8] Økland, Ø. 1998. *Convection in highly-insulated building structures*. PhD thesis. NTNC Trondheim.
- [9] Langlais, C., Arquis, E., McCaa, D. J. 1990. *A theoretical and experimental study of convective effects in loose-fill thermal insulation*. ASTM STP 1030. pp.290-318.

TRANSIENT METHODS FOR THE MEASUREMENT OF THERMOPHYSICAL PROPERTIES

Eudovít Kubičár, Vlastimil Boháč

Institute of Physics, Slovak Academy of Sciences, Dúbravská cesta 9, 842 20 Bratislava, Slovakia
E-mail: kubicar@savba.sk

Abstract

The presented paper is focused on the review of the Transient Methods. Data uncertainty is discussed from the point of view of data consistency relation considering measured, published and recommended data. Theory of the methods, experimental arrangement and the measuring regime considering sensitivity coefficients and correlation of the measured parameters are presented. The results of the intercomparison on PERSPEX using Pulse Transient and Step – Wise Transient are presented. Data uncertainties of thermal conductivity are up to 6 % for Perspex.

Key words: transient method, specific heat, thermal diffusivity, and thermal conductivity

1 Introduction

Transient methods are based on the generation of the dynamic temperature field inside the specimen. The measuring process can be described as follows: The temperature of the specimen is stabilized and uniform. Then a small disturbance in the form of a pulse of heat or a heat flux in the form of a step-wise function is applied to the specimen. A thermometer either unified with the heat source or placed apart from the heat source measures the temperature change (temperature response). From the temperature response to this small disturbance, the thermophysical parameters can be calculated according to the model used. Technically, the dynamic temperature field is generated by the passage of the electric current through a line or a plane electrical resistance. Basic characteristics of the transient methods are the following:

- heat source – sample geometry
- way of generation of the temperature field
- heat source – thermometer configuration
- number of measured thermophysical parameters.

Experimental arrangement corresponding to the described measuring process gives a group of methods that are specified in Table 1 together with the parameters that can be obtained by use of specific method [1].

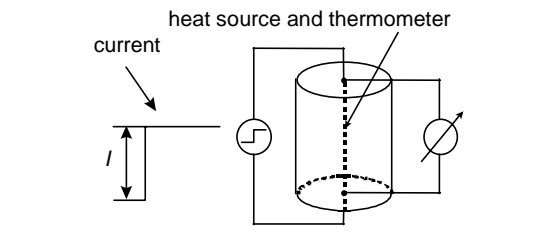
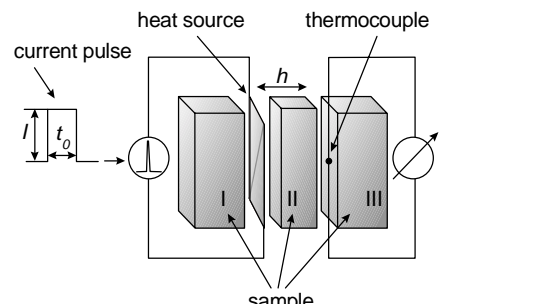
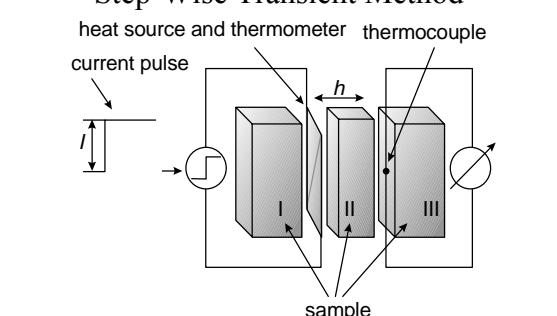
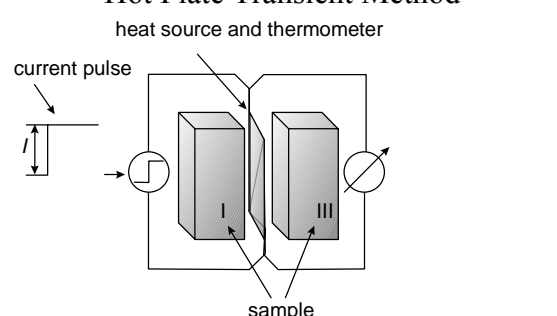
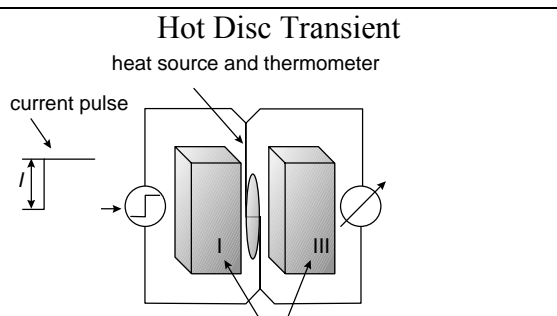
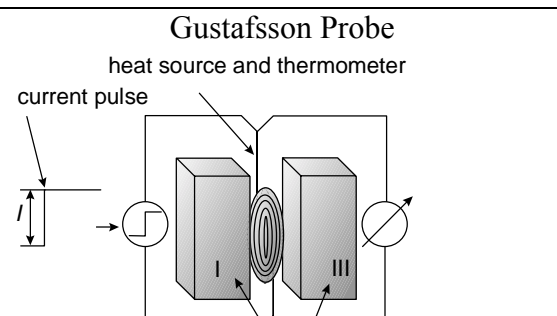
Any transient experiment require the answer to the following questions:

1. How long should be realised the transient?
2. In which time interval of the transient should be applied the evaluation procedure?

3. What size relation of the sample to the heat source – thermometer configuration should be used?

Present contribution discusses measuring regime, theory, experimental arrangement and intercomparison measurements made on PERSPEX by pulse transient [2] and step-wise transient [3] method. The paper should give the answer the above mentioned questions. Pulse transient and step – wise transient methods will be chosen for the analysis and PERSPEX for intercomparison.

Table 1.: Transient methods.

<p style="text-align: center;">Hot Wire Method heat source and thermometer</p>  <p style="text-align: center;">thermal conductivity</p>	<p style="text-align: center;">Pulse Transient Method heat source thermometer</p>  <p style="text-align: center;">specific heat, thermal diffusivity and thermal conductivity</p>
<p style="text-align: center;">Step-Wise Transient Method heat source and thermometer thermocouple</p>  <p style="text-align: center;">specific heat, thermal diffusivity and thermal conductivity</p>	<p style="text-align: center;">Hot Plate Transient Method heat source and thermometer</p>  <p style="text-align: center;">thermal effusivity</p>
<p style="text-align: center;">Hot Disc Transient heat source and thermometer</p>  <p style="text-align: center;">thermal conductivity, thermal diffusivity and specific heat</p>	<p style="text-align: center;">Gustafsson Probe heat source and thermometer</p>  <p style="text-align: center;">thermal conductivity, thermal diffusivity and specific heat</p>

2 Comments on accuracy

Data reliability depends on intercomparison measurements using various methods in different laboratories. Criterion of data reliability is data consistency relation

$$\lambda = ac\rho \quad (1)$$

where c is specific heat, a thermal diffusivity, λ thermal conductivity and ρ is density. Data consistency relation includes thermophysical parameters that are defined in different way considering thermodynamic state. A crucial problem exists regarding data consistency relation when different methods are used. Intercomparison measurements include, usually, various kinds of methods. **General question is what data agreement can be achieved when using different methods.** High precision might be achieved when intercomparison is performed on stable materials where heat transport obeys Fourier law, only. The presented analysis will be performed within the limitation given by Fourier law.

3 Theory of the method

The model of a method is characterized by a temperature function. The temperature function is a solution of the partial differential equation with boundary and initial conditions corresponding to the experimental arrangement. We will concentrate on the pulse transient [2] and step-wise transient [2] methods.

The thermophysical parameters can be found using the temperature function by appropriate fitting technique. The sensitivity coefficients and correlation give measuring time (time during which the temperature response is scanned) and time window in which the evaluation technique can be applied over the temperature response. The sensitivity coefficient [4] is given by $\beta_p = p \frac{\partial T_i(h,t)}{\partial p}$ and correlation [5] by $\gamma(t) = \beta_a / \beta_c$

where p is parameter to be analysed and $T_i(h,t)$ is the temperature function. The calculated temperature functions the corresponding sensitivity coefficients and correlation are shown in Fig. 1 for pulse transient and step wise transient as functions of the Fourier number $F = at/h^2$. Calculations were performed using data for PERSPEX, i.e. thermal diffusivity $a = 0.12 \cdot 10^{-6} \text{ m}^2 \text{ sec}^{-1}$, density $\rho = 1184 \text{ kg m}^{-3}$, specific heat $c_p = 1254 \text{ J kg}^{-1} \text{ K}^{-1}$ and specimen thickness $h = 0.005 \text{ m}$.

Correlation for both started to be serious for Fourier number $F > 2$. Thus measuring time (time during which the temperature response is scanned) should be $F < 2$. Time window for data evaluation should be in the range where sensitivity coefficients have high value and low correlations. For pulse transient method the time window is $0.2 < F < 0.5$ while for step - wise transient it is $0.5 < F < 1.8$.

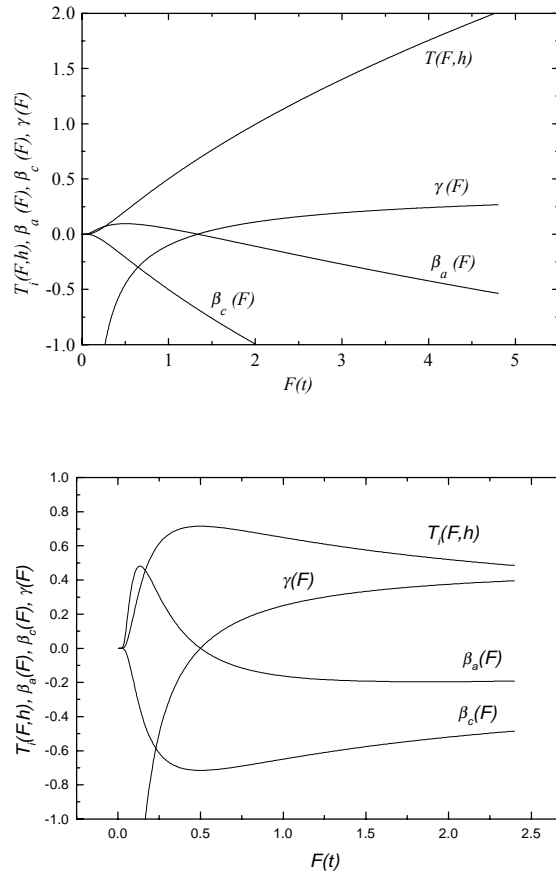


Fig. 1.: Temperature functions $T_i(h,t)$ sensitivity coefficients β_a and β_c and correlation $\gamma(t) = \beta_a / \beta_c$ as functions of the Fourier number $F = at/h^2$ for Pulse Transient (up) and for Step Wise Transient (down). Curves are calculated for PERSPEX.

3.1 Modelling of experiments

Results of difference analysis of theoretical temperature responses give a detailed picture regarding a choice of time windows in which data are evaluated [3]. Difference analysis is based on the fitting of the temperature function over the theoretical points. The points were calculated using, again, the temperature function every 0.2 sec when output was represented by 3 valid numbers for pulse transient and every 0.5 sec when output was represented by 4 valid numbers for step-wise transient methods. A strobe (time interval) of 4 sec for pulse transient and 30 sec for pulse transient was chosen in which the fitting procedure was applied over a part of the theoretical response using, again, temperature function. The strobe was consecutively shifted over theoretical temperature response starting from 0.2 sec up to 400 sec in steps 0.2 sec for pulse transient. Strobe of 30 sec was applied on calculated temperature response shown in Fig. 1 starting from 0.5 sec up to 500 sec in steps 0.5 sec for step – wise transient. Fitted values of specific heat and thermal diffusivity are shown in Table 3 as functions of the Fourier number \bar{F} that corresponds to the mean time of the strobe. Data stability is poor outside the interval $0.4 < \bar{F} < 0.6$ for specific heat and $\bar{F} < 0.4$ for thermal diffusivity

when pulse transient is used. Different picture can be obtained when one uses step-wise transient. Data stability for that case is poor for both specific heat and thermal diffusivity outside the interval $0.9 < \bar{F} < 1.7$.

The temperature response is scanned up to the moment when the correlation of the sensitivity coefficients starts to be high, i.e. up to $\bar{F} \sim 2$. This criterion gives the measuring time and it follows from figure 2. Time window in which the fitting procedure can be applied is $0.4 < \bar{F} < 0.6$ for specific heat and $\bar{F} < 0.4$ for thermal diffusivity when pulse transient is used and for both, i.e. for specific heat and thermal diffusivity within the interval $0.9 < \bar{F} < 1.7$ when step-wise transient is used.

3.2 Ideal model

Temperature functions shown in Fig. 2 that, in fact, are solutions of partial differential equations are valid for ideal model. Clear differences exist between the ideal model and the real one. Table 1 lists differences between the ideal model and the real one and it specifies the criteria that should be experimentally arranged to approach the ideal model. When using real models then temperature functions have a more complicated form. Formally, the difference is expressed in a suitable form of boundary or initial condition. Then the solution corresponding to real experimental setup can be formal rewritten in a form

$$T(x,t) = T_i(x,t) f(x,t, \alpha, \beta, \gamma, \dots) \quad (6)$$

Table 2.: Differences between the ideal and the real models.

Ideal model	Real arrangement	Criteria of reliable data
Non-limited specimen	Limited specimen	Influence of the heat loss from the specimen surface should be limited
Negligible thickness of the heat source	Actual thickness of the heat source	Heat capacity of the heat source should be negligible in comparison to the specimen
Material of the heat source and the specimen are the same	Heat source is made of metal that, usually has different thermophysical parameters as the specimen	
Ideal thermal contact between the heat source and the specimen exists	Non-ideal thermal contact exists between the heat source and the specimen	Thermal contact resistance should be negligible in comparison to the thermal resistance of the specimen
Negligible mass of the thermometer made of the same material as the specimen	Non-negligible mass of the thermometer made of different material as the specimen	Heat capacity of the thermometer should be negligible

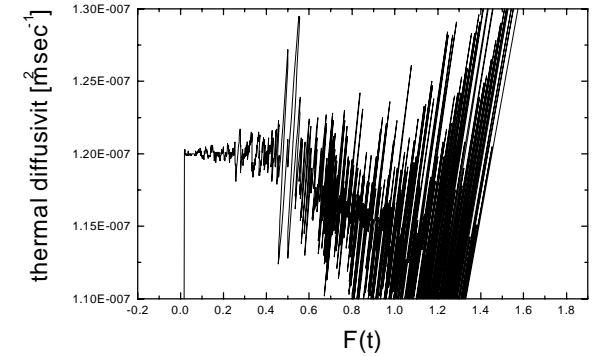
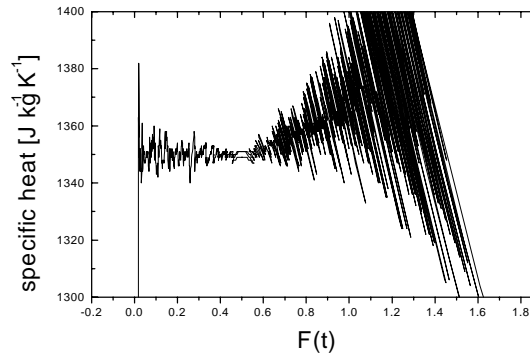
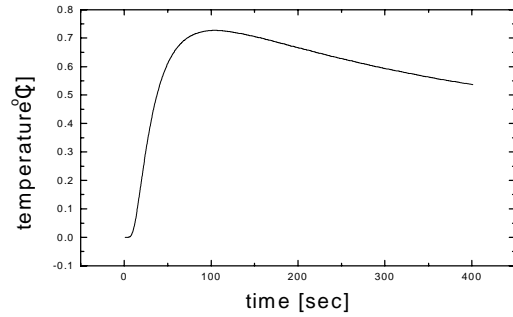
Table 3.: Modeling of experiment. PERSPEX $c = 1350 \text{ J kg}^{-1} \text{ K}^{-1}$, $a = 0.12 \times 10^{-6} \text{ m}^2 \text{ sec}^{-1}$, $r = 1184 \text{ kg m}^{-3}$

Pulse transient

Calculation 1 – 400 sec, step 0.2 sec

$\Delta t = 4 \text{ sec}$, $\Delta F = 0.0192$

Output 3 valid numbers



Step – wise transient

Calculation 1 – 400 sec, step 0.5 sec

$\Delta t = 30 \text{ sec}$, $\Delta F = 0.144$

Output 4 valid numbers

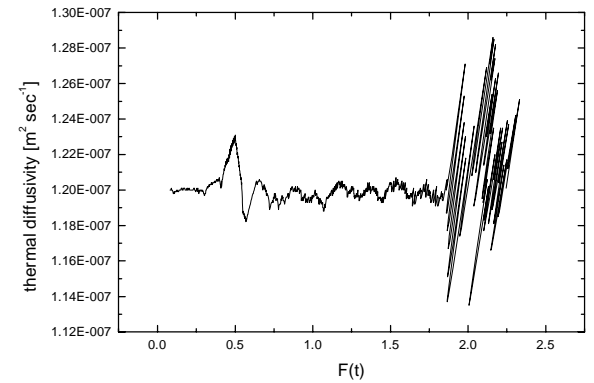
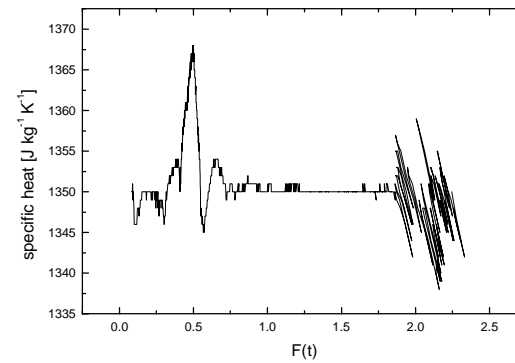
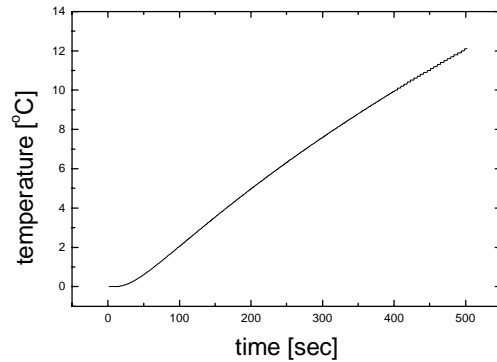
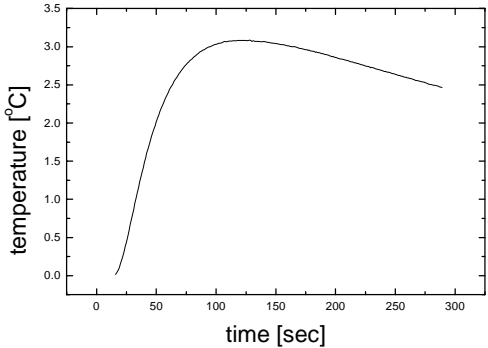
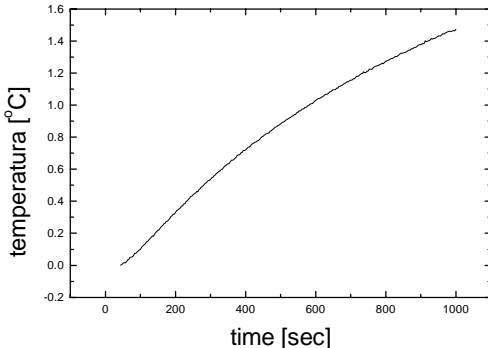
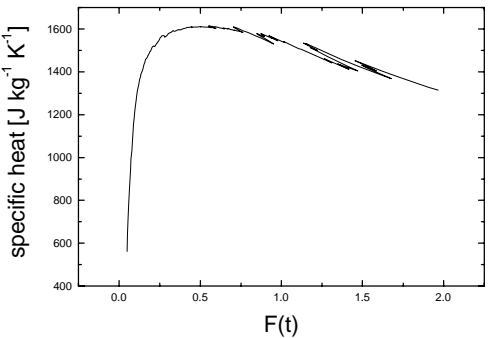
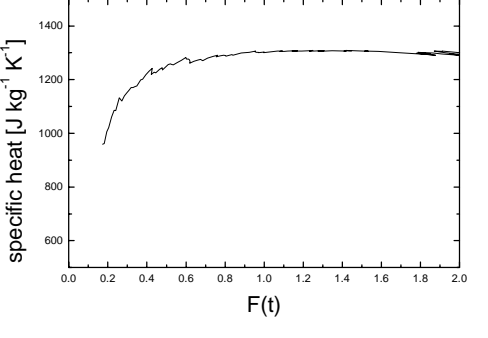
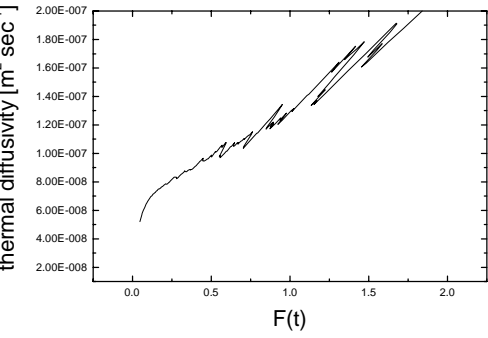
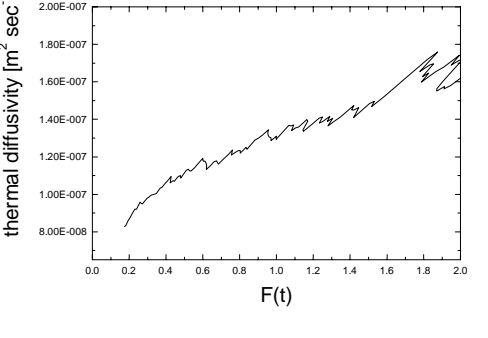


Table 4. Experimental analysis of the measuring regime

Pulse transient	Step wise transient
	
<p>$\Delta t = 10 \text{ sec}, \Delta F = 0.033$</p> 	<p>$\Delta t = 66 \text{ sec}, \Delta F = 0.22$</p> 
	

where $T_i(x,t)$ is the temperature function of an ideal model, in our case the temperature shown in Fig. 1, $f(x,t,\alpha,\beta,\gamma,\dots)$ is a correction function characterising the deviation from the ideal models, and $\alpha, \beta, \gamma, \dots$ are parameters characterising heat capacity of the heat source, contact thermal resistance, heat loss from the specimen surface, etc. [2]. For $f(x,t,\alpha,\beta,\gamma,\dots) \rightarrow 1$ one obtains criteria for use of the ideal models, in fact for use of the temperature functions valid for ideal model.

3 Experiment

The Thermophysical Transient Tester RT 1.02 (Institute of Physics SAS) was used for experiment. Both the pulse transient and the step-wise transient regime were used for intercomparison measurements. A test of correlation was made to find experimentally the measuring time and the time window suitable for evaluation in the following way: The temperature response was scanned over 300 sec for pulse transient and 300 sec for step – wise transient method (measuring time up to $F = 2$). Time difference between two scans was 3.3 sec. Difference analysis was performed to find the measuring time and time window for data evaluation in a similar way as in paragraph 3.2. A strobe of 10 sec ($\Delta F = 0.033$) for pulse transient and 66 sec ($\Delta F = 0.22$) for step-wise transient was chosen in which the specific heat and thermal diffusivity was found by fitting procedure. The strobe was consecutively shifted over experimental temperature response. The results of this analysis are shown in Table 3. Specific heat for both pulse transient and step-wise transient method have a plateau where data are stabilised and are near to recommended value. However data of thermal diffusivity show systematically progress. A more detailed study needs to be performed to find agreement between the theory and the experiment when time window for thermal diffusivity is searched for.

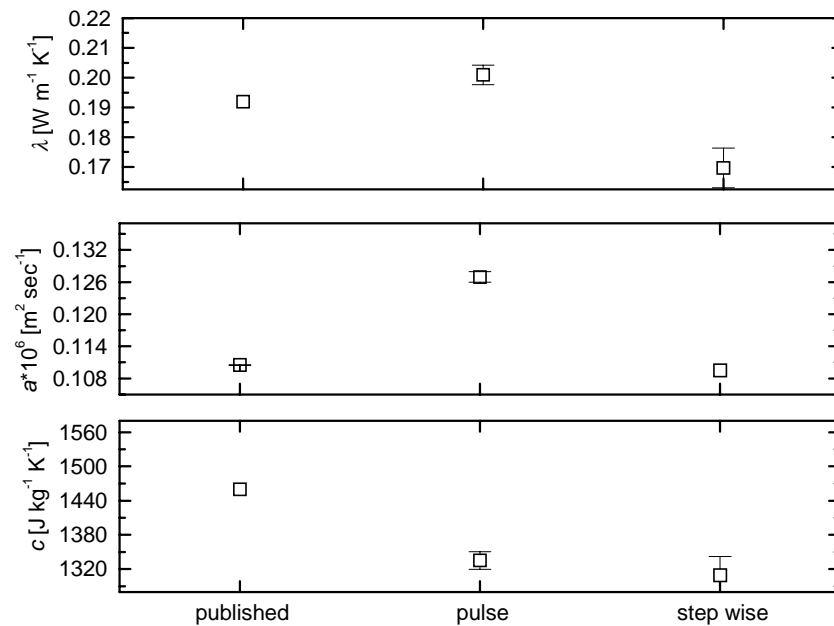


Figure 2.: Results of intercomparison on PERSPEX.

Results of intercomparison made on PERSPEX are shown in Fig. 2. Variations in heat pulse width and energy, heat flux, reassembling and surrounding atmosphere were used. Mean values and standard deviation of the thermal diffusivity, specific heat and the thermal conductivity were obtained by averaging of all data excluding values that show large shifts for both the pulse transient and the step – wise transient. The error bars characterizing the precision of the experimental set up are shown. Shifts of experimental data for both the pulse transient and the step – wise transient methods can be found. This indicates that discrepancies still exists between the model and the experimental set up.

5 Conclusions

A new class of the methods known as transient methods for measuring specific heat, thermal diffusivity and thermal conductivity is presented. Experimental set-up and methodology for pulse transient and step – wise transient is discussed. Results of intercomparison measurements made on PERSPEX are presented. Data are intercompared with published and recommended ones. Data shift was found. Although data uncertainty is for specific heat within 2%, for thermal diffusivity within 4% and thermal conductivity within 4.5% [2], data shift is within 10%. Data shift is caused by differences between ideal models and the real experimental set-up, choice of the time window for data evaluation and the contribution of the radiation component to the heat transport [7].

Acknowledgements

The authors are grateful to the Thermophysical Properties Section at the National Physical Laboratory for providing specimens PERSPEX and to Mr. Markovic for the assistance during experiment. This work was supported by grant agency VEGA under Nr. 2/5084/2000.

References

- [1] L. Kubičár; V. Boháč; Review of several dynamic methods of measuring thermophysical parameters in Proc. of 24th Int. Conf on Thermal Conductivity / 12th Int. Thermal Expansion Symposium October 26 – 29 1997 Eds. P S Gaal and D E Apostolescu, (Lancaster: Technomic Publishing Company 1990), p.135 – 149.
- [2] L. Kubičár; Pulse Method of Measuring Basic Thermophysical Parameters, in Comprehensive Analytical Chemistry Vol. XII Thermal Analysis Part E Ed Svehla G (Amsterdam, Oxford, New York, Tokyo: Elsevier 1990), pp. 350.
- [3] L. Kubičár; V. Boháč; A step wise method for measuring thermophysical parameters of materials, Meas. Sci. Technol. 11, 1 (2000) p. 252 - 258
- [4] J. V. Beck; K. Arnold; Parameter Estimation in Engineering and Sciences (New York, London, Sidney, Toronto, John Willey 1977)
- [5] M. Raynaud; Strategy of experimental design and the estimation of parameters, High Temp. High Press. 31 (1999) 1 – 15
- [6] L. Kubičár; V. Boháč; Accuracy analysis of intercomparison measurements of thermophysical properties, Proc. of TEMPECO '96 Ed Piero Marcarino (Torino: Levrotto & Bella 1996) pp 505 - 511
- [7] P. Koniorczyk; J. Zmywaczyk; Investigation of the coupled conductive-radiative heat transfer in plexiglas, Proc. of TEMPECO '96 Ed Piero Marcarino (Torino: Levrotto & Bella 1996) pp 543 – 547

THICKNESS DEPENDENCY OF THERMOPHYSICAL PROPERTIES OF PERSPEX

Vlastimil Boháč¹, Ľudovít Kubičár¹ and Mattias K. Gustafsson²

¹ Institute of Physics, Slovak Academy of Sciences, Dúbravská cesta 9, SK-84228 Bratislava, Slovak Republic

² Department of Thermo and Fluid Dynamics, Chalmers University of Technology, Gothenburg, Sweden
Email: bohac@savba.sk, mkgu@ftd.chalmers.se

Abstract

PERSPEX is material that is easy to produce with the reproducible physical properties. PERSPEX - PMMA is a vinyl polymer, made by free radical vinyl polymerization from the monomer methyl methacrylate. This material was chosen as the Certified Reference Material (CRM) for the measurement of thermal conductivity by Guarded Hot Plate Method (NPL). Using literature data, steady state method, and transient methods, that give thermal conductivity, thermal diffusivity and specific heat within a single measurement, one can intercompare thermophysical data providing that data consistency relation $\lambda = \rho * c * a$ is used. The intercomparison, usually, indicates data shift depending on method used. Intercomparison of the thermophysical data measured by two different dynamic methods - Pulse Transient and Gustafsson Probe Methods, literature data and recommended data is discussed. The specimen thickness dependency of thermophysical parameters of PERSPEX measured by Pulse Transient Method was found. Similar thickness dependency of thermal conductivity measured by Guarded Hot Plate Method was referred in the literature.

Key words: PMMA, PERSPEX, thickness dependency of thermophysical parameters, Pulse Transient Tester, Hot Disk Thermal Constants Analyser, methodology.

1 Introduction

The necessity of CRM and the perfect knowledge of its properties are evident, especially when developing new methods as well as their methodologies. Thermophysical data of PERSPEX were intercompared using data found in the literature, data recommended by NPL [3] as well as data measured by different dynamic methods (Gustafsson Probe, Pulse Transient Method). Several material sources were used for experiments. Totally, in this paper, there were compared data measured by three different experimental methods using four various material sources. Different specimens were used for intercomparison (Table 1). All data are compared in a review graph for thermal conductivity (Figure 4). In our paper we used PERSPEX for investigation of the dependency of thermophysical data on specimen thickness.

Table 1. List of methods and PERSPEX (PMMA) specimens used for intercomparison

Method	Specimen origin	Specimen diameter
Pulse transient	Commercial batch 1 [1]	18 mm
Pulse transient	NPL	20 and 30 mm
Pulse transient	Commercial batch 2	30 mm
Gustafsson probe	Commercial batch 2	50 mm
Guarded hot plate	Not specified [2]	200 mm
Guarded hot plate	NPL [3]	76 mm

2 Experimental techniques

Transient methods for measuring the specific heat, thermal diffusivity and thermal conductivity were used [1], [4]. The methods allow to investigate the specific heat, thermal diffusivity and thermal conductivity within single measurement.

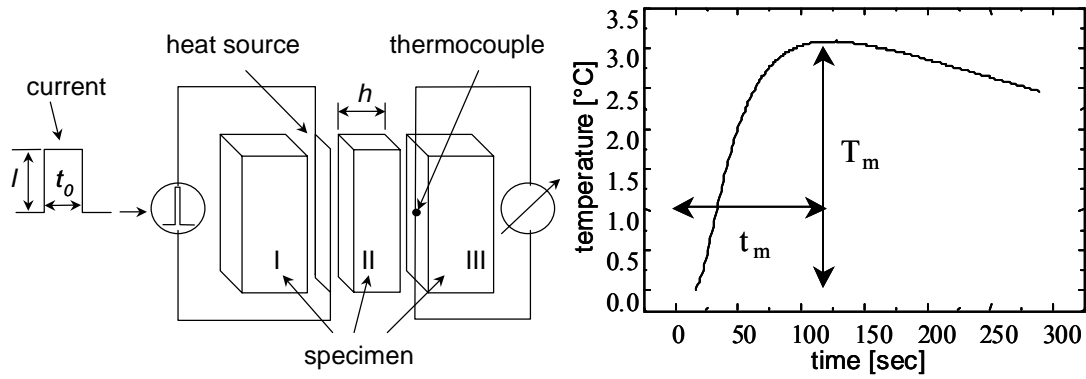


Figure 1. Principle of the Pulse Transient Method and example of the transient record.

The principle of the Pulse Transient Method and specimen arrangement is shown in Figure 1. The heat pulse is generated by the passing of the electrical current through the plane electrical resistor made of a metallic foil of 20 μm thick. The temperature response is measured by the thermocouple with diameter of 50 μm . All measurements were made at room temperature and in air as well as in vacuum of 0.1 Pa. The thermophysical parameters are calculated from the temperature response to the heat pulse. Then the thermal diffusivity is given as

$$a = \frac{h^2}{2t_m} \quad , \quad (1)$$

the specific heat as,

$$c = \frac{Q}{\sqrt{2\pi e\rho h T_m}} \quad , \quad (2)$$

and the thermal conductivity as

$$\lambda = ac\rho \quad , \quad (3)$$

where $Q = RI^2t_0$ and R is the electrical resistance of the heat source, ρ is density and other parameters are given in the Figure 1.

The Hot Disk Thermal Constants Analyser™ [4] sometimes referred to as the Transient Plane Source or Gustafson Probe [4] was used as second dynamic method. The principle of the method drawn in Figure 2 is based on the transient heating of a plane double spiral sandwiched between two pieces of the investigated material. By passing an electrical current through the spiral and recording the resistance increase of the sensor at the same time, the temperature change is obtained. Temperature record is used to determine both transport coefficients - the thermal conductivity and the thermal diffusivity from one single transient. The parameters are found by fitting of the temperature function (4) on the temperature record providing rules given in [4]. *Specific heat* is calculated from data consistency relation $\lambda/a=c$.

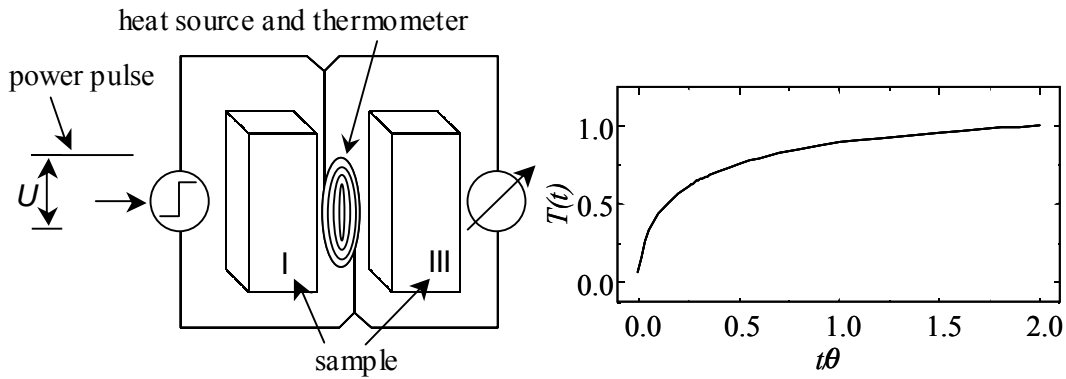


Figure 2. Principle of the Hot Disk Thermal Constants Analyser and example of the transient record (t/θ means dimensionless time constant).

The temperature function has a form

$$\overline{\Delta T(\tau)} = \frac{P_0}{\sqrt{\pi^3 r \lambda}} D(\tau) , \quad (4)$$

where P_0 is the total output of power in the sensor and the $D(\tau)$ is a dimensionless time function of the probe

$$D(\tau) = \frac{1}{[m(m+1)]^2} \times \int_0^\tau \sigma^{-2} d\sigma \left[\sum_{l=1}^m l \sum_{k=1}^m k \exp\left\{-\frac{l^2 + k^2}{4m^2\sigma^2}\right\} I_0\left(\frac{lk}{2m^2\sigma^2}\right) \right] , \quad (5)$$

and

$$\tau = \sqrt{t/\theta} , \quad (6)$$

$$\theta = \frac{r^2}{a} , \quad (7)$$

$$R(t) = R_0 [1 + \alpha \overline{\Delta T(\tau)}] , \quad (8)$$

θ is referred to as the characteristic time of the transient record, t is the time for the temperature record, r is the radius of the outer concentric circle, and m is the number of electrically conducting ring sources; R_0 is the initial electrical resistance and α is the Temperature Coefficient of Resistivity (TCR) of the probe. A detailed description of this experimental technique can be found elsewhere [4].

2 Experimental results

2.1 Intercomparison results

The Figure 3 shows the intercomparison of the thermophysical parameters measured by Transient Pulse Method [1] and Gustafsson Probe [4]. The data used representing properties of the same material batch (material batch 2). The specimen of 30 mm in diameter and 6 mm thick was used for the Pulse transient Method.

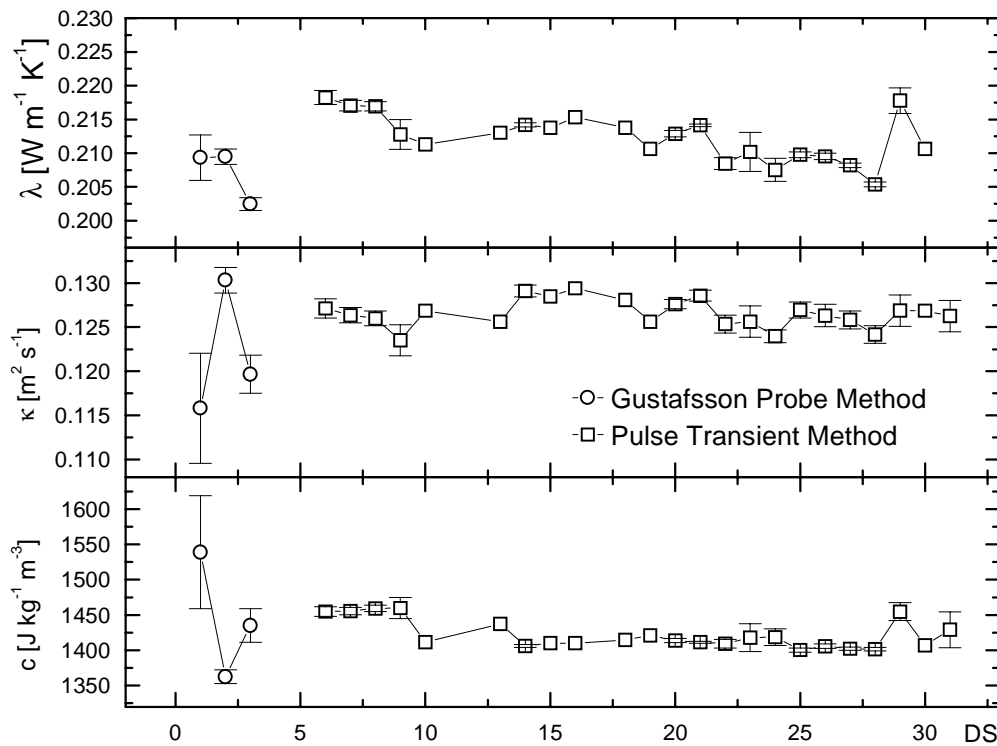


Figure 3. Thermophysical parameters of PMMA (PERSPEX) measured by Pulse Transient Method and Gustafsson Probe Method. The first three points were measured by Gustafsson probe method on sensors of different diameters (6.6mm, 13mm 20mm). Every point represents an average that were obtained at the same experimental conditions (heat pulse energy, pulse width, test of reproducibility after reassembling) for Pulse Transient Method.

Averaged values with standard deviations were calculated for all points shown in Figure 3 that were measured by Pulse Transient Method. The largest percentage difference is 4.5% for thermal diffusivity. Difference in thermal conductivity and specific heat is less than 1.6%. All data are in reasonable coincidence.

In the case of Gustafsson Probe the specimen diameter was 50 mm. Each of three points represents statistics of at least 5 measurements performed at different radius of the probe.

2.2 Thickness dependency

Data in Figure 4 were collected from various sources in the literature [1,2] and are compared with our data measured by the Pulse Transient Method and Gustafsson Probe Method. Data measured on PERSPEX of NPL origin by Pulse Transient Method show clear thickness dependency of thermophysical parameters for both 20 and 30 mm of diameter specimen sets. Similar behavior was observed on Hot Guarded Disk Method [2]. The value of thermal conductivity $\lambda=0.192$ certified by NPL is depicted in figure too. The penetration depth (corresponding to the sensor constant and thus the sensor radius) substitutes the thickness of the specimen for Gustafsson Probe.

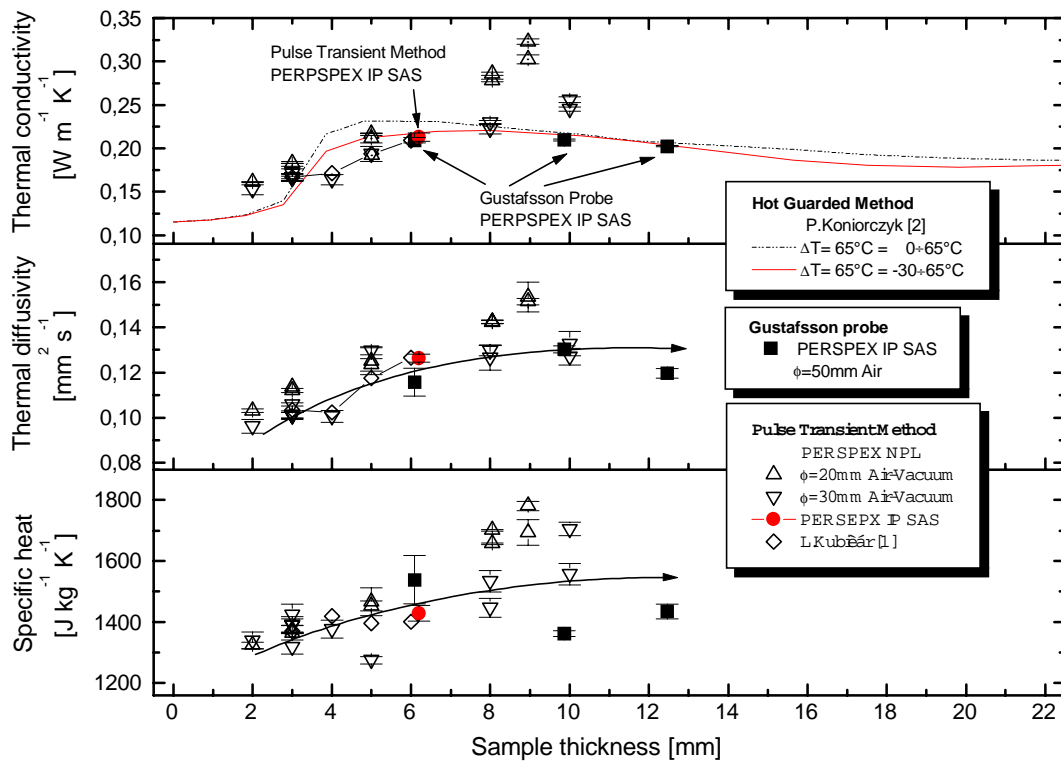


Figure 4. Thermal conductivity, thermal diffusivity and specific heat of PMMA (PERSPEX) measured by Pulse Transient Method and Gustafsson Probe Method. The NPL certified value of thermal conductivity is $0.192 \text{ W m}^{-1} \text{ K}^{-1}$. Specimen origin is given in Table 1.

3 Conclusions

The paper presents the results of the intercomparison measurements and of the study of the thickness dependency that was obtained on PERSPEX. The Pulse Transient Method and Gustafsson Probe Method give data within an experimental error less than 4.5 % for thermal diffusivity and even less than 1.6% for thermal conductivity and specific heat.

Both methods are able to determine thermal diffusivity, thermal conductivity and specific heat within single transient record.

Data measured on PERPSEX (NPL) by Pulse Transient Method on the specimens of 20 and 30 mm diameters clearly show the dependency of thermophysical parameters on thickness of the specimen. This is supported by data previously measured using Pulse Transient Method [1] and by data using Guarded Hot Plate [2]. Data collection represents three different methods and four different PERSPEX origin. The Pulse Transient and Gustafsson Probe method show the same thickness dependency as Hot Guarded Plate Method (Steady state method).

Acknowledgement

The authors are grateful to the Thermophysical Properties Section at the National Physical Laboratory for providing specimens of PERSPEX. Authors wish to thank the Slovak Science Grant Agency for the financial support under the contract 2/6066/20. One of the authors – Bohac is thankful to the Swedish Academy of Sciences - IVA for the financial support on the stay at Chalmers University of Technology, Gothenburg (SE).

References

- [1] Kubičár L.; *Pulse Method of Measuring Basic Thermophysical Parameters*, in Comprehensive Analytical Chemistry Vol. XII Thermal Analysis Part E Ed Svehla G (Amsterdam, Oxford, New York, Tokyo: Elsevier 1990)
- [2] Koniorczyk P., Zmywaczyk J.; *Investigation of the coupled conductive-radiative heat transfer in plexiglas*, Proc. of TEMPECO '96 Ed Piero Marcarino (Torino: Levrotto & Bella 1996) pp 543 – 547
- [3] Salmon D., Thermophysical Properties Section at the National Physical Laboratory Teddington, UK.
- [4] Gustafsson S.E., 1991 Rev. Sci. Instrum. 62, (1991) 797-804
- [5] Gustafsson S.E., Karawacki E., Khan M.N., 1979, J.Phys. D.: Appl. Phys. 12, 1411-1421
- [6] Boháč V., Gustafsson M.K., Kubičár L., Gustafsson S.E., *Parameter estimations for measurements of thermal transport properties with the hot disk thermal constants analyser*, Review of Scientific Instruments, 2000, Vol 71, Iss 6, pp 2452-2455

DETERMINATION OF THE RESPONSE DELAY PARAMETERS FOR A MEASUREMENT SYSTEM USING THE FLASH METHOD

Ján Spišiak, Tatiana Šrámková

Institute of Physics, Slovak Academy of Sciences, Dúbravská cesta 9, 842 28 Bratislava, Slovak Republic
E-mail: fyzijspi@savba.sk, fyzitsra@savba.sk

Abstract

The flash method has become a standard method for measuring thermal diffusivity of various materials. Many factors influence the accuracy of thermal diffusivity determination thermal diffusivity. One of them is transfer function of the measuring system and its time constant. This time constant limits the thickness of measured samples of materials with high thermal diffusivity. The limitations of a simple device used in our institute are discussed in this contribution.

Key words: flash method, transfer function, time constant, response delay

1 Introduction

The flash method has gained a widespread acceptance in the thermophysical community. The method was originally proposed by Parker et al.[1] nearly four decades ago. The concept of the method is simple. A sample is irradiated by a light pulse on the front side and the temperature response at the rear side is detected. The system which detects and processes the measured signal usually consists of a temperature sensor, preamplifier and A/D converter. The time response of such a system influences the precision of the measurement. During the last years the flash method has been successfully applied to measure thin foils or materials with high thermal diffusivity. In this case the transient response of the measurement system can cause a significant error. Therefore it is necessary to know the transient response characteristics of the system. In the paper we present an evaluation of the time constants of the device built at the Institute of Physics SAS [2].

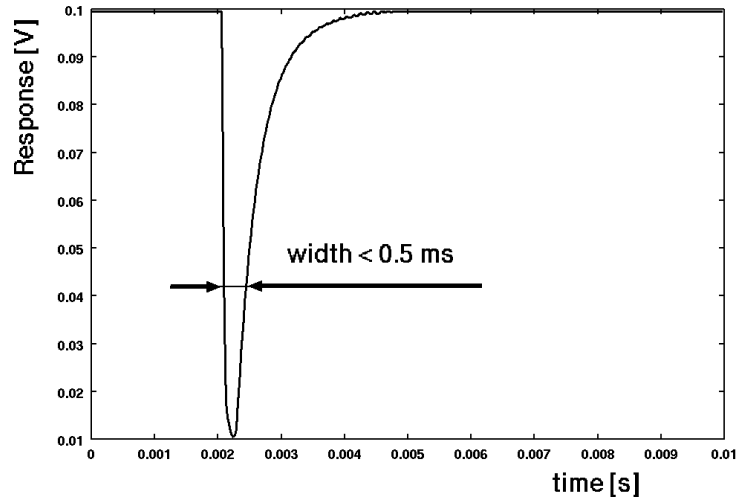
2 Evaluation of the time constant of the measuring system

The motivation to find the transfer function of our apparatus was the intention to measure copper samples of thickness of few mm. In this case the response is fast and could be distorted by the inertia of the apparatus.

The apparatus consists of a flash lamp as a light source, thermocouple as a detector, preamplifier, amplifier and A/D converter. The flash lamp gives just a small amount of energy and therefore we could measure only thin samples. The resulting precision of the measurement could be influenced by the flash pulse duration and delay of the measurement system.

2.1 Duration of the flash pulse

We measured the duration of the flash lamp pulse by a phototransistor. The shape of the detected pulse was influenced by the position of this photodetector. A broader peak was observed when it was placed closer to the light source. So the width of the peak was influenced by the intensity of the measured heat flux. The width of the flash duration was determined to be less than 0.5 ms. A typical response of the photosensor is shown in Fig.1.



2.2 Delay of the measuring system

The response of a 1-st order system with the time constant τ and input $V(t)$ can be written as

$$\Theta(t) = e^{-\frac{t}{\tau}} \left[\int \frac{e^{\frac{t}{\tau}}}{\tau} V(t) dt + C \right] \quad (1)$$

A first order system with the time constant τ_1 and a stepwise input has a response

$$\Theta_1(t) = 1 - e^{-\frac{t}{\tau_1}} \quad (2)$$

Fig. 1: Duration of the flash pulse.

$$\Theta_2(t) = 1 - \frac{\tau_1 e^{-\frac{t}{\tau_1}}}{\tau_1 - \tau_2} - \frac{\tau_2 e^{-\frac{t}{\tau_2}}}{\tau_2 - \tau_1} \quad (3)$$

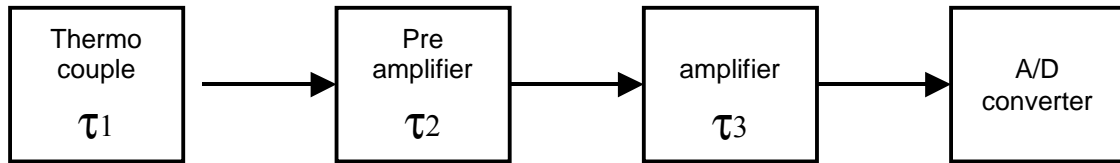


Fig. 2: Scheme of the measuring system.

Our measurement system consists of a thermocouple, preamplifier, amplifier and A/D converter (Fig. 2). Our aim was to evaluate the time constants of individual components by a unit step input. The unit step was realized by the electric circuit depicted in Fig.3.

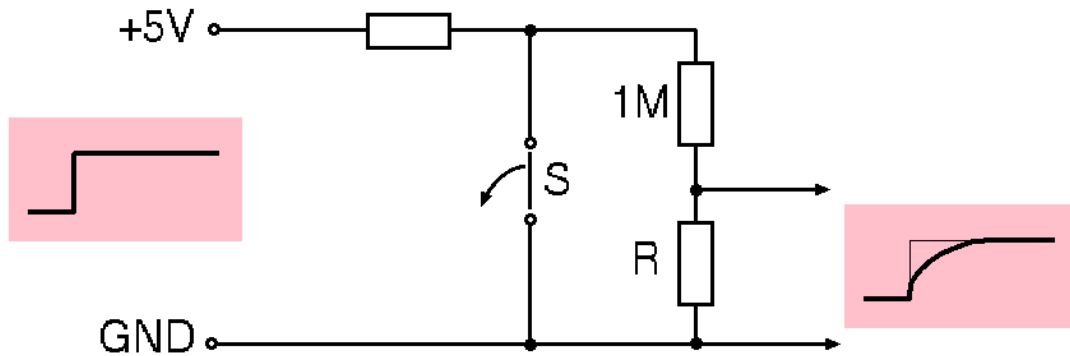


Fig. 3: Scheme of the unit step input.

The A/D converter was Keithley DAS1200 with sampling frequency 50 kHz. The amplifier with the time constant τ_3 was a built-in amplifier on the board of DAS1200 with gains 1, 10, 100 or 500. The measured response to the unit step was under our resolution, so the estimated $\tau_3 < 20 \mu\text{s}$.

The preamplifier is based on MAA 725 with no filter added. The response to the unit step input is shown in Fig.4 (curve τ_2). The time constant τ_2 was estimated by fitting the response to the Eq.(2) using the Levenberg-Marquardt optimization technique. The fitting gave the value of $\tau_2 = (275 \pm 4) \mu\text{s}$.

The tested thermocouple was a chromel-alumel intrinsic thermocouple of diameter $f = 76.2 \mu\text{m}$. The thermocouple was glued to a copper foil of thickness $l = 100 \mu\text{m}$. The unit step was obtained by irradiating the foil with a short burst of radiant energy. The

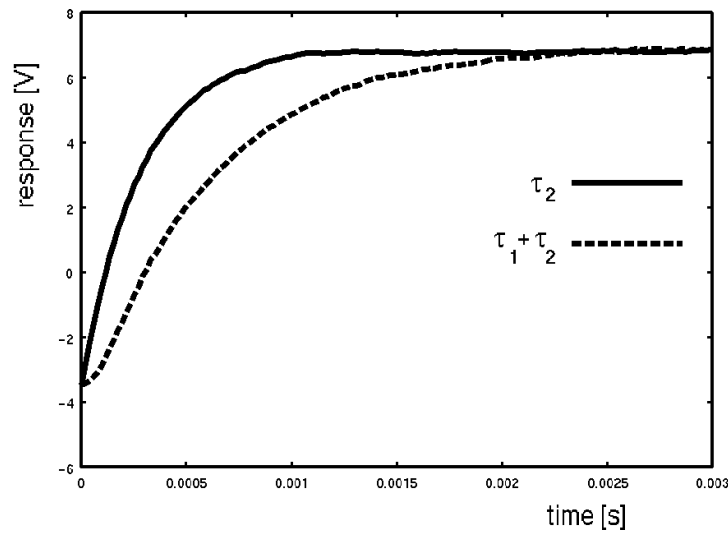


Fig. 4: Responses for the time constant measurements.

time constant of the thermocouple was determined from Eq.(3) by using τ_2 as known from the previous experiment. The estimated value of $\tau_1 = (481 \pm 22) \mu\text{s}$.

3 Conclusion

In the paper we determined the time constant τ of the device for measuring thermal diffusivity by the flash method. Joint time constant ($\tau_1 + \tau_2 + \tau_3$) of the measurement system was estimated to be 1 ms. With this time constant we can measure copper samples of thickness approximately 5 mm for which the characteristic time $T_{1/2}$ is about 100 times longer than estimated τ . When measuring thinner samples a correction of the response is necessary [3].

References

- [1] W.J.Parker, R.J.Jenkins, C.P Butler, and G.L.Abbot, 1961 *J. Appl. Phys.*, **32**, 1679-1684.
- [2] T. Šrámková and T. Log, 1995 *Int.J.Heat Mass Transfer*, 15 **38**, 2885-2891.
- [3] N.Araki, D.W.Tang, M.Suzuki, and A.Makino, 2000 *Int. J. Thermophys.* **21**, 495-502.

DETERMINATION OF TEMPERATURE-DEPENDENT THERMAL CONDUCTIVITY WITHOUT INTERNAL MEASUREMENTS

Jozefa Lukovičová, Jozef Zámečník

Department of Physics, Faculty of Civil Engineering, Slovak University of Technology, Radlinského 11, 813 68 Bratislava, Slovakia
Email: lukovico@svf.stuba.sk, zamecnik@svf.stuba.sk

Abstract

Determining the temperature dependent thermal conductivity based on solution of the inverse heat conduction problem of functional estimation using conjugate gradient algorithm is presented. Estimation of the thermal conductivity is obtained by using just boundary measurements of temperature (i.e., internal measurements are unnecessary) and no prior information is available on its functional form.

1 Introduction

This paper presents the inverse method, which can be considered as a reasonable alternative to the classical methods for measuring thermal properties of solid material (the steady-state method, the probe method, the periodic heating method, the pulse method, etc.). With just temperature measurements taken at media boundaries and no a priori information about the unknown thermal conductivity as function of temperature it is possible to determine thermal conductivity for wide temperature range.

This method solves inverse transient heat conduction as a general optimization problem by applying the adjoining equation approach coupled to the conjugate gradient algorithm.

2 Formulation of the problem

We consider the one-dimensional, non-linear heat conduction problem in slab geometry. The dimensionless mathematical formulation of this problem can be expressed as

$$\frac{\partial T(x,t)}{\partial t} = \frac{\partial}{\partial x} \left(k(T) \frac{\partial T(x,t)}{\partial x} \right) \quad (x,t) \in (0,1) \times (0,1] \quad (1a)$$

$$-k(T) \frac{\partial T(x,t)}{\partial x} = q_0 \quad \text{at } x=0, \quad t \in (0,1] \quad (1b)$$

$$-k(T) \frac{\partial T(x,t)}{\partial x} = q_1 \quad \text{at } x=1, \quad t \in (0,1] \quad (1c)$$

$$T(x,t) = T_0 \quad \text{for } t=0, \quad x \in [0,1] \quad (1d)$$

Where the following dimensionless quantities are defined:

$$x = \bar{x} \bar{L}, \quad T = \bar{T} / \bar{T}_r, \quad k = \bar{k} / \bar{k}_r, \quad q = \bar{q} \bar{L} / \bar{k}_r \bar{T}, \quad t = \bar{t} \bar{k}_r / \bar{\rho} \bar{C}_r \bar{L}^2,$$

\bar{T}_r and \bar{k}_r refer to the nonzero reference temperature and thermal conductivity, respectively, $\bar{\rho} \bar{C}_r$ is the heat capacity per unit volume. We assume $\bar{T}_0 = \bar{T}_r$, i.e., $T_0 = 1$ in the direct problem (1).

In the present problem, the thermal conductivity $k(T)$ is regarded as unknown, but everything else in equation (1) is known. In addition, temperature readings taken at some appropriate locations are considered available. The temperature readings taken over the time period t_e are denoted by $Y(x_i, t) \equiv Y_i(t)$, $i = 1$ to m , where $i = 1$ and m are always corresponding to $x = 0$ and 1 (i.e., boundary measurements), respectively.

The inverse problem for ideal situation is defined as follow: find $k(T)$ such that $Y_i(t) = \mathbb{T}(x_i, t; k)$, for $i = 1$ to m and over the time period t_e . Since the measured temperature $Y_i(t)$ contains measurement errors, this equation needs to be solved in the least square sense. Then the inverse problem is stated as follows: by utilising the measured temperature data $Y_i(t)$, estimate the unknown $k(x, t)$ over t_e . This is classified as the function estimation for the determination of the non-linear thermal conductivity $k(T)$, because no prior information is available on the functional form of $k(x, t)$. The unknown thermal conductivity $k(T)$ is obtained in such a way that the following functional is minimised:

$$J|k(T)| \equiv J|k(x, t)| = \int_0^{t_e} \sum_1^m |T_i(x_i, t) - Y_i(x_i, t)|^2 dt \quad (2)$$

here, the quantities $T_i(x_i, t)$ are calculated from the solution of the direct problem by using an estimated $\hat{k}(x, t)$ for the exact $k(x, t)$ at the measurement locations $x = x_i$.

The direct problem (1) is nonlinear since thermal conductivity is function of temperature, therefore, an iterative technique is needed (finite difference method by the solver LSODA [1]). $k(T)$ cannot be replaced by $k(x, t)$, since is unknown before the direct problem calculations. However, when the temperatures $T(x, t)$ are converged by iterative technique under some initial and boundary conditions, the values of $k(x, t)$ should be fixed because temperatures $T(x, t)$ are known and fixed at any (x, t) .

For the estimation $k(x, t)$ by minimizing the functional (2) is using the following iterative process based on the conjugate gradient method [2]

$$\hat{k}^{n+1}(x, t) = \hat{k}^n(x, t) - \beta^n P^n(x, t) \quad \text{for } n = 0, 1, 2, \dots \quad (3a)$$

where β^n is the search step size in going from iteration n to iteration $n + 1$ and

$P^n(x, t)$ is the direction of descent given by

$$P^n(x, t) = J'^n(x, t) + \gamma^n P^{n-1}(x, t) \quad (3b)$$

which is a conjugation of the gradient direction $J''^n(x, t)$ at iteration n and the direction of descent $P^{n-1}(x, t)$ at iteration $n-1$. The conjugate coefficient is determined from

$$\gamma^n = \int_0^1 \int_0^{t_e} (J''^n)^2 dt dx / \int_0^1 \int_0^{t_e} (J''^{n-1})^2 dt dx \quad (3c)$$

with $\gamma^0 = 0$ for any n . The convergence of this iterative procedure is guaranteed in [3].

3 Iterative process

To perform the iterations (3), it is needed to compute β^n and J''^n .

To compute the step size β^n : It is assumed that when $k(x, t)$ undergoes a variation $\Delta k(x, t)$, $T(x, t)$ is perturbed by $T(x, t) + \Delta T(x, t)$. Then replacing k by $k + \Delta k$ and T by $T + \Delta T$ in direct problem (1), subtracting from the resulting expressions the direct problem (1), the system of equations for sensitivity function $\Delta T(x, t)$ is obtained:

$$\frac{\partial}{\partial x} \left[k(x, t) \frac{\partial \Delta T(x, t)}{\partial x} \right] + \frac{\partial}{\partial x} \left[\Delta k(x, t) \frac{\partial T(x, t)}{\partial x} \right] = \frac{\partial \Delta T(x, t)}{\partial t} \quad 0 < x < 1 \quad (4a)$$

$$-k(x, t) \frac{\partial \Delta T(x, t)}{\partial x} = \Delta k(x, t) \frac{\partial T(x, t)}{\partial x} \quad \text{at } x = 0 \quad (4b)$$

$$-k(x, t) \frac{\partial \Delta T(x, t)}{\partial x} = \Delta k(x, t) \frac{\partial T(x, t)}{\partial x} \quad \text{at } x = 1 \quad (4c)$$

$$\Delta T(x, t) = 0 \quad \text{for } t = 0 \quad (4d)$$

The functional $J(\hat{k}^{n+1})$ for iteration $n+1$ is obtained from (2) and (3a), such that

$$J(\hat{k}^{n+1}) = \int_{t=0}^{t_e} \sum_{i=1}^m [T_i(\hat{k}^n) - \beta^n \Delta T_i(p^n) - Y_i]^2 dt \quad (5)$$

where $T_i(\hat{k}^n)$ is the solution of the direct problem by using estimate $\hat{k}(x, t)$ at $x = x_i$.

The sensitivity function ΔT_i is taken as the solutions of (4) by letting $\Delta k = p^n$. The step size β^n is determined by minimising the functional (5) with respect to β^n , as follows

$$\beta^n = \int_{t=0}^{t_e} \sum_{i=1}^m (T_i - Y_i) \Delta T_i dt / \int_{t=0}^{t_e} \sum_{i=1}^m (\Delta T_i)^2 dt \quad (6)$$

In order to calculate the gradient of the functional $J'(\hat{k}^n)$, it is needed to determine an adjoint function $\lambda(x, t)$ in addition to the sensitivity function $\Delta T(x, t)$ [4]:

Equation (1a) is multiplied by the adjoint function $\lambda(x, t)$ and resulting expression is integrated over the time and corresponded space; then the result is added to (2), such that

$$J[k(x, t)] = \int_{t=0}^{t_e} \sum_{i=1}^m [T_i - Y_i]^2 dt + \int_{x=0}^1 \int_{t=0}^{t_e} \lambda \left\{ \frac{\partial}{\partial x} \left[k(T) \frac{\partial T(x, t)}{\partial x} \right] - \frac{\partial T(x, t)}{\partial x} \right\} dt dx \quad (7)$$

the variation ΔJ is obtained by perturbing k by Δk and T by ΔT from (7); the initial and boundary condition of the sensitivity problem (4) then leads to the adjoint problem for determination of function $\lambda(x, t)$

$$\frac{\partial}{\partial x} \left[k(x, t) \frac{\partial \lambda(x, t)}{\partial x} \right] + \sum_{i=2}^{m-1} 2(T_i - Y_i) \delta(x - x_i) + \frac{\partial \lambda(x, t)}{\partial t} = 0 \quad \text{for } 0 < x < 1 \quad (8a)$$

$$-k(x, t) \frac{\partial \lambda(x, t)}{\partial x} = 2(T_1 - Y_1) \quad \text{at } x = 0 \quad (8b)$$

$$-k(x, t) \frac{\partial \lambda(x, t)}{\partial x} = 2(T_m - Y_m) \quad \text{at } x = 1 \quad (8c)$$

$$\lambda(x, t) = 0 \quad \text{for } t = t_e \quad (8d)$$

Finally gradient $J'(x, t)$ is calculated from

$$J'(x, t) = -\frac{\partial \lambda(x, t)}{\partial x} \frac{\partial T(x, t)}{\partial x} \quad (9)$$

In each iteration step it is needed to solve the direct problem, the sensitivity problem and the adjoint problem.

The check condition is specified as

$$J|\hat{k}^{n+1}(x, t)| < m\delta^2 t_e \quad (10)$$

where δ is the stand deviation of the measurements (we assume that the temperature reziduals may be approximated by $T_i - Y_i \approx \delta$, which is assumed to be constant).

4 Results

In the verification of the conjugate gradient method in predicting $k(T)$ by the inverse analysis from the temperature recordings, we employed an artificial numerical example. The thermal conductivity $k(T)$ is assumed to vary with temperature in the form

$$k(T) = K_0 + K_1 \sin(T / K_2) + K_3 \exp(T / K_4) \quad (11)$$

where the constants K_0, K_1, K_2, K_3, K_4 are taken as 1, 2.5, 5, 80 and 2.5 respectively. The initial guess of $\hat{k}(x, t)$ used to begin the iteration is taken 10. The space and time increments are taken as $\Delta x = 0.1$ and $\Delta t = 0.1$, respectively; the boundary heat fluxes are taken as $q_1 = 20$ and $q_0 = 14$; the total measurement time $t_e = 7$ and the measurement time step is taken the same as Δt .

The estimation of $k(x, t)$ by using 11 and 2 (boundary) sensors with exact measurements shows a very good agreement with exact values $k(x, t)$. Therefore, the conjugate gradient method provides to determine temperature-dependent thermal conductivity without the necessity of using interior sensors.

In order to evaluate the results for situations involving random measurement (input) errors, we assume normally distributed no-correlated errors with zero mean and constant standard deviation. The simulated inexact measurement data are expressed as

$$Y = Y_{exact} + \omega\delta, \quad (12)$$

where Y_{exact} is the solution of the direct problem with an exact $k(T)$, δ is the standard deviation of the measurements and ω is a random variable that is generated using the Monte-Carlo treatment and is within -2.576 to 2.576 for a 99.9% confidence bounds. The average relative error between exact and estimated values is defined as

$$\left(\sum_{i=1}^m \sum_{j=1}^n \left| \frac{k(x_i, t_j) - \hat{k}(x_i, t_j)}{k(x_i, t_j)} \right| \right) : (n.m)100\% \quad (13)$$

where m and n represent the total discrete number of position and time increments, respectively.

When the dimensionless measured temperatures with errors $\delta = 0.00$ and $\delta = 0.08$ are obtained according to (8), the inverse solutions using these inexact measurements are compared to exact values. The average relative errors between exact and estimated values are 1.350 and 6.071%, respectively. For the case when $\delta = 0.08$, the dimensionless measured temperature errors are within -0.19 to 0.19 for a 99% confidence bounds, which implies that a total of about 0.38 dimensionless temperature error is allowed. According to Fig. 1. the dimensionless temperature at $x = 0.06$ is range from 1 to 12, thus the average relative measurement error is about 2 %. By using this 2 % measurement error, one could estimate the thermal conductivity with an average relative error of about 6 %. This proves that the measurement errors are not amplified the errors of estimated thermal conductivity.

The experiment values are from the furnace-slag based concrete with bulk density 1430 kg.m^{-3} . The length of material sample is 0.2 m. The space and time increments, boundary heat fluxes, total measurement time and measurement time step are taken identically as in the numerical example. Realistic physical values of thermal conductivity as function of temperature with just boundary temperature measurements are showed on Fig. 2.

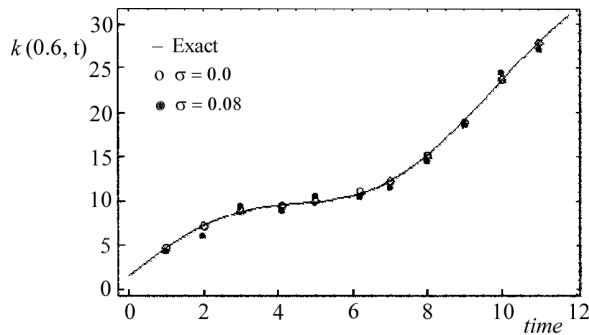


Fig. 1 Exact and estimated values of $k(T)$ at $x = 0.6$

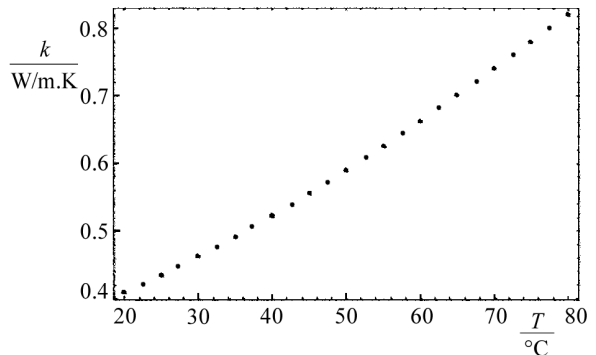


Fig. 2 Realistic physical values of thermal conductivity as function of temperature

5 Conclusion

The conjugate gradient method is applied for the solution of the inverse problem to determine the temperature-dependent thermal conductivity without the necessity of using interior sensors. The measurement errors do not amplify the errors of estimated thermal conductivity, and therefore, the present technique provides a confident estimation.

References

- [1] Constales D, Automatic differentiation in LSODA. In preparation.
- [2] Alifanov O M, 1972 Solution of an inverse problem of heat conduction by iteration methods. *J. Engineering Physics*, **26**, 471-476 (in russian).
- [3] Budak B, Vasilev F, 1969 Numerical methods in optimization equations, Moscow, MGU, 1969 (in russian)
- [4] Jarny Y, Ozisik M N, Bardon J P, 1991 A general method using adjoint equation for solving multidimensional inverse heat conduction. *Int. J. Heat Mass Transfer* **34**, 2911-2919

UNCERTAINTY OF THE THERMAL CONDUCTIVITY MEASUREMENT BY THE TRANSIENT HOT WIRE METHOD

Gabriela Labudová¹, Vlasta Vozárová²

¹ Department of Physics, Faculty of Natural Sciences, Constantine the Philosopher University, Tr. A. Hlinku 1, SK-94974 Nitra, Slovakia

² Department of Physics, Faculty of Mechanical Engineering, Slovak Agricultural University, Tr. A. Hlinku 2, SK-94976 Nitra, Slovakia

Email: glabudova@ukf.sk, vozarova@afnet.uniag.sk

Abstract

This paper deals with uncertainty analysis of the thermal conductivity measurement using the transient hot wire method. The characterization is made on the sample of low-density, polyethylene BRALEN SA 200-22. The measurements are performed on the air at the room temperature. The sources of measurement errors are analyzed and uncertainty of the measured value of the thermal conductivity is evaluated. The analysis shows that the combined standard uncertainty of the thermal conductivity measurement is about $\pm 3.3\%$ for 68 % confidence level.

Key words: transient hot wire method, thermal conductivity, components of the uncertainty

1 Introduction

The reliability of every measurement confirms a quantitative statement of its uncertainty that accompanies it. General rules for evaluating and expressing uncertainty in measurement, which can be followed at various levels of accuracy, have been established as the GUM method (Guide to the Expression of Uncertainty in Measurement) [1,2]. The method has been adopted by various regional metrology and related organizations worldwide.

The GUM approach has been followed in expressing the uncertainty of an estimation of several thermophysical properties including the thermal conductivity using the transient hot strip technique [3] or the guarded hot plate technique [4] as well as the thermal diffusivity using the laser flash method [5].

Here we present uncertainty analysis of the thermal conductivity measurement using the transient hot wire method [6], which is a standard test method of the measuring the thermal conductivity.

2 Classification of uncertainty components

Every measurement is affected by measurement errors that cause the difference between the measured value of the estimated property (in our case the thermal conductivity) and its true value. The true is only an approximation of the value subjected to the measurement.

The uncertainty of the result of a measurement consists of several components, which may be grouped into two categories according to the method used to estimate their values:

Type A standard uncertainties are evaluated by the statistical analysis of series of observations.

Type B evaluation of standard uncertainty is usually based on scientific judgment using all the available relevant information, which may include previous measurement data.

All the individual uncertainties of the result measurement can be combined. *The combined standard uncertainty* $u_c(y)$ of a measurement result y is obtained by combining the individual standard uncertainties u_i arising from a Type A or a Type B evaluation. Taking a first order Taylor series approximation of the measurement equation $Y = f(X_1, X_2, \dots, X_N)$ the equation referred to as the law of propagation of uncertainty can be received in the form

$$u_c^2(y) = \sum_{i=1}^N \left(\frac{\partial f}{\partial x_i} \right)^2 u_i^2 + 2 \sum_{i=1}^{N-1} \sum_{j=i+1}^N \frac{\partial f}{\partial x_i} \frac{\partial f}{\partial x_j} u_{i,j} \quad (1)$$

The partial derivatives of f with respect to the x_i are sensitivity coefficients, u_i is the standard uncertainty associated with the input estimate x_i ; and $u_{i,j}$ is the estimated covariance associated with x_i and x_j . If the probability distribution characterized by the measurement result is approximately normal (Gaussian), then it is believed with an approximate level of confidence of 68 % that the measurement result (measurand Y) can be written as $Y = y \pm u_c(y)$.

The expanded uncertainty U is the measure of uncertainty which can be obtained by multiplying $u_c(y)$ and by a coverage factor k and it is confidently believed that $Y = y \pm U$. When the normal distribution applies and u_c is a reliable estimate of the standard deviation of y , $U = 2u_c$ (i.e., $k = 2$) defines an interval having a level of confidence of approximately 95 % and when $U = 3u_c$ (i.e., $k = 3$) a level of confidence is greater than 99 %.

3 Hot wire method

The ideal analytical model assumes an ideal - infinite thin and infinite long line heat source (hot wire), operating in an infinite, homogeneous and isotropic material with uniform initial temperature T_0 . If the hot wire is heated since the time $t = 0$ with constant heat flux q per unit wire length, the radial heat flow around the wire occurs. The temperature rise $\Delta T(r,t)$ in any distance r from the wire as a function of time describes the simplified equation [7]

$$\Delta T(r,t) = \frac{q}{4\pi k} \ln \frac{4at}{r^2 C} \quad (2)$$

where k is the thermal conductivity, a thermal diffusivity and $C = \exp(\gamma)$, with γ the Euler's constant. The thermal conductivity is calculated from the slope S of the temperature rise $\Delta T(r,t)$ vs. natural logarithm of the time $\ln t$ evolution using the formula

$$k = \frac{q}{4\pi S} \quad (3)$$

The hot wire method can be applied in several experimental modifications [8].

4 Experimental apparatus

The utilized computer-controlled experimental apparatus, that allows the determination of the thermal conductivity of solid, powders and granular materials is described in details elsewhere [9]. It allows to utilize one of three measurement techniques: standard (cross) wire technique, resistance potential lead method and the probe modification of hot wire method.

In the present study results of measurement obtained using the cross technique are analyzed. A wire cross is embedded in ground grooves between two equally sized samples. The cross consists of a linear heat source - the kanthal wire 0.4 mm in diameter (Bulten Kanthal AB) and of a spot welded thermocouple, K type, made from Ni-NiCr wires (Heraeus) 0.1 mm in diameter which acts as the temperature sensor. The hot spot of the thermocouple is in the direct contact with the heating wire and it is placed in the center of the sample. The cold junction is put on the reference place in Dewar cup at 0°C.

The current flowing through the heating wire is produced by the stabilized regulated direct current supply Z-YE-2T-X (Mesit) operated by PC via remote control unit JDR-1 (Mesit). High resolution data acquisition board PCL-818HG (Advantech) with lock in pre-amplifier Z-35 (Metra) is used for serial measurements of transient *emf* of the thermocouple, and the transient voltage corresponding to temperature rise. A proportional feedback temperature controller practices the temperature regulation of the electro-resistive furnace. The apparatus allows measurement on air or in a controlled environment, under atmospheric pressure, in the temperature range from room temperature up to 1200 °C.

5 Samples and experimental results

The measurements have been performed on the plastic samples made of low-density polyethylene (BRALEN SA 200-22). The Research Institute for the Processing and the Application of the Plastic Materials (VUSAPL Nitra) has prepared the samples from granulates produced by Slovnaft. The 'wire cross' was embedded between two sample blocks of 50 times 100 times 100 mm. The thermal contact was improved using the silicon sink compound paste (Dow Corning 340). We have performed measurement utilizing two different currents – 0.6 and 0.7 A. The measurements were performed at room temperature, on air under atmospheric pressure. Fig. 1 presents typical temperature rise vs. time evolution.

Achieved thermal conductivity results for two independent sets of measurements and calculated standard deviations are summarized in the Tab.1. The thermal conductivity values presented there are values calculated for each measurement as the average of five values obtained from a least-squares-fit of the linear part of recorded temperature rise vs. time data.

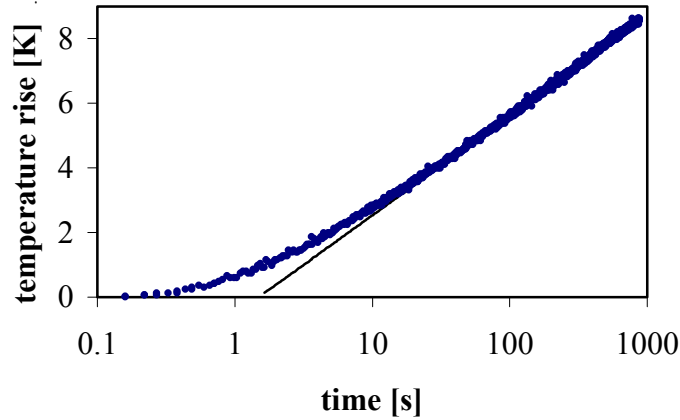


Fig. 1 Typical experimental temperature rise vs. time data and its least-squares-fit

To compare achieved results of the thermal conductivity of the test material (from the same sample) has been measured on the guarded heat flow meter installed in the Austrian Research Centers in Seibersdorf. These values have been taken as the reference values in the measurement.

Table 1. Results of the thermal conductivity measurement and their comparison

No	k [Wm ⁻¹ K ⁻¹]	U [Wm ⁻¹ K ⁻¹]	u [%]	k_{ref} [Wm ⁻¹ K ⁻¹]
1	0.318	0.0121	3.08	0.319
2	0.312	0.0034	1.07	0.314
mean	0.315			0.317

We see very good agreement with the recommended values k_{ref} – values obtained independently in another laboratory.

6 Uncertainty analyses

The thermal conductivity is obtained estimating the slope of the measured temperature rise vs. time evolution in logarithmical scale over a defined time interval using the transient hot wire method. The sources of uncertainties in the thermal conductivity measurement are connected with the measurement of the temperature, stability of the time axis and stability of the power supply. The main sources of the non-measurement errors cause differences between the real conditions and the assumptions of the analytical model i.e., that the heating wire has finite non-zero diameter and the real heat capacity, that there is a thermal barrier between the wire and the sample, between the temperature sensor and the wire, that the sample and the wire have finite dimensions and that there the heat exchange between the sample surface may occur. The random component of the uncertainty is evaluated statistically analyzing the repeated measurement.

6.1 Type A uncertainty

The relative standard deviation values in Table 1 represent the A Type uncertainties. It can be concluded that 3.1 % is the value that well represents the A Type uncertainty component.

6.2 Type B uncertainty

Because of several sources of this type of uncertainty, they will be discussed individually.

Measurement errors

Temperature measurement, time base stability, power supply

The temperature is measured using the K type thermocouple made from spot-welded Ni-NiCr wires. Manufacturer specifies the typical accuracy better than 0.4 % of the measured value. If we take account of the uncertainties the thermocouple *emf* measurement that is in accordance with the PCL-818HG data acquisition board manufacturer of order 0.08 % we may estimate the uncertainty of the temperature measurement at value 0.5 %. It is supposed that the effect causes mainly systematic error in the temperature measurement. We can guess that the uncertainty of the thermal conductivity is about 0.1 %.

The time base is based on the PCL-818HG data acquisition board time system. The manufacturer specifies the stability and the uncertainty better than 0.01 %. The influence is so small that we do not have to consider it as a source of the thermal conductivity uncertainty.

The current is produced by the stabilized power source Z-YE-2T-X working in the stabilized current supply mode. Manufacturer specifies the current stability at level of 0.05 %. The influence on the thermal conductivity uncertainty is then 0.1 %.

Non-measurement errors

Deviations of real experimental conditions from the ideal analytical model considered in the theory cause deformation of the temperature rise curve.

Non-linearity of the beginning and of the end of the graph of $\Delta T(r,t)$ vs. $\ln t$.

Non-linearity of the initial part of the data is caused by finite radius and non-zero heat capacity of the wire and similar influence has the thermal contact resistance between the hot wire and the sample and between the hot wire and the temperature sensor. To overcome this we need to find the certain minimum time t_{\min} , which corresponds to the beginning of the linear part of the curve. The time t_{\min} can be determined either analytically - calculated with respect of the complex theory [9]. In our approach we utilize interactive calculating of the time t_{\min} searching the linear part of graph of temperature rise against natural logarithm of the time. We can not directly evaluate the uncertainty of the thermal conductivity estimation caused by these effects. We try to eliminate these effects experimentally (using of thin wires, by improvement of the thermal contact using a silicon paste). Because of the way of the data reduction based on the checking of the least-squares fit of the data to the analytical model, we suppose that uncertainty is included in the random uncertainty (presented as the A Type).

Deformation of the end of experimental curve is caused mainly as a result of finite dimensions of the sample and finite length of the hot wire. Heat exchange at the sample surface can be eliminated when the thermal conductivity value is calculated from the least squares fitting on the linear part of the curve $\Delta T(r,t)$ vs. $\ln t$. Similar like time t_{\min} , the maximal time t_{\max} can be calculated analytically or could be find by an interactive searching [9]. In our experiment we use the second approach. To eliminate the other boundary effects experimentally we use relatively large samples. We eliminate the influence of the finite length of the hot wire by the measurement of the temperature evaluation in the center of the sample. We consider that the influence of the accuracy of the measurement on these effects is in our case negligible.

All the A and B Type components of the uncertainty are considered to be independent. Using the law of uncertainty propagation (Eq. 1) we can assure the combined standard uncertainty of the thermal conductivity better than 3.3 %.

7 Conclusion

The study presents the uncertainty analysis of the thermal conductivity measurement using the transient hot wire method. The performed series of test measurements on the plastic sample BRALEN SA 200-22 on air at room temperature show that the combined standard uncertainty of the thermal conductivity measurement is better than 3.3 % within 68 % confidence level.

Acknowledgement

Authors wish to thank the Slovak Science Grant Agency for the financial support under the contract 1/6115/99.

References

- [1] Guide to the Expression of Uncertainty in Measurement (GUM), ISO - TAG 4, WG 3, 1993
- [2] B N Taylor and C E Kuyatt, 1994 Guidelines for Evaluating and Expressing the Uncertainty of NIST Measurement Results, NIST Technical Note 1297, NIST
- [3] U Hammerschmidt and W Sabuga, 2000 Transient Hot Strip (THS) Method: Uncertainty Assessment, *Int. J. Thermophys.* **21** 217-248
- [4] U Hammerschmidt, Messunsicherheit bei Wärmeleitfähigkeitsbestimmungen mit dem Plattengerät, PTB, Braunschweig, (report)
- [5] D E Stroe and A Millea, 2000 Metrological Evaluation of a High Temperature Laser Flash Thermal Diffusivity Instrument, *14th Symp. on Thermophys. Prop.*, (Boulder, CO, USA) to be published
- [6] A L Schieirmacher, 1988 *Ann. Phys. Chem.* **34** 623
- [7] H S Carslaw and J C Jaeger, 1959 *Conduction of Heat in Solid*, 2nd. Ed., (Oxford Univ. Press, Oxford)
- [8] J de Boer, J Butter, B Grosskopf and P Jeschke, 1980 Hot Wire Technique for Determining High Thermal Conductivities, *Refract. J.* **22** 1-6
- [9] L Vozár, 1996 A Computer-Controlled Apparatus for Thermal Conductivity Measurement by the Transient Hot Wire Method, *J. Therm. Anal.* **46** 495-505

MODELLING OF THE THERMAL CONDUCTIVITY PROPERTIES OF ULTRA-THIN LAYERS 1-DIMENSIONAL CASE

Aba Teleki

Department of Physics, Faculty of Natural Sciences, Constantine the Philosopher University, Tr. A. Hlinku 1, SK-94974 Nitra, Slovakia
Email: ateleki@ukf.sk

Abstract

We assume constant and homogenous thermal properties characterizing our physical system. In this case we can define boundary conditions modelling a time dependent source, acting on the boundary with a non-perfect thermal contact between two massive layers. We show below that some assumptions about the entropy of the boundary (an ultra-thin layer in real a case) give the third kind of Dirichlet's boundary conditions in the form $k_- \partial_x T_-(0^-, t) + h_{\mp} [T_-(0^-, t) - T_+(0^+, t)] = V(t)$. After combining several ultra-thin layers the structure of the function $V(t)$ may be very complicated. In any case the integrated heat-source $V(t)$ consists of linear combinations of heat-sources acting on individual ultra-thin layers only.

Key words: layered structures, thermal contact resistance, heat source on a boundary

1 Introduction

Let us have a system of plan-parallel slides (infinitely extended in directions of planes). The thermal characteristics inside of any slide are constant and homogenous (such thermal conductivity, thermal diffusivity, etc.). We consider a system with three layers indexed by 1, 2 and 3 (thermal properties of layers are indexed accordingly to the slides). The boundary between layers k and l is indexed as kl ($k, l = 1, 2, 3$) and are considered to be constant and homogenous too.

In this case we can write the equations of the heat transfer through the system in the form

$$\partial_{xx} T_j(x, t) - \alpha_j^{-1} \partial_t T_j(x, t) + k_j^{-1} g_j(x, t) = 0, \quad j = 1, 2, 3, \quad (1)$$

$$h_{j,j+1}^{-1} k_j \partial_x T_j(x, t) + [T_j(x_{j,j+1}^-, t) - T_{j+1}(x_{j,j+1}^+, t)] = 0, \quad j = 1, 2 \text{ and} \quad (2)$$

$$k_j \partial_x T_j(x_{j,j+1}^-, t) - k_{j+1} \partial_x T_{j+1}(x_{j,j+1}^+, t) = 0, \quad j = 1, 2, \quad (3)$$

with initial conditions

$$T_j(x, 0) \equiv F_j(x), \quad j = 1, 2, 3. \quad (4)$$

Here $T(x, t)$ denotes temperature, $g(x, t)$ heat source, α thermal diffusivity, k thermal conductivity and h heat-transfer coefficient. We use the abbreviation

$$L(\xi^+) \stackrel{\text{def}}{=} \lim_{\varepsilon \rightarrow 0} L(\xi + \varepsilon) \quad \text{and} \quad L(\xi^-) \stackrel{\text{def}}{=} \lim_{\varepsilon \rightarrow 0} L(\xi - \varepsilon), \quad (\varepsilon > 0), \quad (5)$$

for any form L .

In some cases, it is possible to describe the modelling of non-trivial thermal properties on the boundaries between two adjoining layers in one-dimensional multi-layer system.

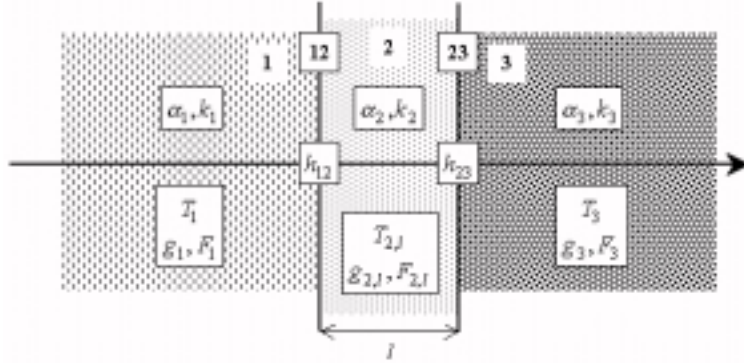


Fig 1 Ultra-thin layer bounded by two massive layers.

One of the most straightforward methods of modelling nontrivial thermal properties of a boundary is the modelling shown by Landau [1]. Landau assumed zero initial temperature in all layers ($F_j(x) \equiv 0$) and perfect heat conduction between the layers ($h_{j,j+1}^{-1} = 0$, $j = 1, 2$). He considered layer 2 with thickness $l \equiv x_{23} - x_{12}$ and with heat source $g_2(x, t)$ acting on it. In case $l \rightarrow 0$ the influence of the layer 2 is reduced to new boundary conditions between layer 1 and 3

$$T_1(x_{13}^-, t) - T_3(x_{13}^+, t) = 0, \quad (6)$$

$$k_1 \partial_x T_1(x_{13}^-, t) - k_3 \partial_x T_3(x_{13}^+, t) = g_2(t) \stackrel{\text{def}}{=} \lim_{l \rightarrow 0} \int_{x_{12}}^{x_{23}+l} dx g_2(x, t). \quad (7)$$

It is easy to see that the boundary conditions

$$k_j \partial_x T_j(x_{j,j+1}^-, t) + T_j(x_{j,j+1}^-, t) = f_{j,j+1}(t), \quad k_{j+1} \partial_x T_{j+1}(x_{j,j+1}^+, t) + T_{j+1}(x_{j,j+1}^+, t) = f_{j,j+1}(t) \quad (8)$$

used by Özisik is the same as (6) and (7), where f represents the heat source acting on the boundary $j, j+1$. Özisik considered (as in [1] too) the $h_{j,j+1}^{-1} = 0$ cases only.

2 One simple nontrivial case

We consider a multi-layer system with 3 layers described in Introduction. Let us have nontrivial conductivity properties ie.

$$h_{12}^{-1} \neq 0 \quad \text{and} \quad h_{23}^{-1} \neq 0. \quad (9)$$

Remark 1 We assume, that $T_j(x,t), \mathcal{G}_j(x,t) \in C^\infty(I_j \times R_+)$ and $F_j(x) \in C_0^\infty(I_j)$, where $I_j \equiv (x_{j-1}, x_{j,j+1})$, $R_+ \equiv (0, \infty)$ and $C^\infty(I)$ is the set of functions with continuous derivatives of all order on the set I . We denote $C_0^\infty(I)$ all functions from $C^\infty(I)$ which have a compact support on the set I .

These properties of $T(\cdot)$ are not real restrictions from the physical point of view. We can extend all our conclusions of $T(\cdot)$ -s to the domain of appropriate closed differential form. This domain is a subset of the closure $\overline{C^\infty(I)} = L^2(I)$. ■

Integrating the equation (1) for the middle layer ($j = 2$) on the interval $\langle x_{12}, x_{23} \rangle$ we obtain (for a given time $t > 0$)

$$\begin{aligned} & \int_{x_{12}}^{x_{23}} dx [\partial_x T_2(x,t) - \alpha_2^{-1} \partial_t T_2(x,t) + k_2^{-1} \mathcal{G}_2(x,t)] = \\ & = -\partial_x T_2(x_{12}^+, t) + \partial_x T_2(x_{23}^-, t) + k_2^{-1} \mathcal{G}_2(t) - \alpha_2^{-1} \int_0^t dx \partial_t T_2(x,t) = 0 \end{aligned} \quad (10)$$

where $x_{12} = 0$.

Combining the equations (3) for $j = 1$ and $j = 2$ with (10) we find

$$k_1 \partial_x T_1(x_{12}^-, t) - k_3 \partial_x T_3(x_{23}^+, t) = \mathcal{G}_2(t) - k_2 \alpha_2^{-1} \int_0^t dx \partial_t T_2(x,t). \quad (11)$$

Equation (2), for $j = 2$ gets replaced by

$$h_{23}^{-1} k_3 \partial_x T_3(x_{23}^+, t) - [T_2(x_{23}^-, t) - T_3(x_{23}^+, t)] = 0, \quad (12)$$

and combining with (2) for $j = 1$ we obtain

$$h_{12}^{-1} k_1 \partial_x T_1(x_{12}^-, t) + h_{23}^{-1} k_3 \partial_x T_3(x_{23}^+, t) + [T_1(x_{12}^-, t) - T_3(x_{23}^+, t)] = T_2(x_{12}^+, t) - T_2(x_{23}^-, t). \quad (13)$$

Using (11) it is easy to see that we can rewrite (13) as

$$\begin{aligned} & k_1 \partial_x T_1(x_{12}^-, t) + k_3 \partial_x T_3(x_{23}^+, t) + h_{13} [T_1(x_{12}^-, t) - T_3(x_{23}^+, t)] = \\ & \tilde{h}_{13} \mathcal{G}_2(t) - \tilde{h}_{13} k_2 \alpha_2^{-1} \int_0^t dx [\partial_t T_2(x,t)] + h_{13} [T_2(x_{12}^+, t) - T_2(x_{23}^-, t)] \end{aligned} \quad (14)$$

where

$$h_{13}^{-1} = \frac{1}{2} (h_{12}^{-1} + h_{23}^{-1}) \quad \text{and} \quad \tilde{h}_{13} = \frac{1}{2} (-h_{12}^{-1} + h_{23}^{-1}). \quad (15)$$

We express the simplest nontrivial case using the conditions

$$\Delta_2^-(t) \stackrel{\text{def}}{=} \lim_{l \rightarrow 0} \left\{ k_2 \alpha_2^{-1} \int_0^l dx [\partial_t T_2(x,t)] \right\} = 0 \quad \text{for } t > 0, \quad \text{and} \quad (16)$$

$$\Delta_2^+(t) \stackrel{\text{def}}{=} \lim_{l \rightarrow 0} \{ h_{13} [T_2(x_{12}^+, t) - T_2(x_{23}^-, t)] \} = 0 \quad \text{for } t > 0. \quad (17)$$

Remark 2 Temperature $T_2(x, t)$ depends on l as well and the answer to the question of existence of these limits is complicated in a general case. From a physical point of view equation (16) becomes true if sources g_j ($j = 1, 2, 3$) vary slowly in time so that the relaxation period in the super-thin layer (layer 2) is negligibly small in comparison with changes of the heat source. ■

Using our assumption in Remark 1 that $T_2(x, t) \in C^\infty((0, l) \times \mathbb{R}_+)$ for any l there exists some $\xi_1 \in (0, l)$ for which

$$\int_0^l dx \partial_x T_2(x, t) = \int_0^l dx \partial_x T_2(\xi_1, t) = \partial_x T_2(\xi_1, t). \quad (18)$$

Now, we can write

$$\Delta_2^-(t) = k_2 \alpha_2^{-1} \lim_{l \rightarrow 0} \{\partial_x T_2(\xi_1, t)\}. \quad (19)$$

Remark 3 In (18) and (19) ξ_1 depends on l , therefore the identity $\Delta_2^-(t) \equiv 0$ may be false in general. ■

Now look at the equation (17). There is physical reason for the validity of (17). For an individual atom it is not correct to define properties such as temperature. We cannot define left hand side or right hand side temperature for one atom. Therefore the limit in (17) has no good interpretation for a layer with thickness of an atom.

On the other hand, this layer may consist a macroscopic set of atoms. This mass of atoms may cumulate heat and has well-defined entropy. This gives a possibility to introduce the temperature for this layer with thickness of one atom unambiguously. This is the only temperature with what one can characterize the layer. No left or right hand side temperatures there exist.

Therefore we write

$$\lim_{l \rightarrow 0} \{T_2(0, t) - T_2(l, t)\} \quad \text{and} \quad \Delta_2^+(t) \equiv 0. \quad (20)$$

Therefore we can rewrite the boundary conditions (11) and (14) into the relation joining the layers 1 and 3 immediately

$$k_1 \partial_x T_1(0^-, t) - k_3 \partial_x T_3(0^+, t) = G_2(t), \quad t > 0 \quad (21)$$

$$h_{13}^{-1} k_1 \partial_x T_1(0^-, t) + h_{13}^{-1} k_3 \partial_x T_3(0^+, t) + [T_1(0^-, t) - T_3(0^+, t)] = \tilde{h}_{13}^{-1} G_2(t), \quad t > 0, \quad (22)$$

where is

$$G_2(t) \stackrel{\text{def}}{=} g_2(t) - \Delta_2^-(t). \quad (23)$$

The more symmetric form of these boundary conditions (similar to the Özisik kind of boundary conditions) is

$$h_{13}^{-1} k_1 \partial_x T_1(0^-, t) + [T_1(0^-, t) - T_3(0^+, t)] = h_{23}^{-1} G_2(t) \quad (24)$$

$$h_{13}^{-1} k_3 \partial_x T_3(0^+, t) + [T_1(0^-, t) - T_3(0^+, t)] = -h_{12}^{-1} G_2(t) \quad (25)$$

Remark 4 The modified source $G_2(t)$ consists of two parts. The first one described by the classical heat source $g_2(t)$ acting on the system; and a second one characterized by the heat accumulation properties of the ultra-slim layer 2. ■

3 Combining simple nontrivial cases

In this section we construct the final form of the modelling of the ultra-thin layer. We assume 5 layers, where layer 2 and 4 are ultra-thin, and layer 3 is free of any heat source, i.e. $g_3(x,t) \equiv 0$. (26)

After some simple calculations we obtain

$$h_{15}^{-1}k_1\partial_x T_1(0^-,t) + [T_1(0^-,t) - T_3(0^+,t)] = h_{13}(h_{15}^{-1}h_{23}^{-1} + h_{12}^{-1}h_{35}^{-1})G_2(t) - h_{45}^{-1}G_4(t), \quad (27)$$

$$h_{15}^{-1}k_5\partial_x T_5(0^-,t) + [T_3(0^-,t) - T_5(0^+,t)] = -h_{12}^{-1}G_2(t) + h_{35}(h_{13}^{-1}h_{45}^{-1} - h_{15}^{-1}h_{34}^{-1})G_4(t). \quad (28)$$

where

$$h_{35}^{-1} = \frac{1}{2}(h_{34}^{-1} + h_{45}^{-1}) \quad \text{and} \quad h_{15}^{-1} = h_{13}^{-1} + h_{35}^{-1} \quad (29)$$

and $G_4(t)$ is defined on layer 4 similarly as $G_2(t)$ on layer 2. The result does not depending on the dimension $l_3 \stackrel{def}{=} (x_{34} - x_{23})$ and we can calculate the limit $l_3 \rightarrow 0$ easily.

It is easy to see, that the right hand side of (27) and (28) are linearly independent. We obtained the most general form of boundary conditions deduced from the simple case

$$k_- \partial_x T_-(0^-,t) + h_- [T_-(0^-,t) - T_+(0^+,t)] = V(t), \quad t > 0 \quad (30)$$

$$k_- \partial_x T_-(0^-,t) - k_+ \partial_x T_+(0^+,t) = W(t), \quad t > 0. \quad (31)$$

where the sign “-” respectively “+” signed the “left hand side” respectively “right hand side” of the boundary. The functions $V(t)$ and $W(t)$ are one’s like (with respect the Remark 1). Combining more ultra-thin layers into the ultra-thin system will not change the structure of (30) and (31). From (27) and (28) it is easy to see, that $V(t)$ and $W(t)$ represent some linear combination of elementary heat-sources $g_n(t)$ acting on individual ultra-thin layers only.

4 Conclusion

A physically important case has been presented here. Source acting on a boundary with nontrivial thermal parameters generates more general boundary conditions for thermal conductivity. Our meaning of nontrivial thermal parameters on boundary is non-perfect thermal contact between two layers.

The general structures of boundary conditions lead us to non-continuous temperatures on the boundary. This is similar to the situation presented in (7), where the continuity of x -derivative of the temperature is broken.

This is not critical in the sense that the differential form (1) has a closure. Boundary conditions (7), (30) and (31) present limit cases of real physical situations only. They are unique and well defined in the sense of closed differential form (1). We can use them safely reflecting to the Remark 1.

Acknowledgement

Author wishes to thank the Slovak Science Grant Agency for the financial support under the contract 1/6115/99.

References

- [1] Landau L D and E M Lifshitz *Hydrodynamics*, Pergamon, Tarrytown, New York, 1980, §50
- [2] Özisik M H *Radiative Transfer and Interactions with Conduction and Convection*, Wiley Interscience, New York, 1973

HIGH-TEMPERATURE ALUMINA ROD DILATOMETER

Igor Štubňa, Libor Vozár

Department of Physics, Faculty of Natural Sciences, Constantine the Philosopher University, Tr. A. Hlinku 1, 949 74 Nitra, Slovakia

Abstract

A new vertical difference dilatometer has been developed for the temperature region of 20 – 1000 °C. This dilatometer is constructed from alumina rods passing through an oven. A difference transformer acting as a linear displacement transducer is on one side of the rods, and a zeroing screw is on the opposite side. The dilatometer is calibrated by sapphire etalon. The dilatometer's sensitivity is around $1 \cdot 10^{-7}$ m.

1 Introduction

Linear thermal expansion coefficient (LTEC) α is an important performance property of a material. Thermal expansion of the sample is, in general, influenced by structure, chemical composition of the material and temperature. An experimental study of the influence of the temperature on thermal expansion (called thermodilatometry) records the changes of the structure on a dilatometric curve [1, 2]. For more complex understanding of these changes it is useful to combine thermodilatometry with a measurement of further physical parameters [3].

Linear thermal expansion coefficient (LTEC) α is introduced by a definition

$$\alpha = \frac{1}{l_0} \frac{dl}{dt} \quad , \quad (1)$$

where l_0 is an initial length of the sample, and dt is a sufficiently short temperature interval. In practice it is 1 – 5 °C [2]. As it follows from Eq. (1), the LTEC cannot be measured at one temperature but a temperature interval must be taken. Then LTEC can be calculated for such interval

$$\alpha_{1-2} = \frac{1}{l_1} \frac{l_2 - l_1}{t_2 - t_1} \quad , \quad t_2 > t_1 \quad , \quad (2)$$

where l_1, l_2 is the length of the sample at the temperature t_1, t_2 respectively.

Absolute or relative methods are used for experimental determination of the relative thermal expansion $\Delta l/l_1$ (RTE). The principle of the absolute method is based on a direct measurement of the position of the sample ends. It needs optical apparatus, mostly an interferometer, for solving this task [2]. Relative methods are, in fact, differential methods and usually compare the RTE of the measured sample to the RTE

of the sample made from a reference material. Commonly used reference materials are silica glass (for $t < 800$ °C) and alumina (for higher temperatures) [1, 2].

Let us assume that the initial length of both samples is identical at the room temperature t_0 and an output signal of the linear displacement pickup Δp is set to zero. The value of Δp is a function of the difference between the sum of lengths of the sample l_x and the piston l_1 on the one side, and the sum of lengths of the reference sample l_r and rod l_2 on the other side

$$(l_1 + l_x) - (l_2 + l_r) = \Delta p = 0 \quad . \quad (3)$$

At the temperature t we have

$$[(l_1 + \Delta l_1) + (l_x + \Delta l_x)] - [(l_2 + \Delta l_2) + (l_r + \Delta l_r)] = \Delta p \neq 0 \quad , \quad (4)$$

where Δl_1 , Δl_x , Δl_2 , Δl_r , are expansions of the piston, the measured sample, the rod and the reference sample respectively. The piston and the rod are made from the same material, and their lengths at the temperature of t_0 can be considered equal. Then $l_1 = l_2$ and $\Delta l_1 = \Delta l_2$. Because the initial lengths of both samples were the same, we can rewrite Eq. (4) as

$$\Delta l_x - \Delta l_r = \Delta p \quad . \quad (5)$$

This equation is suitable only for an ideal dilatometer which keeps $\Delta p = 0$ over the used temperature course if two reference samples are in the dilatometric cell. In such a case the transducer usually gives a non-zero output signal Δp_0 , which must be subtracted from Δp . We can determine the RTE from equation

$$\frac{\Delta l_x}{l_0} = \frac{\Delta p - \Delta p_0}{l_0} + \frac{\Delta l_r}{l_0} \quad , \quad (6)$$

where l_0 is the initial length of the sample at the temperature t_0 . The value Δp is measured, the function $\Delta p_0(t)$ is previously experimentally determined, and the function $\Delta l_r/l_0(t)$ is known.

To complete the Thermophysical Laboratory at Constantine the Philosopher University, a new simple, low-cost differential dilatometer was designed and constructed. This dilatometer is described below.

2 Dilatometer

The dilatometric system is designed from aluminum rods (Degussa, Germany). Both ends of four rods are firmly attached to duraluminium blocks. This supporting construction is vertically oriented. The differential induction transducer (INPOS, CR), which measures the linear displacement, is fixed to the upper block. The transformer core is not fixed and freely passes through the coils of the transformer. The core is in a

mechanical contact with the upper end of the piston of the dilatometer. The supporting rod is inserted in the lower block. This supporting rod lies on the zeroing screw. The measured sample is put between the piston and supporting rod. The piston and the supporting rod are also made from aluminum rods. The scheme of the dilatometric system is shown in Fig. 1.

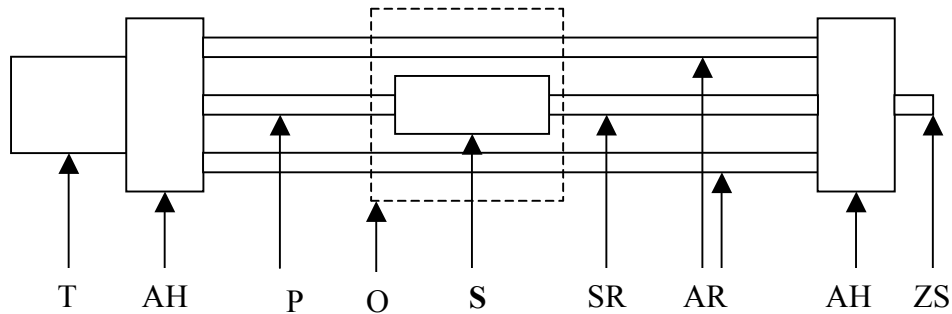


Fig. 1 – Construction of the dilatometer. T – transducer, AH – aluminium holders, P – piston, S – sample, SR – supporting rod, AR – alumina rods, ZS – zeroing screw, O - oven

The zeroing screw carries the supporting rod, the sample, the piston and the transformer core. The whole system can be moved in a vertical direction with help of the zeroing screw, performing rough zero setting. A wide shift of the zero screw permits to use samples with a length of 18 – 22 mm. The fine set of zero can be reached with a complementary electrical scheme on the output of the transducer.

The dilatometric system is combined with an oven made from porous alumina bricks (Alporit, CR) and SiC heating rods (Silit, Germany). Six heating rods are connected in series and supplied from the autotransformer. A secondary current is controlled by a temperature PI programmer. Temperature is measured by a chromel – alumel thermocouple in proximity of the sample. The oven is in an aluminum enclosure.

The dilatometer is connected to a computer, which performs the following functions:

a) control of the temperature regime, b) measurement and acquisition of the output signal of the transducer, c) measurement and acquisition of the temperature, d) plotting the dilatometric curve during the experiment.

3 Results

As it follows from Eq. (6), the dependence of the RTE of the reference sample (made from aluminum rod in our case) on the temperature has to be known. To calculate the RTE we need to know the temperature relationship of the zero signal Δp_0 . This relationship can be experimentally found with the help of the sample made from alumina rod. Another way, which we used to correct the transducer output signal, is measuring the sapphire etalon sample (delivered from NII of Metrology, Leningrad, together with temperature dependence of RTE). The RTE of the sapphire etalon can be expressed by a polynomial

$$\frac{\Delta l}{l_0} = -8 \times 10^{-1} t^3 + 3 \times 10^{-6} t^2 + 5.8 \times 10^{-3} t - 0.1556 \quad (7)$$

The dilatometric curve of the sapphire etalon sample obtained by our dilatometer can be fitted by a function

$$\frac{\Delta p}{l_0} = (-2 \times 10^{-11} t^3 + 9 \times 10^{-9} t^2 + 6 \times 10^{-5} t - 0.002) \frac{k}{l_0}, \quad (8)$$

where $k = 2.8435$ mm/V is an experimentally found coefficient. From comparing Eq. (7) with Eq. (8) we obtain the correction function. This correction takes into account the “zero dilatometric curve” as well as the alumina rod correction. The corrected values of the RTE can be calculated using a formula

$$\frac{\Delta l_x}{l_0} = \left[U + (1 \times 10^{-11} t^3 + 1 \times 10^{-8} t^2 - 2 \times 10^{-5} t + 0,009) \right] \frac{k}{l_0}, \quad (9)$$

where U is a transducer voltage output.

As an example, a dilatometric measurement of the unfired electroceramic sample was carried out. The sample of the length of $l_0 = 20$ mm and diameter of 3 mm was made from a mixture of quartz (25 %), kaolin (50 %) and feldspar (25 %). The dilatometric curve shows that typical consequences of phase changes occurred during the firing of such ceramics (dehydroxylation, $\alpha \rightarrow \beta$ change of quartz, creation of spinel phase), Fig. 2. This curve is in a good agreement with the one measured by a quartz differential dilatometer [3].

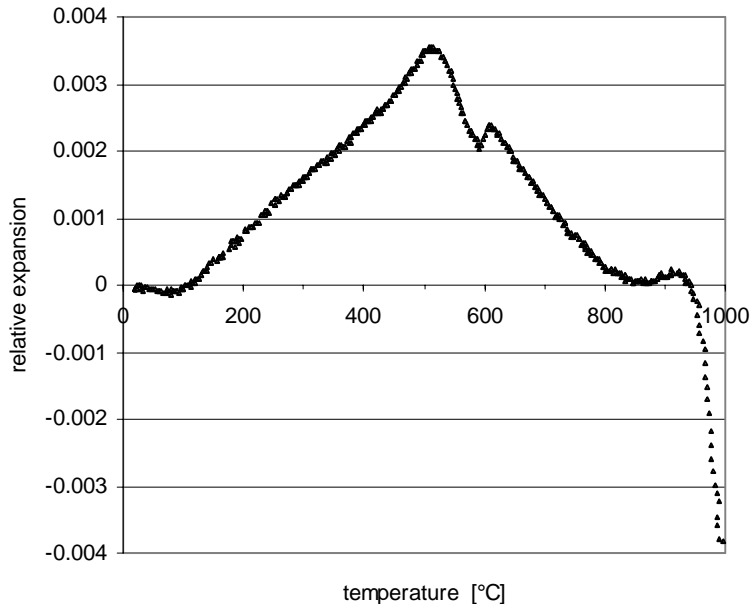


Fig 2 – Dilatometric curve of the unfired electroceramic sample.

Acknowledgement

Authors wish to thank the Slovak Science Grant Agency for the financial support under the contract 1/6115/99.

References

- [1] Brož P et al, 1985 *Základy fyzikálního měření I*. Praha, SNTL
- [2] Mazurin OV et al, 1969 *Teplovoe rasširenje stekla*. Leningrad, Izd. Nauka
- [3] Štubňa I, Trnovcová V, 1998 The effect of texture on thermal expansion of extruded ceramics. *Ceramics - Silikáty* **42** pp. 21-24

AN APPARATUS FOR THE THERMAL DIFFUSIVITY MEASUREMENT USING THE FLASH METHOD

Libor Vozár¹, Wolfgang Hohenauer²

¹Department of Physics, Faculty of Natural Sciences, Constantine the Philosopher University, Tr. A. Hlinku 1, SK-94974 Nitra, Slovakia

² Department of Materials Technology, Austrian Research Centers, A-2444 Seibersdorf, Austria

Email: vozar@uniag.sk, wolfgang.hohenauer@arcs.ac.at

Abstract

The paper deals with the measurement of the thermal diffusivity using the laser flash methods. Here the concept and the analytical basis of the standard laser flash method as well as the flash method with repeated pulses are summarized. Here the experimental apparatus is described in details and results of the thermal diffusivity measurements on samples made of austenitic steel and TiAl alloys are presented and compared.

Key words: thermal diffusivity, flash method, flash method with repeated pulses

1 Introduction

The laser flash method, proposed by Parker et al [1], has become the standard method of measuring the thermal diffusivity of solids. Here the front face of a plane sample receives a short pulse of radiant energy provided by a laser. The resulting temperature rise on the opposite (rear) face of the sample is measured, and the thermal diffusivity is computed from the temperature rise vs. time data.

To overcome particular experimental difficulties associated with the measurement of poor thermal conductive materials and/or the measurement of large samples that limit an extension of the general use of the flash method especially in the case of an investigation of insulators, temperature sensitive materials, large-grain heterogeneous materials, measurements near the phase transition, the modification of the method – the flash method with repeated pulses was proposed [2,3]. In the flash method with repeated pulses the pulse energy is split into several consecutive (laser) pulses and applied periodically to the sample front face. The thermal diffusivity is estimated from the resulting temperature rise of the rear surface, as in the standard laser flash technique.

2 Mathematical basis

The ideal adiabatic model considers a homogeneous opaque thermally insulated slab of thickness e with uniform and constant thermophysical properties and the density ρ . If the sample front face is exposed to instantaneous heat pulses repeated with the period t_p , analytically described by the shape $\phi(t) = Q\delta(t - kt_p)$; $k = 0, 1, \dots, p$, with Q - the heat

supplied by a pulse to the unit area of the front face, $\delta(t)$ the Dirac's function and $(p+1)$ the number of pulses, the temperature $T(t)$ at the rear face conforms the equation

$$T(t) = \frac{Q}{\rho c e} \left\{ k + 1 + 2 \sum_{n=1}^{\infty} (-1)^n \sum_{i=0}^k \exp[v_n (i t_p - t)] \right\}. \quad (1)$$

Here t is the time, c the specific heat, a the thermal diffusivity and parameter $k = 0, 1, \dots, p-1$ when $k t_p \leq t < (k+1)t_p$, or $k = p$ in case of $t \geq p t_p$, respectively, and

$$v_n = n^2 \pi^2 \frac{a}{e^2}.$$

The non-ideal model that is more realistic in a wider temperature range considers heat transfer between the sample and its environment. Let us have a cylindrical sample of the radius r_s , with the thickness e and the pulse shape $\phi(t)$ as in the case of the ideal model. If we take account of heat loss from the sample, governed by Biot numbers H_0 , H_e and H_r at the front, rear and radial faces, the transient temperature $T(t)$ in the center of the sample rear face can be expressed in the form of Fourier series

$$T(t) = \frac{Q}{\rho c e} \sum_{n=1}^{\infty} A_n(H_0, H_e) \sum_{m=1}^{\infty} B_m(H_r) W_{nm}(t), \quad (2)$$

with the time terms

$$W_{nm}(t) = \sum_{i=0}^k \exp[v_{nm}(i t_p - t)],$$

where

$$A_n(H_0, H_e) = \frac{2u_n^2 (u_n^2 + H_e^2) \left(\cos u_n + \frac{H_0}{u_n} \sin u_n \right)}{(u_n^2 + H_0^2)(u_n^2 + H_e^2) + (H_0 + H_e)(u_n^2 + H_0 H_e)}, \quad H_0 > 0; H_e > 0$$

$$B_m(H_r) = \frac{2H_r}{J_0(w_m)(w_m^2 + H_r^2)}, \quad H_r > 0$$

$$k = \begin{cases} 0, 1, \dots, p-1 & ; \quad k t_p \leq t < (k+1)t_p \\ p & \quad t \geq p t_p \end{cases}$$

$$v_{nm} = \left(u_n^2 + w_m^2 \frac{e^2}{r_s^2} \right) \frac{a}{e^2},$$

and u_n and w_m are the positive roots of equations

$$(u^2 - H_0 H_e) \tan(u) = (H_0 + H_e) u,$$

$$w J_1(w) = H_r J_0(w),$$

and J_0 a J_1 are Bessel functions of the first kind, order 0 and 1.

3 Experimental apparatus

The computer controlled laser flash experimental apparatus was built at the Materials Research Division of the Austrian Research Centre in Seibersdorf where it is regularly used for measurements of the thermal diffusivity of solids.

The apparatus consists of Nd:Cr:GGG (gallium-gadolinium garnet doped with neodymium) glass laser (BLS400, Baasel Lasertech) working at wave length $\lambda=1.064$ μm with the justified pulse energy $\sim 10 \text{ J}\cdot\text{cm}^{-2}$. The transient temperature is measured by the liquid nitrogen cooled HgCdTe infrared detector (HCT-80, Infrared Associated, Inc.) with preamplifier (PPA-15-DC). The detector has a time constant of about 300 ns and is set to detect radiation from the central square area ($\sim 4 \text{ mm}^2$) at the sample rear face. The sample is supported in a horizontal position in the vacuum chamber. A short tantalum tube acts as the resistance heater and allows measurements in the temperature range from 20 up to 1900 °C. Furnace is powered by a DC current from the power source (TN 10-5000, Heinzinger Elektronik). The sample temperature sensor consists of the steel encapsulated K-type (NiCr/Ni) thermocouple of 1 mm in diameter, or spot welded S-type (Pt/PtRh10) thermocouple made from wires of 0,35 mm in diameter (Heraeus). All data acquisition and control is performed using the standard measurement hardware (PCI 20001C-A carrier, PCI 20002M 12bit A/D, 20003M 12bit D/A, PCI 20007M Timer/IO, Burr-Brown). The software is built in Borland's C++ and runs on a PC under MS DOS [4].

The apparatus is constructed in two axes as illustrated in Fig. 1. A laser is placed horizontally. The laser beam is reflected by a bending mirror and follows vertically through a glass window (BK7) into a water-cooled stainless-steel vacuum chamber. The vacuum is stabilized using the turbo pump (TPH 110, A. Pfeiffer Wakuumtechnik) at values of 10^{-5} Pa order. The sample holder consists of three molybdenum rods that fix the sample in a horizontal position in the central zone of the furnace. The construction allows the irradiation of the lower (front) face of the sample and the measurement of temperature and temperature response on the upper (rear) face of the sample. The detachable top of the vacuum chamber fixes the IR temperature sensor that is focused with CaF_2 lens and mechanical iris. The chamber top contains the movable tubes that allow the setting and through a window the checking of the thermocouples' position.

The data reduction – an estimation of the thermal diffusivity consists of a least squares (LSQ) fitting of the theoretical curves, to the measured temperature rise vs. time evolution. Because we have semi-linear LSQ tasks - working expressions (1) and (2) linearly depend on the heat flux term $Q/\rho c e$, the algorithm described elsewhere [5,6] that shifts the fitting to solving a set of algebraic equations can be utilized effectively. The data reduction - depending on the ideal adiabatic model (equation 1), or the non-ideal 'heat loss' theory (equations 2), gives the appropriate thermal diffusivity a_{ID} , or a_{HH} , respectively.

4 Experimental results

The test measurements were performed on a sample made of austenitic steel X10NiCrMoTiB1515 (Nr.1.4970) the material with known thermophysical properties. The sample was disc shaped with 2.18 mm thick and 10 mm in diameter. The second test sample had a thickness $e = 1.49$ mm and was made from TiAl alloy. In order to improve the laser light absorption the front faces of the samples were blackened. All

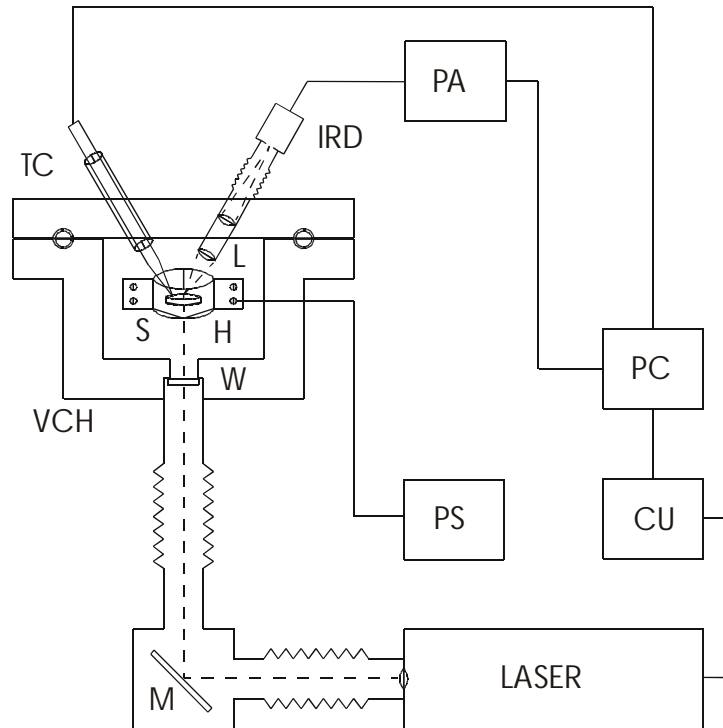


Fig 1 Schematic view of the experimental apparatus (TC-thermocouple, IRD - infra-red detector, PA - preamplifier, L - lens, S - sample, H - heater, W - window, VCH - vacuum chamber, M - mirror, PS - power source, PC - personal computer, CU - controller unit)

measurements were taken in a vacuum at 300 °C.

Thermal diffusivity results obtained analyzing the experimental data (Fig. 5 and 6) measured under different measuring conditions are summarized in the Table 1 and 2. Relatively good agreement of thermal diffusivity values obtained utilizing the standard ‘one-pulse’ flash method (No.1) and the flash method with repeated pulses can be seen.

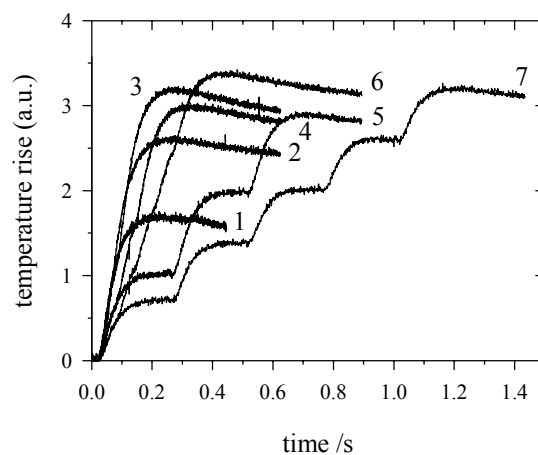


Fig 2 Experimental temperature rise vs. time curves (material - CrNi steel, curves labels correspond to the notation in the Table 1)

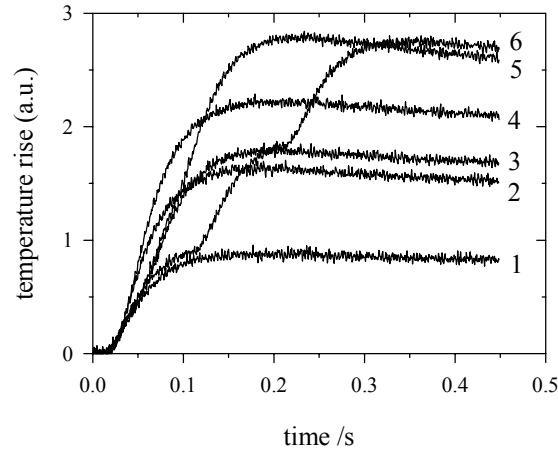


Fig 3 Experimental temperature rise vs. time curves (material - TiAl alloy, curves labels correspond to the notation in the Table 2)

Table 1 Results of thermal diffusivity estimation of austenitic CrNi steel. Here f is the pulse frequency, t_p the period and $p+1$ the number of pulses, a_{ID} and a_{HH} are the thermal diffusivities calculated using the equation (1), or (2), respectively. Recommended thermal diffusivity value is $a_R = 4.24 \cdot 10^{-6} \text{ m}^2 \text{ s}^{-1}$.

Case	f Hz	t_p s	$p+1$	a_{ID} $10^{-6} \text{ m}^2 \text{ s}^{-1}$	$(a_{ID} - a_{ID1})$ $/a_{ID}$ %	a_{HH} $10^{-6} \text{ m}^2 \text{ s}^{-1}$	$(a_{HH} - a_R)/a_R$ %
1			1	4.69	0	4.25	0.24
2	16	0.062	2	4.55	-2.98	4.33	2.12
3	64	0.016	3	4.51	-3.84	4.34	2.36
4	16	0.062	3	4.48	-4.48	4.26	0.47
5	4	0.250	3	4.70	0.21	4.24	0
6	16	0.062	5	4.67	-0.42	4.43	4.48
7	4	0.250	5	5.01	6.82	4.2	-0.94

Table 2. Results of thermal diffusivity estimation of TiAl alloy (Ti48Al). For the used parameters see Table 1. Recommended thermal diffusivity is $a_R = 5.95 \cdot 10^{-6} \text{ m}^2 \text{ s}^{-1}$.

Case	f Hz	t_p s	$p+1$	a_{ID} $10^{-6} \text{ m}^2 \text{ s}^{-1}$	$(a_{ID} - a_{ID1})$ $/a_{ID}$ %	a_{HH} $10^{-6} \text{ m}^2 \text{ s}^{-1}$	$(a_{HH} - a_R)/a_R$ %
1			1	6.16	0	5.86	-1.54
2	100	0.01	2	6.18	0.32	5.95	0
3	25	0.04	2	6.18	0.32	5.97	0.36
4	100	0.01	3	6.26	1.62	6.04	1.49
5	25	0.04	3	6.36	3.24	6.12	2.78
6	10	0.1	3	6.44	4.54	5.93	-0.34

Any significant difference between the dispersion of the thermal diffusivity values estimated from ‘several pulses’ recordings and the usual dispersion of the standard ‘one pulse approach’ of the experimental apparatus used haven’t been observed. The shapes of the experimental curves and the comparison of the measured values a_{ID} and a_{HH} indicate that the experimental conditions are non-ideal and the heat loss should be taken into account.

5 Conclusion

The paper shows that the laser flash method apparatus can be successfully applied to the measurement of thermal diffusivity using the flash methods. Experimental results show that the level of the thermal diffusivity measurement accuracy and reproducibility using the standard one-pulse flash method is comparable to the repeated pulses approach's flash method.

Acknowledgement

Authors wish to thank the Hertha Firnberg Foundation of the ARC Seibersdorf and the Slovak Science Grant Agency for the financial support under the contract 1/6115/99.

References

- [1] Parker W J, Jenkins R J, Butler C P and Abbott G L, 1961 Flash Method of Determining Thermal Diffusivity, Heat Capacity and Thermal Conductivity, *J. Appl. Phys.* **32**, 1679-1684
- [2] Vozár L, Groboth G, Hohenauer W, Hübner E, 1999 An Application of the Laser Flash Method with Repeated Pulses for the Thermal Diffusivity Measurement, in *Proceedings of the 10th Int. Conf. on Photoacoustic and Phototherm. Phen.*, (Eds. F. Scudieri, M. Bertolotti, New York: AIP Woodbury), pp. 351-353
- [3] Vozár L, Hohenauer W, 2000 Measurement of the Thermal Diffusivity Using the Laser Flash Method with Repeated Pulses, *High Temp. High Press.* (in press)
- [4] Vozár L, Gembarovič J, Majerník V, 1993 FLASH - A Software Package for Data Acquisition and Data Analysis in the Flash Method, *High Temp. High Press.* **25**, 421-425
- [5] Gembarovič J, Vozár L, Majerník V, 1990 Using the Least Squares Method for Data Reduction in the Flash Method, *Int. J. Heat Mass Transfer* **33**, 1563-1565
- [6] Vozár L, Šrámková T, 1997 Two Data Reduction Methods for Evaluation of Thermal Diffusivity from Step Heating Measurements, *Int. J. Heat Mass Transfer* **40**, 1647-1655